Doctoral Thesis

Laser Plasma Study through Simulation and Theory: Raman Scattering and Plasma Dipole Oscillation

Hyung Seon Song

Department of Physics

Ulsan National Institute of Science and Technology

2023

Laser Plasma Study through Simulation and Theory: Raman Scattering and Plasma Dipole Oscillation

Hyung Seon Song

Department of Physics

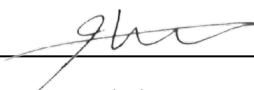Ulsan National Institute of Science and Technology

Laser Plasma Study through Simulation and Theory: Raman Scattering and Plasma Dipole Oscillation

A thesis/dissertation submitted to

Ulsan National Institute of Science and Technology

in partial fulfillment of the

requirements for the degree of

Doctor of Philosophy

Hyung Seon Song

06.05.2023 of submission

Approved by

_____

Advisor
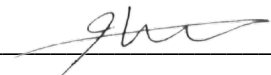
Min Sup Hur

Laser Plasma Study through Simulation and Theory: Raman Scattering and Plasma Dipole Oscillation

Hyung Seon Song

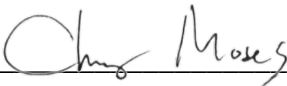This certifies that the thesis/dissertation of Hyung Seon Song is approved.
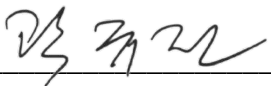
06.05.2023 of submission

Signature

_____

Advisor: Min Sup Hur
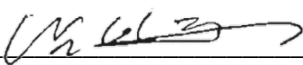
Signature

_____

Moses Chung

Signature

_____

Kyujin Kwak

Signature

_____

Hyyong Suk

Signature

_____

Inhyuk Nam

Abstract

Stimulated Raman Scattering (SRS) is a fascinating physical phenomenon that arises from the interaction between a plasma medium and high-energy laser radiation. It involves the transfer of laser energy to plasma waves, resulting in the generation of new waves and the scattering of the incident laser beam. SRS is an important phenomenon in laser plasma interaction, with various applications in fields such as laser fusion, particle acceleration, and high-energy-density physics. The SRS process begins when a high-intensity laser beam interacts with a plasma medium. The laser energy excites plasma waves, which can be longitudinal or transverse depending on the direction of the laser polarization. These waves then undergo a resonance process, where they interact with the plasma ions and transfer energy to them. As a result, new waves are generated, and the incident laser beam is scattered in a different direction. One of the most significant features of SRS is its threshold behavior. SRS only occurs when the laser intensity exceeds a certain threshold value. Below this value, the plasma waves cannot reach the resonance condition and do not transfer energy to the plasma ions. Above the threshold value, however, the plasma waves grow exponentially, leading to a rapid increase in the scattered light intensity. SRS has various applications in laser plasma interaction. In laser fusion, SRS can be a significant obstacle as it leads to the loss of laser energy and can damage the laser system. Researchers have developed various methods to mitigate SRS, such as using frequency conversion techniques, plasma shaping, and polarization smoothing. In particle acceleration, SRS can be used to generate high-energy electron beams. By controlling the laser intensity and plasma conditions, researchers can create plasma wakefields that accelerate charged particles to high energies.

Plasma density diagnostics are crucial to understanding the laser plasma interaction process. One diagnostic method involves using a probe laser to measure the plasma density through the interaction with the plasma electrons. Other diagnostic methods include interferometry, Thomson scattering, and Langmuir probes. Raman scattering diagnostics are a powerful tool for measuring the plasma density in a wide range of applications. This technique relies on the inelastic scattering of light from the plasma, which results in a shift in the frequency of the scattered light. By measuring the frequency shift, researchers can determine the plasma density and gain insight into the plasma's behavior. Overall, Raman scattering diagnostics are a powerful tool for measuring plasma density in a wide range of applications. These techniques can provide valuable insight into the plasma's behavior and are essential for the development of advanced plasma technologies. Ongoing research continues to improve the sensitivity and accuracy of Raman scattering diagnostics, ensuring that these techniques remain at the forefront of plasma research.

Plasma dipole oscillations are a type of collective motion that can occur in a plasma medium when it is excited by an external electromagnetic field. These oscillations result from the motion of the plasma electrons in response to the electromagnetic field, creating a dipole moment that oscillates at a characteristic frequency. Plasma dipole oscillations are an important phenomenon in plasma physics and

have various applications, including as a radiation source for plasma diagnostics. Plasma dipole oscillations can also act as a radiation source for plasma diagnostics. When the dipole moment of the plasma oscillates, it generates electromagnetic radiation at the same frequency. This radiation can be in the THz-band depending on the plasma parameters. This characteristics create new diagnostic method for plasma density. More easily usage of PDO method, we shot the laser pulse obliquely.

The magnetization of the PDO induces the formation of three modes in gyrating electrons: the upper hybrid (H) mode, the right circular mode (R), and the left circular mode (L). The H-mode acts as a resonance point that prevents transmission to the vacuum, whereas X-modes can be transmitted through the plasma. The H-mode diminishes as the magnetic field increases, while X-modes become more prominent. This results in more energy being extracted from the PDO in the form of radiation. This effect is demonstrated by the effective flow, where in the weak field regime, electrons are well organized, resulting in effective longitudinal flow, while in the strong field regime, electron phases are randomized, and circular flows prevail, forming X-modes instead of H-mode.

Contents

List of Figures

I   Plasma Raman Instability in the Laser Plasmas

1.1   Introduction

Laser plasma research incorporates plasma physics, optics, high-energy physics, and laser technology. It is fascinated by the complicated interactions that take place when intense laser beams collide with plasmas, which are ionized gases composed of free electrons and ions. The primary objective of laser plasma research is to understand the fundamental physics behind laser-plasma interactions. Complex physical processes such as laser light absorption [1, 2], particle acceleration [3, 4], plasma heating [5, 6], and the formation of intense electromagnetic fields [7, 8] are examples of these interactions. By studying these phenomena, researchers hope to understand more about the fundamental physics principles and complicated dynamics that occur in laser-produced plasmas.

One captivating phenomenon observed during the propagation of a high-intensity laser through a plasma is self-focusing [9]. The physical process of self-focusing is determined by the competition of two dimensionless components. The first value indicates the charge-displacement nonlinearity's contribution to the relative strength of the diffraction in proportion to the relativistic electron mass nonlinearity, and the second parameter represents the laser intensity in relativistic units. An optical beam can expand into spikes of unlimited amplitude over a finite propagation distance. This is referred to as wave collapse (blow-up) [10], giving rise to self-sustaining regions of remarkably high laser intensity known as laser filaments [11]. These filaments exhibit extraordinary propagation characteristics, enabling them to traverse significant distances within the plasma medium or even the air.

Laser-driven particle acceleration represents another focal point within the laser plasma field. Through the generation of powerful electric fields, laser-plasma interactions propel charged particles, such as electrons or ions, to attain high energies. Notably, techniques like laser wakefield acceleration (LWFA) [12] and direct laser acceleration (DLA) [13] hold immense promise for achieving compact and high-energy particle accelerators, thereby revolutionizing the field of particle acceleration.

Moreover, the synthesis of high harmonics is being actively researched utilizing the principal mechanism, an oscillating mirror activated by a laser pulse. The plasma-vacuum contact that occurs at the surface of the solid target is the nonlinear medium underpinning the harmonic generating process. Harmonics are produced by electron mobility in the laser beam at the plasma-vacuum interface. Consider the contact between the critical-density surface of the plasma and the vacuum to be an oscillating mirror, with the mirror oscillation caused by the laser field acting on the mirror's electrons. The two primary driving factors are the laser's electric field and the ponderomotive force or light pressure, which results in the creation of both odd and even harmonics [14]. This groundbreaking technique enables the generation of coherent and short-wavelength X-ray or extreme ultraviolet (EUV) radiation [15].

Furthermore, in the pursuit of fusion energy experiments, laser plasma interactions play a crucial role, particularly in the domain of inertial confinement fusion (ICF) [16]. ICF employs intense lasers to compress and heat a plasma, with the aim of initiating and sustaining a controlled fusion reaction. As the plasma absorbs the laser energy, it gives rise to a highly energetic and dense plasma environment that is

conducive to efficient fusion processes.

Finally, at high intensities, lasers have the ability to induce the breakdown of gases, leading to the creation of plasma channels or filaments. These plasma channels serve as effective waveguides [17] for subsequent laser pulses, enabling precise control and manipulation of laser beams over considerable distances.

As a main focus of this chapter in the field of laser plasmas, stimulated Raman scattering (SRS) [18] takes center stage. When a high-intensity laser beam interacts with a plasma, a nonlinear optical process occurs, resulting in coherent Raman scattered light. When light interacts with plasmas, it experiences a frequency shift [19], which is known as Raman scattering. The incident laser beam transfers some of its energy to plasma waves during SRS. These waves are produced by the interaction of the laser with charged particles, namely plasma electrons. The energy transfer method is based on the principles of stimulated scattering, in which the presence of the incident laser beam causes the scattered light to be amplified. When incoming laser photons contact with the plasma, they scatter into two new photons: a Stokes-shifted photon with a downshifted frequency and an anti-Stokes-shifted photon with an up-shifted frequency. The magnitude of the frequency shift is determined by the energy exchange between the laser and the plasma waves.

I'll go over the laser plasma convention briefly before getting into the SRS. Incident electromagnetic (EM) waves can interact with electrons in plasmas and give rise to various interesting phenomena such as plasma grating [20, 21] and plasma mirror [22]. Plasma acts as linear and nonlinear media depending on the external field intensity [23]. Field intensity classifies dynamical regimes, once the perturbation is enhanced, nonlinear current is generated. Various feedback interaction makes very complex phenomenon, which cannot be described by analytic equations resulting in a difficulty to interpret them [24, 25]. Instead of these complex things, I will start the basic equation of motion in the presence of the plane EM wave.

$$m\frac{dv_0}{dt} = -eE \tag{1}$$

where, m is electron mass, v_o is quiver velocity [26], e is elementary charge and E is electric field. Electric field can be represented by vector potential for EM wave. With the cgs unit,

$$E = -\frac{1}{c}\frac{\partial A}{\partial t} \tag{2}$$

where, c is speed of light and A is vector potential. In the laser plasma field, vector potential is usually normalized for the simplicity.

$$\frac{eA}{mc^2} = a_0 \tag{3}$$

Substitute all things into the equation of motion, quiver velocity can be obtained

$$\frac{v_0}{c} = a_0 \tag{4}$$

This representation is crude for describing many body problems with the analytic derivations [27]; however, it does give practical usage. Because laser plasma is commonly believed to be in a cold fluid [28],

Debye length becomes very tiny, allowing the long-range Columb interaction between particles to be ignored [29]. I convert it into practical parameters including the laser intensity.

$$a_0^2 = 7.3 \times 10^{-19} [\lambda(\mu m)]^2 I(W/cm^2) \tag{5}$$

Final form of parameter is

$$\frac{v_0}{c} = 8.85 \times 10^{-10} \lambda(\mu m) \sqrt{I(W/cm^2)} \tag{6}$$

For the CO_2 laser, when the intensity is $10^{16} W/cm^2$, oscillating velocity becomes comparable to the speed of light. Over the laser intensity $10^{16} W/cm^2$, relativistic treatments need to be considered.

Normalized laser intensity over the 1 means relativistic plasma waves can occur. It was shown by Dawson that wave breaking in a cold plasma [30] occurs when elements of the plasma electron fluid that started out in different positions overtake each other while moving back and forth during the passage of the wave. For both non-relativistic and relativistic plasmas,this overtaking happens when the peak fluid velocity equals the phase speed of the plasma wave. A direct consequence of this is that a large fraction of the plasma electrons get trapped in and accelerated by the plasma wave.

$$E_{max} > \frac{m\omega_p c}{e} \tag{7}$$

where $\omega_p = \sqrt{\frac{e^2 n_0}{m\varepsilon_0}}$, n_0 is background density and ε_0 is vacuum permitivity. Relativistic threshold is also obtained by the Akhiezer and Polovin [31].

$$E_{max} > \sqrt{2(\gamma - 1)} \tag{8}$$

,where $\gamma = \frac{1}{\sqrt{\beta_\phi^2 - 1}}$ and β_ϕ is normalized phase velocity by speed of light.

In the non-relativistic regime, considering a plane wave, the amplitude of the pump is required to satisfy the condition:

$$a_0 \ll 1 \tag{9}$$

In an un-magnetized plasma, the hydrodynamic equations describe the presence of three waves: the electron plasma wave (EPW), the ion acoustic wave (IAW), and the electromagnetic wave (EMW) [32]. However, studying each wave individually in a homogeneous plasma provides limited insight into their interactions with one another. A second-order analysis is required to understand non-linear interactions [33], which involves considering the product of two oscillating quantities. This approach can help explain the lowest-order example of non-linear interaction, known as a three-wave instability. A three-wave instability is a non-linear interaction between three waves that results in the transfer of energy between them. This phenomenon has important implications for plasma-based applications, such as inertial confinement fusion [34], plasma heating and current drive [35], and particle acceleration [36]. The transfer of energy can lead to the generation of new waves, such as sidebands or harmonics, and can significantly modify the behavior of the original waves. In the context of a plasma wave driven by a high-amplitude laser, the laser interacts with an EPW, generating scattered light [37] that is Doppler-shifted due to the electrons' longitudinal collective motion in the wave. The scattered light wave beats

with the laser light, creating a beat-wave whose envelope reinforces the original EPW via the pondero-motive force [38]. This force is proportional to the gradient of the energy density of the beat EMW. This process is known as the Raman scattering process and has important implications for laser-plasma interactions and the generation of high-energy particles.

To introduce the theory of three coupled waves, we can start by considering the case of three coupled oscillators, as described by Nishikawa in 1968 [39]. In this scenario, each wave has a locally linear dispersion relation characterized by angular frequency and wave-number (ω, k). A small non-linear coupling between the waves allows us to conclude that each of the three waves can be described by a set of coupled non-linear differential equations, which can be solved using perturbation theory. By solving these equations, we can understand how the perturbations associated with one wave might affect one or more of the other waves present in the plasma. The non-linear interaction of the EPW, IAW, and EMW in a plasma is investigated, with the necessity of fulfilling the frequency and wave-number matching constraints, which guarantees that the energy and momentum conservation rules are met. It demands, specifically, that the total of the interacting waves' wave vectors (wave numbers) be zero and that their frequencies fulfill a precise connection. This condition guarantees that the waves' energy and momentum are balanced, allowing for effective energy exchange. In particular, the real components of the frequencies and wave-numbers must be matched for each wave, which may be represented as

$$
\begin{aligned}
\omega_0 &= \omega_1 + \omega_s \\
k_0 &= k_1 + k_s
\end{aligned}
\tag{10}
$$

The matching conditions discussed above are crucial in the context of resonant energy exchange between waves. This occurs when three waves interact: a large-amplitude laser wave with frequency ω_0 and wave number k_0, a plasma wave with frequency ω_1 and wave number k_1, and a scattered light wave with frequency ω_s and wave number k_s. By fulfilling the matching conditions, resonant energy exchange can occur between the waves, leading to efficient transfer of energy and influencing each wave's behavior through nonlinear processes.

The plasma under consideration is assumed to be infinite in extent and spatially homogeneous, mean-ing that its properties, such as density and temperature, do not vary significantly across the plasma. Additionally, it is assumed that there is no pump depletion, which means that the energy of the large-amplitude laser wave is conserved during the interaction. To analyze the nonlinear interaction of the large-amplitude laser wave, plasma wave, and scattered light wave in this simplified scenario, a further simplification is made by modeling these waves as three oscillators. Each oscillator is described by the equation for a damped harmonic oscillator, which takes the form:

$$
\left[\frac{d^2}{dt^2} + 2\gamma_i \frac{d}{dt} + \omega_i^2 \right] X_i(t) = 0
\tag{11}
$$

where X_i represents the amplitude of the oscillation for wave i (with i corresponding to the laser, plasma wave, or scattered light wave), γ_i is the damping coefficient, ω_i is the natural frequency. Since wave 0 (the laser) has large amplitude and is not significantly damped, and we assume no pump depletion, the

lowest order coupling of these waves gives the coupled system.

$$\left[\frac{d^2}{dt^2} + \omega_0^2\right] X_0(t) = 0$$

$$\left[\frac{d^2}{dt^2} + 2\gamma_1\frac{d}{dt} + \omega_1^2\right] X_1(t) = 2\alpha X_0(t) X_s(t) \tag{12}$$

$$\left[\frac{d^2}{dt^2} + 2\gamma_s\frac{d}{dt} + \omega_s^2\right] X_1(t) = 2\beta X_0(t) X_1(t)$$

where α and β are constants and coupling factors. 1 is plasma wave and s is scattered wave respectively. When the coupling factors α or β is large, the laser wave can efficiently transfer energy to the plasma wave or scattered wave, leading to significant amplitude modulation and modification of the each wave's behaviors. The solution of simple harmonic oscillator is

$$X_0(t) = \bar{X}_0(t) e^{i\omega_0 t} \tag{13}$$

$X_1(t)$ will be standing waves $\cos(\omega_1 t)$ or there are $\omega \pm \omega_0$ components. Taking the Fourier transform of other damped equations

$$\left[\omega^2 + 2i\gamma_1\omega - \omega_1^2\right] X_1(\omega) + \alpha\bar{X}_0\left[X_s(\omega - \omega_0) + X_s(\omega + \omega_0)\right] = 0$$

$$\left[\omega^2 + 2i\gamma_s\omega - \omega_s^2\right] X_s(\omega) + \beta\bar{X}_0 X_1(\omega \pm \omega_0) = 0 \tag{14}$$

Defining $D_s(\omega) = \omega^2 + 2i\gamma_s\omega - \omega_s^2$, solution for ω must satisfy

$$D_1(\omega) = \alpha\beta\bar{X}_0^2\left[\frac{1}{D_s(\omega + \omega_0)} + \frac{1}{D_s(\omega - \omega_0)}\right] \tag{15}$$

Consider the real and imaginary parts of $\omega = \omega_r + i\gamma$ separately. The exponential growth rate is given by:

$$(\gamma + \Gamma_1)(\gamma + \Gamma_s)\left[1 + \left(\frac{\Delta\omega^2}{2\gamma + \Gamma_1 + \Gamma_s}\right)^2\right] = \gamma_0^2 \tag{16}$$

where γ_0 is the coupling constant given by:

$$\gamma_0 = \frac{\bar{X}_0}{2}\sqrt{\frac{\alpha\beta}{\omega_1\omega_s}} \tag{17}$$

Examining the limiting cases of the dispersion relation gives the following key results for the growth of a three-wave parametric instability in an infinite, homogeneous plasma. Firstly, when the frequency mismatch ($\Delta\omega = \omega_0 - (\omega_1 + \omega_s)$) and damping rates of both daughter waves are zero, the instability has a maximum growth rate given by the coupling constant γ_0. Secondly, when $\Delta\omega = 0$ but both waves have finite non-zero damping, the growth rate is given by:

$$\gamma = \gamma_0\sqrt{1 + \left(\frac{\Gamma_s - \Gamma_1}{2\gamma_0}\right)^2} - \frac{\Gamma_1 + \Gamma_s}{2} \tag{18}$$

This indicates that there is a threshold amplitude induced by damping; if the amplitude of the pump laser goes below the threshold, the damping effect takes over, and the instability cannot expand. In other

words, the energy transmitted from the pump laser to the plasma wave and dispersed light wave becomes inadequate to overcome the dissipation processes, causing the instability to be suppressed.

$$I > I_{\text{threshold}} \propto \Gamma_1 \Gamma_s \qquad (19)$$

The final comment on this idealized solution is that we assumed $X_1, X_s \ll X_0$ in order to begin solving for ω. However, the analysis presented above shows that X_1, X_s will grow exponentially for $I > I_{\text{threshold}}$, which will soon make this assumption invalid. When we consider more realistic situations such as pump depletion, finite plasma length, and plasma density gradients, things become much more intractable. When I consider more realistic situations, such as pump depletion, finite plasma length, and plasma density gradients, the dynamics of the system become much more complex and challenging to analyze. Pump depletion occurs when the energy of the pump laser is gradually transferred to the plasma waves and scattered light, leading to a reduction in the pump laser's amplitude over time. This depletion causes further nonlinear effects and changes the genesis and interaction of waves. Furthermore, the limited length of the plasma introduces boundary effects that can have a significant impact on wave dynamics. The presence of density gradients inside the plasma further complicates the research by causing geographic variances in plasma properties and wave quality. My Raman study, on the other hand, aims to provide a straightforward technique for plasma diagnostics. This level of complexity is not necessary for the procedure. As a result, I disregard this part.
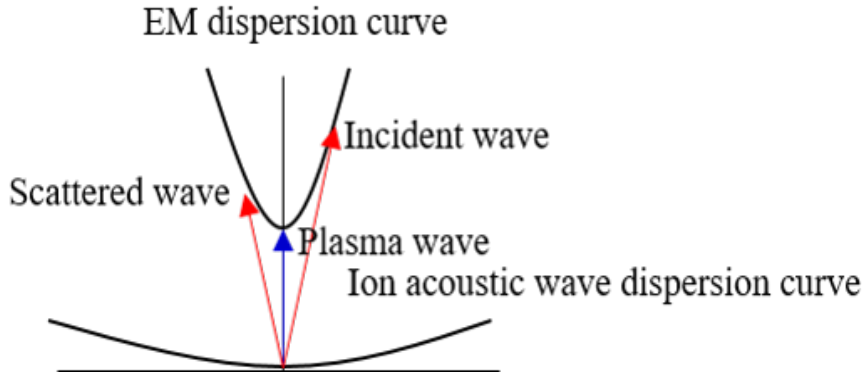
Figure 1: Dispersion curves of electromagnetic and ion acoustic wave, arrows represent dispersion relation of scattered wave and plasma wave respectively.

1.2 Raman Instability

Parametric plasma instability [40] refers to a phenomenon in which the plasma exhibits an unstable behavior due to the nonlinear coupling [41] between different wave modes or frequencies. This instability arises from the exchange of energy between interacting waves, leading to the growth or amplification of wave modes. The interaction between waves occurs through a nonlinear process known as parametric

amplification [42,43]. This process involves the transfer of energy between waves with different frequencies and wave numbers, typically satisfying certain resonance conditions. The interaction occurs when the frequency and wave number differences between the waves satisfy specific relationships determined by the plasma's properties.

Depending on the kind of interacting waves, parametric conditions are different and name is also different. Parametric Decay Instability (PDI) [44] occurs when a high-frequency pump wave decays into a lower-frequency daughter wave and a sideband wave. The decay process involves the conservation of energy and momentum, and the resonance conditions are determined by the frequency and wave number differences between the pump, daughter, and sideband waves.

$$\omega_0 = \omega_{daughter} + \omega_{side}$$
$$k_0 = k_{daughter} + k_{side}$$

(20)

Stimulated Brillouin Scattering (SBS) [45] is another type of parametric instability that occurs when a high-frequency pump wave interacts with a low-frequency ion acoustic wave in a plasma. The pump wave transfers energy to the ion acoustic wave, leading to the scattering of the pump wave and the generation of a scattered wave with a frequency upshift (anti-Stokes-shifted wave).

$$\omega_0 + \omega_s + \omega_{ion}$$
$$k_0 = k_s + k_{ion}$$

(21)

Among the various parametric instabilities that can occur in plasmas, the Raman instability involves the interaction of two electromagnetic plasma waves and one electrostatic plasma wave, resulting in complex dynamics and wave-wave interactions within the plasma system. The dispersion relations associated with each wave play a crucial role in determining the parametric conditions necessary for the occurrence of the Raman instability. The Raman instability arises due to a resonant coupling between the three waves involved. This resonant interaction occurs when the frequencies and wave vectors of the interacting waves satisfy specific conditions dictated by their dispersion relations. The dispersion relation of a wave describes the relationship between its frequency and wave vector, encapsulating important information about its propagation characteristics and behavior within the plasma medium. To understand the parametric conditions for the Raman instability, we need to examine the dispersion relations of the electromagnetic and electrostatic plasma waves involved. The dispersion relation of an electromagnetic plasma wave describes the relationship between the wave's frequency and wave number in a plasma medium. In general, the dispersion relation for an electromagnetic wave propagating through a plasma can be derived by considering the Maxwell's equations and the equation of motion for the charged particles in the plasma. To derive the dispersion relation of an electromagnetic plasma wave, we start by considering Maxwell's equations in a plasma and the equation of motion for charged particles. We assume a linear, homogeneous, and unmagnetized plasma for simplicity. Maxwell's equations in a plasma

are given by

$$\vec{\nabla} \cdot \vec{E} = \frac{\rho}{\varepsilon_0}$$

$$\vec{\nabla} \cdot \vec{B} = 0$$

$$\vec{\nabla} \times \vec{E} = -\frac{\partial \vec{B}}{\partial t} \tag{22}$$

$$\vec{\nabla} \times \vec{B} = \mu_0 \varepsilon_0 \frac{\partial \vec{E}}{\partial t} + \mu_0 \vec{J}$$

Where $\vec{E}$ is the electric field, $\vec{B}$ is the magnetic field, ρ is the charge density, $\vec{J}$ is the current density, and μ_0 is the vacuum permeability. I assume a plane wave solution of the form:

$$E = E_0 e^{i(k \cdot r - \omega t)}$$

$$B = B_0 e^{i(k \cdot r - \omega t)} \tag{23}$$

Where E_0 and B_0 are the amplitudes of the electric and magnetic fields, k is the wave vector, r is the position vector, ω is the angular frequency, and t is time. Substituting plane wave solutions into Maxwell equations, I obtain:

$$i\vec{k} \cdot \vec{E} = \frac{\rho}{\varepsilon_0}$$

$$i\vec{k} \cdot \vec{B} = 0$$

$$i\vec{k} \times \vec{E} = i\omega \vec{B} \tag{24}$$

$$i\vec{k} \times \vec{B} = \mu_0 \varepsilon_0 i\omega \vec{E} + \mu_0 \vec{J}$$

From equation 22, we find that $\vec{k}$ and $\vec{B}$ are perpendicular to each other, which implies that the wave is transverse. Taking the curl of equation and substituting equation, I get dispersion relation of electromagnetic plasma wave and electrostatic plasma wave.

$$\omega^2 = c^2 k^2 + \omega_p^2 \tag{25}$$

$$\omega = \omega_p \tag{26}$$

Momentum and energy conservation regulate the resonance conditions of Raman instability. These fundamental conservation laws play a crucial role in determining the wave number of the plasma waves involved in the instability. Momentum conservation ensures that the total momentum of the interacting waves and the plasma remains conserved throughout the instability process. This conservation law imposes constraints on the wave vectors of the waves participating in the Raman instability. The interaction between the waves leads to a transfer of momentum, which must be balanced to satisfy momentum conservation.

Similarly, energy conservation governs the exchange and redistribution of energy between the participating waves and the plasma medium. Energy transfer occurs as a result of the resonant interaction,
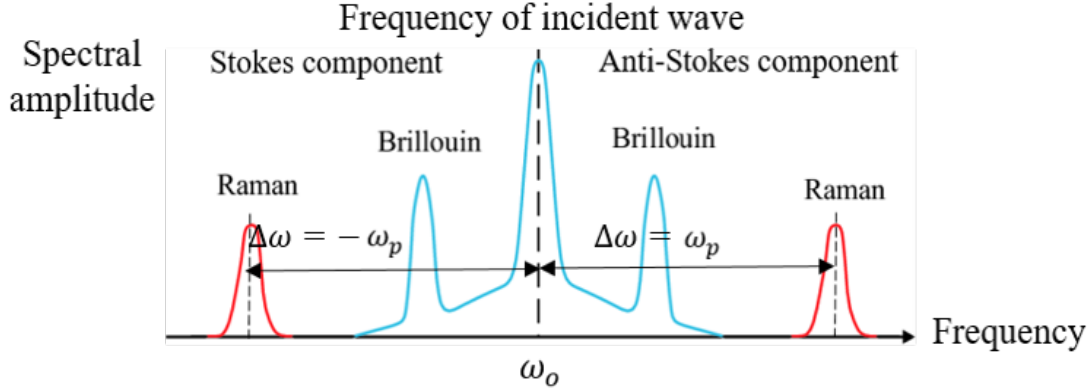
Figure 2: Spectrum of scattering between incident electromagnetic waves and plasmas

where the energy from one wave is transferred to the other waves involved in the instability. The conservation of energy provides further restrictions on the frequencies of the waves.

To satisfy both momentum and energy conservation, the wave numbers of the plasma waves are typically set to the plasma wave number, denoted as ω_p/c, where ω_p is the plasma frequency and c is the speed of light. The plasma wave number represents the characteristic spatial scale associated with the collective oscillations of the plasma particles. By setting the wave number of the plasma waves to ω_p/c, the resonance conditions for the Raman instability can be satisfied, ensuring the conservation of momentum and energy. This choice of wave number facilitates efficient energy transfer and allows for the resonant coupling between the waves, leading to the growth and amplification of the instabilities.

1.3 Spectrum of SRS

Several scattering mechanisms can occur when a laser pulse interacts with plasma, including Rayleigh scattering, Brillouin scattering, and Raman scattering. Each of these scattering processes has unique properties, notably in terms of frequency changes in the scattered light spectrum. Consider the quasi-neutral plasma as an example. Ions are significantly heavier than electrons, which are assumed to be fixed in the femto-second scale. I'll concentrate on the electron's reaction to an incoming electromagnetic wave because it scatters significantly more energy than the proton. I can approximate the electron's equation of motion by re-polarizing the wave electric field in the x-direction.

$$m_e \frac{d^2x}{dt^2} = -m_e \omega_0^2 x - eE_0 \sin(\omega t). \tag{27}$$

The second component on the right represents the perturbing force caused by the electromagnetic wave, whereas the first term represents the (linearized) electrostatic attraction between the electron and the proton. In actuality, I'm illustrating the hydrogen atom as a simple harmonic oscillator with a natural frequency of ω_0. Following a momentary interruption, the typical frequency of electromagnetic radiation emitted by the atom is ω_0. In other words, *omega*$_0$ should indicate the frequency of one of the hydrogen spectral lines in this model. In general, if I give the frequency of a spectral line to ω_0, I may apply the

9

(a) Interaction

Incident wave

dipole

(b) Post-Interaction
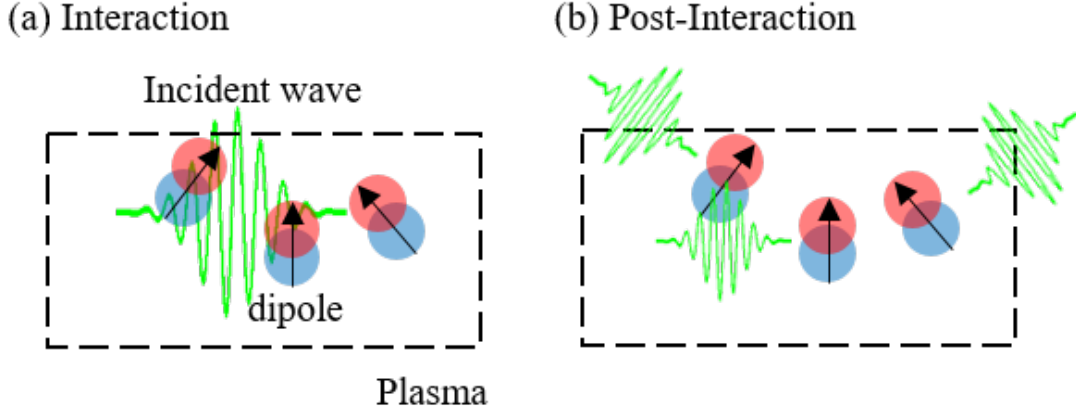
Plasma

Figure 3: Rayleigh scattering diagram, (a) incident wave stimulates dipoles in plasma, (b) after incident wave passes through plasma, surviving dipole emits radiation.

aforementioned model to nearly any sort of atom. The solution of equation 27 is

$$x = \frac{eE_0}{m_e(\omega^2 - \omega_0^2)} \sin(\omega t). \tag{28}$$

As a result, the electron's dipole moment takes the form $\mathbf{p} = -p_0 \sin(\omega t)\hat{\mathbf{x}}$, where

$$p_0 = \frac{e^2 E_0}{m_e(\omega^2 - \omega_0^2)}. \tag{29}$$

By similarity with the preceding section's study, the differential and total scattering cross-sections of our model atom assume the form

$$\frac{d\sigma}{d\Omega} = \frac{\omega^4}{(\omega^2 - \omega_0^2)^2} r_e^2 \sin^2 \theta, \tag{30}$$

and

$$\sigma = \frac{\omega^4}{(\omega^2 - \omega_0^2)^2} \sigma_T, \tag{31}$$

respectively. This form of scattering is known as Rayleigh scattering. There are two features of Rayleigh scattering that should be discussed. First, it is far weaker than Thompson scattering (since *omegallomega$_0$*). Second, unlike Thompson scattering, it is very frequency dependent. Indeed, the preceding calculations show that high frequency (short wave-length) radiation is significantly more efficiently dispersed than low frequency (long wave-length) radiation. Rayleigh scattering has no energy gain or loss when there is no frequency change in the scattered light's spectrum. It happens as a result of the interaction between the incident laser light and the plasma electrons, which causes the light to re-emit at the same frequency as the incident light.

Brillouin scattering involves the interaction between the laser light and plasma acoustic waves, known as sound waves. Brillouin scattering can be described by the equation set consist of fluid and Maxwell equations with Coulomb gauge. This equation set gives three wave equations for electromagnetic wave, plasma wave and ion sound wave.

$$\left(\frac{\partial^2}{\partial t^2} + 2\gamma_0 \frac{\partial}{\partial t} + \omega_p^2 - c^2 \nabla^2 \right) A_0 = -\omega_p^2 \frac{n_e}{n_0} A_0 \tag{32}$$

The vector potential of the incident wave is A_0, while the perturbed electron density is n_e. The incident wave damping rate, γ_0. The other wave equations for electron and ion are

$$\frac{\partial^2 n_e}{\partial t^2} + 2\gamma_e \frac{\partial n_e}{\partial t} - \frac{5T_e}{3m_e}\frac{\partial^2 n_e}{\partial x^2} + \omega_{pe}^2(n_e - n_i) = \frac{e^2 n_0}{2m_e^3 c^2}\nabla^2(A_0 \cdot A_0) \qquad (33)$$

$$\frac{\partial^2 n_i}{\partial t^2} - 3\frac{T_i}{m_i}\frac{\partial^2 n_i}{\partial x^2} + \omega_{pi}^2(n_i - n_e) = 0 \qquad (34)$$

The three wave equations under consideration exhibit a similar form to the coupled equations introduced in the previous section. The resemblance lies in their underlying mathematical structure, which enables us to analyze the interactions between different waves in a plasma medium. In this section, I discussed the equations governing the interactions between the electron plasma wave (EPW), ion acoustic wave (IAW), and electromagnetic wave (EMW) in a homogeneous plasma. These interactions were characterized by the coupling of oscillating quantities, allowing for the exchange of energy between the waves. In the section on stimulated Raman scattering (SRS), I will explain the essential parameters for the plasma diagnostic approach without deriving the coupled equation for stimulated Raman scattering.

The stability of these equations is tested using harmonic perturbations. The zeroth order density perturbation takes precedence. The first order ± 1 wave must be included in this case. Equations are recast here by fitting the order.

$$\left(\frac{\partial^2}{\partial t^2} + 2\gamma_0\frac{\partial}{\partial t} + \omega_p^2 - c^2\nabla^2\right)A_0 = -\frac{\omega_p^2}{2n_0}(n_e A_-^* + n_e^* A_+) \qquad (35)$$

$$\left(\frac{\partial^2}{\partial t^2} + 2\gamma_\pm\frac{\partial}{\partial t} + \omega_p^2 - c^2\nabla^2\right)A_\pm = -\frac{\omega_p^2}{2n_0}n_e A_\pm^* \qquad (36)$$

$$\frac{\partial^2 n_e}{\partial t^2} + 2\gamma_e\frac{\partial n_e}{\partial t} - \frac{5T_e}{3m_e}\frac{\partial^2 n_e}{\partial x^2} + \omega_{pe}^2(n_e - n_i) = \frac{e^2 n_0}{2m_e^3 c^2}\nabla^2(A_0 \cdot A_-^* + A_0^* \cdot A_+) \qquad (37)$$

$$\frac{\partial^2 n_i}{\partial t^2} - 3\frac{T_i}{m_i}\frac{\partial^2 n_i}{\partial x^2} + \omega_{pi}^2(n_i - n_e) = 0 \qquad (38)$$

Ignoring pump depletion $\gamma_0 = 0$ (weak coupling regime), equation 35 gives the dispersion relation $\omega_0^2 = \omega_{pe}^2 + c^2 k_0^2$. Applying harmonic approximation to the Eq. 36 - 38, dispersion relation of scattering can be obtained.

$$\varepsilon_0 = -\frac{\chi_e(1+\chi_i)}{2}k^2 v_0^2\left[\frac{1}{\bar{\omega}_-^2 - \omega_{pe}^2 - c^2 k_-^2} + \frac{1}{\bar{\omega}_+^2 - \omega_{pe}^2 - c^2 k_+^2}\right] \qquad (39)$$

$$\chi_e = \frac{-\omega_{pe}^2}{\bar{\omega}^2 - \frac{5}{3}k^2 v_e^2}, \quad \chi_i = \frac{-\omega_{pi}^2}{\bar{\omega}^2 - 3k^2 v_i^2}, \qquad (40)$$

,where $\bar{\omega}_\pm = \omega \pm \omega_0 + i\gamma_\pm, k+\pm = k \pm k_0$ and $\bar{\omega} = \omega - i\gamma_e$. Pump wave does not significantly modify the dispersion relation of electrostatic wave in the weak coupling regime. $\omega = \omega_s + \Delta\omega$. $\Delta\omega \ll \omega_s$. When scattering increase is balanced with Landau damping, instability arises at a threshold power when $\omega_0 = \sqrt{c^2(k-k_0)^2 + \omega_p^2} + \omega_s$ and $k \approx 2k_0$. the threshold condition is

$$\frac{v_0^2}{v_e^2} > 8\frac{\gamma_e}{\omega_s}\frac{\gamma_-}{\omega_0}\frac{\omega_0^2}{\omega_{pe}^2} \qquad (41)$$

γ_- is $\nu_{ei}\frac{\omega_p^2}{2\omega_0^2}$, where ν_{ei} is the electron ion collision frequency and γ_e is the Landau damping rate due to electrons and ion. Near threshold, growth rate is

$$Im\omega \approx -\left(\frac{k_0^2 v_0^2}{\omega_s \omega_0}\omega_{pi}^2 - 2\gamma_-\gamma_e\right)/(\gamma_e + \gamma_-) \tag{42}$$

Similarly, Raman scattering involves the interaction between the laser light and plasma density fluctuations. The scattered light in Raman scattering also consists of Stokes and Anti-Stokes components, but the frequency shifts are determined by different mechanisms compared to Brillouin scattering. The Raman shift is typically equal to the plasma frequency and is directly related to the plasma density. By analyzing the frequency shifts in Raman scattering, information about the plasma density profile and variations can be obtained, making it a valuable diagnostic tool for plasma characterization. When a laser pulse exceeds the threshold and propagates into a plasma, it can trigger parametric instability, leading to Raman scattering through the grating of electron plasma. When considering a magnetized plasma wave, its behavior becomes somewhat electromagnetic rather than solely electrostatic. In such cases, the wave can generate X-modes [46], which are characterized by the presence of right circular (R) and left circular (L) modes. These modes play a crucial role in the energy exchange between the incident and scattered waves. The R-mode corresponds to a wave propagating in the same direction as the ambient magnetic field, while the L-mode propagates in the opposite direction. These modes are circularly polarized and exhibit distinct dispersion characteristics in magnetized plasmas. The interaction of these modes with the incident and scattered waves can lead to various interesting phenomena. The pump wave is characterized by $E_0 e^{i(k_0 x - \omega_0 t)}$, and the backward scattered wave and plasma wave have the forms $E_0 e^{-i(k_b x + \omega_b t)}$ and $E_L e^{-i(k_L x + \omega_L t)}$, respectively. The following conditions apply:

$$\omega_b \approx \omega_0 - \omega_L, \quad k_L \approx k_0 + \frac{\omega_b}{c} \approx 2k_0 \tag{43}$$

For forward scattering, there are two types of scattered waves: Stokes and anti-Stokes waves [47]. These waves can be described by $E_f e^{i(k_f x - \omega_f t)}$, with the following matching conditions:

$$\omega_f = \omega_0 \pm \omega_L, \quad \pm k_L \approx k_0 - \frac{\omega_f}{c} \approx \pm\frac{\omega_p}{c} \tag{44}$$

Backward and forward Raman scattering are denoted by the subscripts b and f, respectively, whereas the Langmuir or plasma wave is denoted by the subscript L. According to the equation, the phase velocity of the plasma wave in backward scattering is $v_\phi = \frac{\omega_L}{2k_0} \ll c$, where ω_L is the frequency of the slow wave with a large wavenumber ($\sim 2k_0$), which is quite close to the upper-hybrid frequency shown by the X-mode dispersion curves in Fig.4. $\omega_p = \sqrt{\frac{e^2 n_0}{m_e \varepsilon_0}}$ and $\omega_c = \frac{eB_0}{m_e}$ are used here. The plasma wave involved in forward scattering, on the other hand, is a fast wave with $v_\phi \approx c$, generating $\omega_L = \omega_p$, as seen by the cross-point of the $\omega \approx ck$ line and the X-mode curve in Fig.4.

It is required to determine both the plasma density and the magnetic field while examining magnetized plasma systems. This is accomplished by measuring the forward and reverse scattering signals produced by an electromagnetic pulse traveling through the plasma. The backward scattered signal contains information about both the plasma density and the magnetic field, whereas the forward scattered
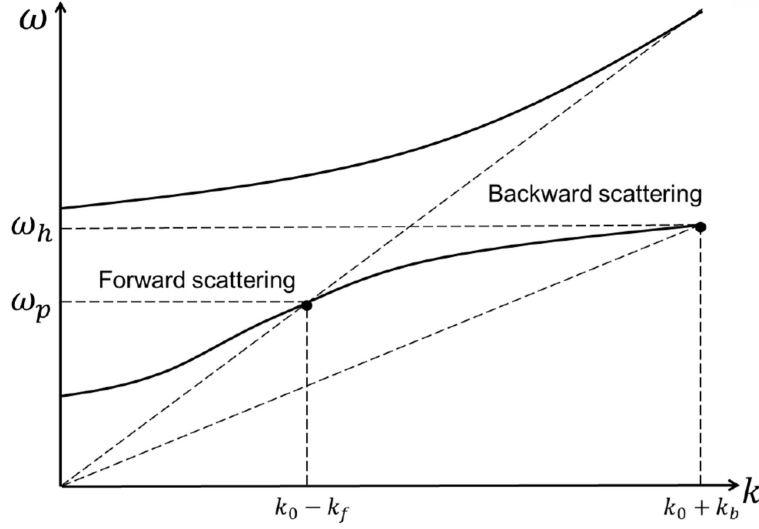
Figure 4: Curves of X-mode dispersion in a magnetized plasma.

signal simply contains density information. However, several variables can affect the precision of measurements acquired from forward and backward scattering signals. These include plasma temperature, probing electromagnetic wave wavelength, and scattering angle [48].

In a non-magnetized plasma, the Raman shift amounts of forward scattering (scattered light in the same direction as the incident light) and backward scattering (scattered light opposite to the incident direction) are typically equal. This symmetry arises from the isotropic nature of the plasma and the absence of a preferential direction due to magnetic fields. As a result, the Raman scattering process in non-magnetized plasmas is characterized by a single Raman shift, which corresponds to the plasma frequency and provides information about the plasma density. However, in magnetized plasmas, the presence of a magnetic field introduces an anisotropy that affects the Raman scattering process. The Raman shift amounts of forward and backward scattering can differ due to the influence of the magnetic field.

This asymmetry arises from the interaction of the scattered light with the magnetic field and the resulting modified dispersion relations of the plasma waves. The discrepancy in the Raman shift amounts between forward and backward scattering in magnetized plasmas opens up an opportunity for simultaneous measurements of plasma density and magnetic field. By analyzing the difference in the Raman shifts, it is possible to extract information about both the plasma density and the magnetic field strength. To measure the plasma density and magnetic field simultaneously, one can utilize the differential Raman shift between forward and backward scattering as a diagnostic tool. By precisely measuring the Raman shifts in both directions and accounting for the known relationship between the shift asymmetry and the plasma parameters, it becomes possible to extract quantitative information about the plasma density and the magnetic field strength.

The shift amounts of forward scattering and backward scattering in a plasma can exhibit different behaviors. In some cases, the shift amounts of the two scattering processes are equal, implying that the spectral shifts observed in both forward and backward directions are symmetrical. This symmetry can

13
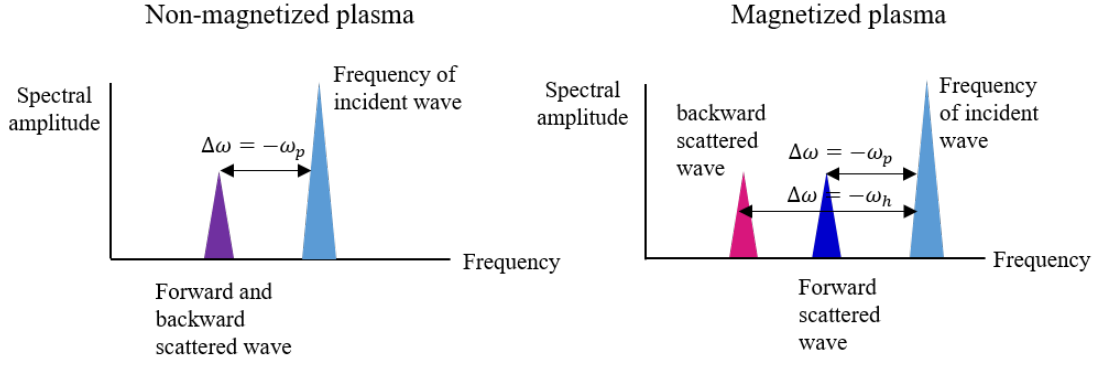
Figure 5: Spectrum of forward and backward scattering

provide valuable information about the plasma properties, such as density and magnetic field, without the need for additional measurements. However, it is also possible for the shift amounts of forward scattering and backward scattering to be different. In such scenarios, the spectral shifts observed in the forward and backward directions do not exhibit symmetrical behavior. This discrepancy can arise due to various factors, including the influence of magnetic fields or plasma density gradients.

Remarkably the differences in forward and backward scattering shift values may be utilized to determine plasma density and magnetic field at the same time. By carefully observing spectrum changes and comparing them to theoretical models or known plasma characteristics, it is possible to obtain information regarding plasma density and magnetic field strength. A valuable diagnostic technique is the simultaneous measurement of plasma density and magnetic field in a magnetized plasma using different shift amounts.

1.4 Growth Rate of SRS in Magnetized Plasma

Irradiating plasma with a short, linearly polarized laser pulse propagating in the x direction with an electric field of $E_0 = E_0(x,t)\cos(k_0 x - \omega_0 t)$, where the external magnetic field is in the x direction parallel to the laser pulse magnetic field. Ions are treated as a stationary background due to their much higher frequency compared to electrons. The growth rate of the RBS and RFS modes can be determined through a detailed analysis of the dispersion relation and the coupling between the interacting waves. The dispersion relation describes the relationship between the wave frequency and wave number for a given wave mode. In the presence of wave mixing, the dispersion relation is modified due to the interaction between the waves. To obtain the specific expressions for the growth rates of the RBS and RFS modes, a detailed analysis of the dispersion relation and the wave coupling equations is required. The growth rates are determined by solving the relevant equations, taking into account the specific parameters and conditions of the plasma and the laser pulse. With the three wave mixing which is described in the
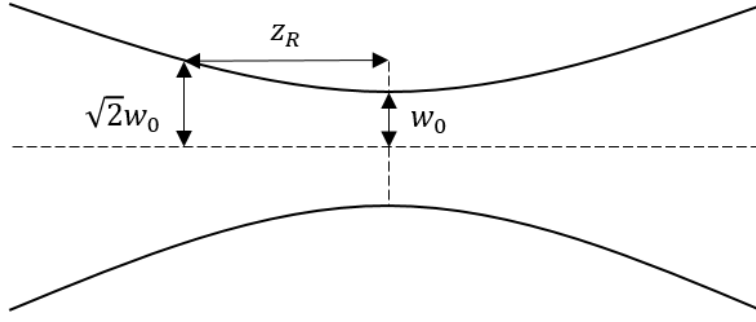
Figure 6: Gaussian beam width

parametric instability session, growth rate of RBS [49] and RFS [50] can be obtained:

$$\gamma_b = \frac{a(x)\omega_0}{2}\sqrt{\frac{\omega_p^2}{\omega_0\omega_h}},$$

$$\gamma_f = \sqrt{K_\pm^2 a(x)^2 - (\Delta\omega)^2},$$

(45)

where $a(x)$ is a vector potential of the pump pulse that has been normalized and its transverse variation follows a Gaussian beam. The intensity distribution of a Gaussian beam follows a Gaussian function in both the transverse (perpendicular to the beam propagation direction) and longitudinal directions. In the transverse direction, the intensity of the beam is highest at the center and decreases gradually towards the edges, forming a symmetric bell-shaped curve. In the longitudinal direction, the intensity also follows a Gaussian distribution, with the maximum intensity typically located at the beam waist, and the intensity decreasing as the beam propagates away from the waist. The shape and properties of a Gaussian beam are determined by several parameters. The key parameters include the beam waist, which represents the region of minimum beam size and maximum intensity, and the beam divergence, which describes how rapidly the beam spreads out as it propagates. The beam waist and divergence are related to the beam's wavelength and the characteristics of the laser resonator. x is the position relative to the focal point. Amplitude of laser pulse is approximately constant within the Rayleigh length $Z_R = \frac{\pi r_0^2}{\lambda}$,

$$a(x) = \frac{a_0}{\sqrt{1 + \frac{x^2}{Z_R^2}}}$$

(46)

where a_0 is the pump pulse's amplitude at the focal, r_0 the spot radius, λ the laser wavelength. The Stokes and anti-Stokes wave coupling coefficients, denoted as K_+ and K_- respectively, play a crucial role in understanding the phenomenon of stimulated Raman scattering (SRS) in a plasma. In SRS, when a high-intensity laser interacts with a plasma, energy is transferred between the incident laser wave, the plasma wave, and the scattered waves. The coupling coefficients K_+ and K_- quantify the strength of this energy transfer process. The coupling coefficients depend on various factors, including the plasma parameters, the laser intensity, and the wave frequencies involved. In particular, they are influenced by the nonlinear nature of the plasma response to the incident laser field. As the laser intensity increases, the nonlinear effects become more pronounced, leading to enhanced energy transfer and a stronger coupling
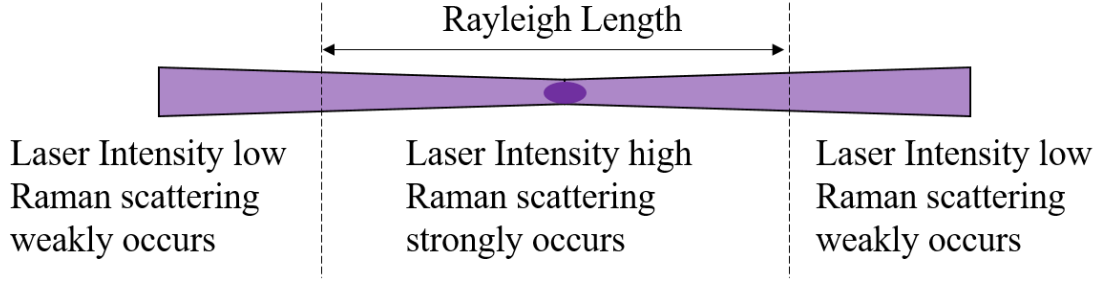
Figure 7: Laser intensity of Gaussian beam induces inhomogenous Raman growing

between the waves. The intensity-dependent frequency shift is another important characteristic of SRS. It refers to the change in frequency experienced by the scattered waves compared to the incident laser wave. This frequency shift is determined by the energy transfer process and is typically proportional to the intensity of the incident laser.

$$K_{\pm} = \frac{e}{2m_e} \sqrt{\frac{\omega_p u_0 u_{\pm}}{2\varepsilon_0 \omega_0 \omega_{\pm}}} \left| \frac{k_0 \omega_{\pm}}{\omega_{\pm} - \omega_c} - \frac{k_{\pm}\omega_0}{\omega_0 - \omega_c} \right| \tag{47}$$

and $\Delta\omega$ is described by

$$\Delta\omega = \frac{K_+^2 a_0^2}{2\delta_+}, \tag{48}$$

$$u_{\pm} = \left(1 + \frac{\omega_c \omega_p^2}{2\omega_{\pm}(\omega_{\pm} - \omega_c)^2} \right)^{-1},$$

$$d_{\pm}(k_{\pm}, \omega_{\pm}) = 1 - \frac{k_{\pm}^2 c^2}{\omega_{\pm}^2} - \frac{\omega_p^2}{\omega_{\pm}^2} \left(1 - \frac{\omega_c}{\omega_{\pm}} \right)^{-1} \tag{49}$$

The subscripts $-$, 0, and $+$ are utilized to represent the Stokes, pump, and anti-Stokes waves, respectively. Group velocity is normalized by speed of light. The velocities of scattered waves are denoted by $u_{\pm}$, pump pulse's is marked by subscript 0. Dispersion function of the stokes and anti-stokes are $d_{\pm}(k_{\pm}, \omega_{\pm})$. In this work, I investigate the cumulative spectra of Raman scattered signals originating from in-homogeneous plasmas characterized by non-uniform density and a magnetic field.

1.5 Laser focusing effect

The growth rate of Raman waves exhibits a direct proportionality to the amplitude of the interacting laser. This means that a stronger interacting laser can lead to more efficient generation and amplification of Raman waves within the plasma medium.

Gaussian beam focusing refers to the phenomenon of concentrating the energy and intensity of a Gaussian-shaped laser beam to a small spot or region. A Gaussian beam is characterized by its bell-shaped intensity profile, where the beam is most intense at its center and gradually decreases towards the edges. The focusing of a Gaussian beam leads to an increased peak intensity at the focal point.

The intensity enhancement is a result of the beam's energy being concentrated into a smaller area. The beam's power remains conserved, but the smaller spot size leads to a higher power density, resulting in a higher intensity.
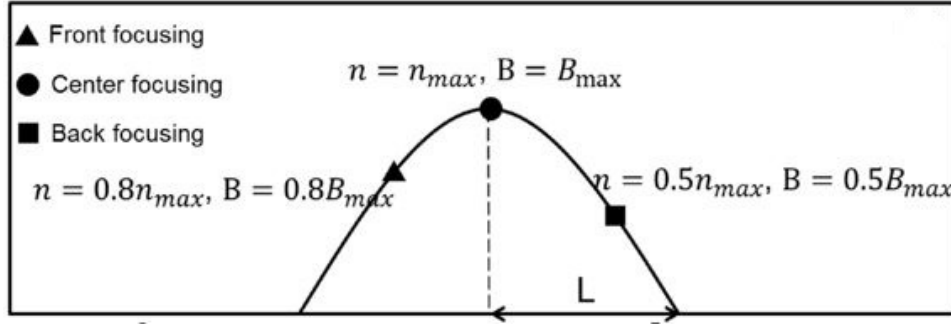
Figure 8: Plasma density and magnetic field profile. Focal points are depicted at the three points.

A tightly focused laser beam enhances the intensity in the focal region, leading to a more pronounced Raman scattering response. In contrast, a less-focused region may produce non-growing Raman signals that are faint and generally insignificant. The targeted area dominates the contribution of Raman signals to the total spectrum.

1.6 Plasma density and magnetic field variation

The parabolic density profile has been used in a number of laser plasma applications, and it is easily created experimentally utilizing a powerful laser and a gas jet. A parabolic plasma density channel is utilized for electron self-injection and acceleration [51]. These profiles, with a total length of 1600 Z_R (where Z_R represents the Rayleigh length), capture the essential characteristics of the plasma under investigation. The magnetic field profile is also parabolic, which is unnatural, but my goal is to demonstrate that the laser focusing effect works.

To investigate laser focusing effect, the power spectrum are analytically calculated for both forward-scattered (RFS) and backward-scattered (RBS) signals at three distinct focal points. Three distinct focal positions are the front, center, and back focal points. Gaussian beam is adopted. Its pulse duration, denoted as $\tau_{eff}\omega_M$, takes on values of 9 and 15 for the different cases considered.

For the short pulse cases, the spectral shape is relatively broad, which makes it challenging to precisely identify the exact positions of the frequency shifts corresponding to the plasma (RFS) or upper hybrid (RBS) frequencies at the three focal points. Due to the broadening effect, the position of the peak is unclear, making precise determination difficult. Consequently, the determination of plasma density and magnetic fields becomes more challenging in these cases. However, in the long pulse case, the spectral shape becomes more sharp, enabling us to accurately determine their position.

When pump pulse interact with plasma, scattered wave is growing according to the equation.

$$\frac{dA_b}{dt} = \gamma_b A_b \tag{50}$$

The pulse duration determines the effective interaction time; within that period, the laser amplitude is sufficient to induce Raman scattering.

$$A_b = A_0 e^{\gamma_b \tau_{\text{eff}}} \tag{51}$$

17

where A_b, A_0, γ, and τ_{eff} are the amplitude of the backward scattered signal, initial value from which the backscattering grows (usually a noise level), growth rates of RBS and effective duration of the growing defined by the pump pulse duration.

In the absence of damping, the RFS signal must travel a sufficient distance, generally Rayleigh length, through a uniform, cold, and collisionless plasma. The frequency of the RFS, however, varies as the pump pulse propagates through the non-uniform plasma. If the Rayleigh length is comparable to the characteristic length and the plasma and magnetic fields do not change much, the RFS signal may have the same form as the RBS with L_{eff} corresponding to the characteristic length.

$$A_f = A_0 e^{\gamma_f L_{eff}/c}, \tag{52}$$

To analyze the scattered wave and extract useful information, we employed the Fourier Transform technique on the accumulated scattered wave signals that had grown during the effective interaction time. The accumulated scattered wave signals encompassed the entire interaction duration, capturing the complete spectral information of the scattered waves. The FT output displayed peaks at specific frequencies, representing the spectral amplitudes at shifted frequencies. By comparing the observed peak positions with theoretical predictions, we were able to extract information about the plasma density and magnetic fields. Fourier Transformed form of scattered wave induced by Gaussian beam is

$$A_0(x) e^{\gamma_{b,f} L_{eff}/c - \frac{\tau_{eff}^2}{4}[\omega - \omega_M]^2}, \tag{53}$$

where ω_M is the Raman shifted frequency of forward and backward scatterings generated in the focused region.
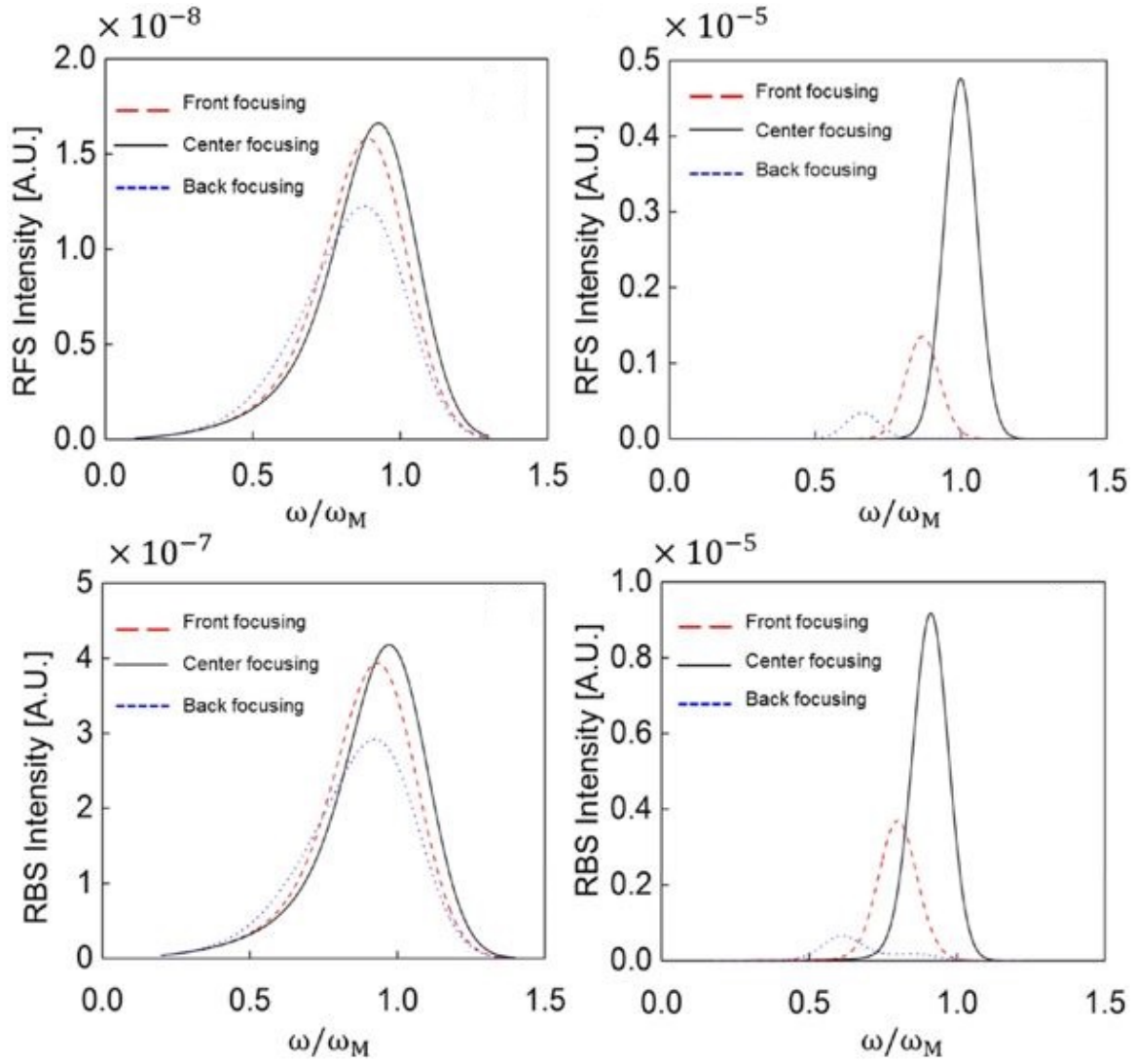
Figure 9: Graphs are separated into the right and left sides by the parameters; effective pulse duration $\tau_{eff}\omega_M = 9$ and $\tau_{eff}\omega_M = 15$.

1.7 Spectral bandwidth of integrated signals of scattered waves

To accurately assess the relationship between the spectral peak shift and the focal location of the pump pulse, I performed numerical calculations to obtain the cumulative spectra. This process involved considering dispersed waves emanating from every point within the plasma medium as wavelets. Each wavelet had an effective duration, τ_{eff}, which matched the duration of the pump pulse. By treating the dispersed waves as wavelets, I aimed to capture the full spectral information and understand how it varied with changes in the focal location of the pump pulse.

To achieve this, I applied Fourier analysis to each wavelet, transforming them into the frequency domain. This allowed me to obtain the spectral representation of the dispersed waves at different locations within the plasma. The numerical calculations provided valuable insights into the behavior of the spectral peak shift as a function of the pump pulse's focal position. By comparing the cumulative spectra obtained from different focal locations, I could observe how the peak positions shifted and identify any corresponding changes in the plasma density or magnetic fields. Figure 10 provides a schematic representation of the approach used for these numerical calculations. It illustrates the wavelets emitted from various points within the plasma and their subsequent transformation through Fourier analysis. This visualization helps to convey the concept of capturing the dispersed waves' spectral information and examining how it relates to the focal location of the pump pulse.

In the context of laser-plasma interactions, the laser pulses used are typically monochromatic, meaning they have a single, well-defined frequency. The magnetic field in the plasma is assumed to be constant, providing a stable environment for the interaction to occur. On the other hand, the plasma density exhibits a small gradient, with a characteristic length comparable to the duration of the laser pulse. Under these conditions, the growth rate of the scattered light, such as in Raman scattering, follows the envelope of the laser pulse. This means that the intensity profile of the laser pulse determines the growth of the scattered wavelets.

In particular, the scattered wavelets experience a growth that is influenced by the shape of the laser pulse. For instance, if the laser pulse has a Gaussian-shaped intensity profile, the scattered wavelets will also exhibit a similar Gaussian growth pattern. This is because the Gaussian-shaped laser pulse serves as the driving force for the scattering process, and the scattered wavelets "inherit" the characteristics of the laser pulse. The growth of these wavelets is directly related to the intensity profile of the laser pulse, with the maximum growth occurring where the laser intensity is highest.

It is important to note that the growth of the scattered wavelets follows the envelope of the laser pulse, rather than the instantaneous intensity. This means that the growth rate is determined by the overall shape of the laser pulse, rather than instantaneous fluctuations in intensity.

$$A_b = A_0 e^{\gamma_b \tau_{eff}} e^{-(t-t_0)^2/(\tau_{eff}^2)} e^{-i\omega_b(t-t_0)} \tag{54}$$

RBS, as well as

$$A_f = A_0 e^{\gamma_f L_{eff}/c} e^{-(t-t_0)^2/\tau_{eff}^2} e^{-i\omega_f(t-t_0)} \tag{55}$$

The cumulative scattered signal from the plasma for the forward scattered (RFS) component can
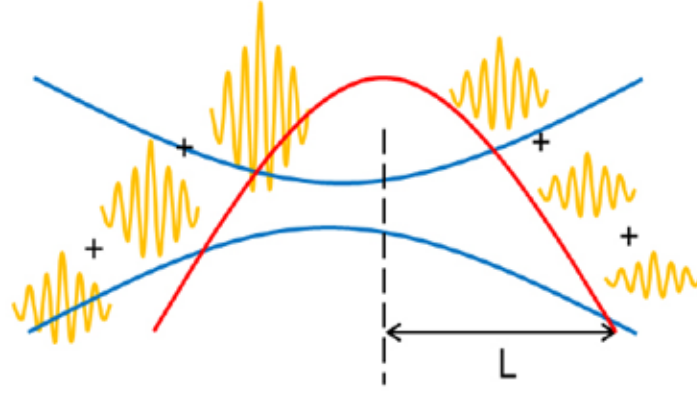
Figure 10: Schematic representation of cumulative wavelet, Amplitude of wavelet generated from the focused spot is highest.

be expressed as the integral of the product of the scattered wave amplitude $A_{b,f}$ and the differential distance dx along the plasma length. This integral represents the accumulation of the scattered signal as the laser pulse interacts with the plasma. Mathematically, it can be written as: $\int_{x_i}^{x_f} A_{b,f} dx$ Here, x_i and x_f represent the starting and ending coordinates of the plasma, respectively. The integral encompasses the entire plasma region of interest. When this is Fourier transformed in terms of time, the result is

$$I_{b,f}(\omega) = \left| \int_{x_i}^{x_f} dx, A_0 e^{\gamma_{b,f} L_{eff}/c - (\tau_{eff}^2)/4[\omega - \omega_{b,f}(x)]^2} \right|^2 \tag{56}$$

where $L_{eff} \to c\tau_{eff}$ for RBS.

To ensure that the peak shift in the integrated power spectrum is distinguishable, it is important to consider the relationship between the maximum shift and the bandwidth of the spectrum. The maximum shift, denoted as $\omega_h(x)$ for RBS or $\omega_p(x)$ for RFS, represents the maximum frequency change experienced by the scattered waves due to the plasma density or magnetic field variations. In order for this peak shift to be identifiable in the spectrum, it should be larger than the bandwidth of the spectrum itself. The bandwidth is determined by various factors such as the pulse duration, the spectral characteristics of the laser pulse, and the scattering process. The effectiveness of identifying the peak shift also depends on the focal location of the pump pulse. If the pump pulse is focused precisely on the peak density (and magnetic field) of the plasma, and the scattering predominantly occurs within the Rayleigh length of the focused spot, then the integrated signals can be approximated as follows.

The integral equation can be simplified by stretching the integrand up to $O(x^2)$ as

$$e^{\gamma_{(b,f)} L_{eff}/c - (\tau_{eff}^2)/4[\omega - \omega_{(b,f)}(x)]^2} \approx e^{\gamma_m L_{eff}/c - (\tau_{eff}^2)/4[\omega - \omega_M(x)]^2} \times \left[1 + \left[\frac{\gamma_m'' L_{eff}}{2c} + (\tau_{eff}^2)/4(\omega - \omega_M) \right] \omega_M'' x^2 \right] \tag{57}$$

where the subscript m of γ and ω indicate that they are evaluated at the point where ω_h (RBS) or ω_p (RFS) reaches its maximum. As a result, $\omega_M' = \gamma_m' = 0$. I obtain by integrating from $-Z_R$ to Z_R using the estimated integrand and setting the focal is located at the center. The Rayleigh range is used because

21

scattering is primarily dominant across that range.

$$I_{b,f}(\omega) \simeq 4A_0^2 e^{2\frac{\gamma_m L_{\text{eff}}}{c} - \frac{\tau_{\text{eff}}^2}{2}[\omega - \omega_M]^2} Z_R^2 \left[1 + B(\Delta\omega) Z_R^2\right]^2 \tag{58}$$

with $\Delta\omega = \omega - \omega_M$ and $B(\Delta\omega) = \frac{\gamma_m'' L_{\text{eff}}}{6c} + \frac{\tau_{\text{eff}}^2 \Delta\omega \omega_M''}{12}$. Full-width half-maximum (FWHM) is commonly used spectral deviation for the spectroscopy. To calculate FWHM, I construct the equation

$$1/2 = e^{-(\tau_{eff}^2)/2\Delta\omega^2 [1 + B(\Delta\omega)Z_R^2]^2} \tag{59}$$

from which I obtain

$$-\ln 2 \approx -\frac{\tau_{eff}^2}{4}\Delta\omega^2 + B(\Delta\omega)Z_R^2 \tag{60}$$

Since $B(\Delta\omega)$ is a linear function of $\Delta\omega$, the final form of the equation is a straightforward quadratic. The spectral peak's FWHM is the difference between the two roots of the equation.

$$\Delta\omega_{\text{FWHM}} \approx \frac{4}{\tau_{\text{eff}}} \sqrt{\ln\sqrt{2} + \frac{\gamma_m'' L_{\text{eff}}}{6c} Z_R^2 + \frac{\tau_{\text{eff}}^2 \omega_M''^2}{144} Z_R^4}$$

When the plasma scale length is greater than the Rayleigh length, i.e. $\omega_M'' Z_R^2 \sim \gamma_m'' Z_R^2 \ll 1, \Delta\omega_{FWHM} \approx \frac{4\sqrt{\ln(\sqrt{2})}}{\tau_{eff}}$. To be able to discern the spectral peak position,

$$2.4/\tau_{eff} < \omega_M$$

The detection of the Raman instability and the subsequent scattered light outside the plasma require a sufficient growth of the instability, which typically takes a few plasma oscillations. While the growth rate is indeed an important factor for the Raman instability, the observed spectrum of the scattered signals, as evidenced by the integrated signals, is primarily influenced by the pulse duration rather than the growth rates.

In Fig.11, the numerical computation of the Fourier-transformed amplitude for RBS and RFS is presented. This computation is dependent on the effective duration of the pump pulse, denoted as τ_{eff}, and is performed when the pump pulse is concentrated on the location that yields the highest frequency shift, represented by ω_M. The figure illustrates how the spectrum of the scattered signals varies with different pulse durations. It shows that the shape and characteristics of the spectrum are more prominently influenced by the pulse duration rather than the specific growth rates of the Raman instability.

The pulse duration, τ_{eff}, determines the effective interaction time between the laser and the plasma, and therefore plays a crucial role in shaping the resulting spectrum. By carefully selecting the pulse duration and optimizing the interaction conditions, it is possible to manipulate the spectral characteristics of the scattered signals and enhance the detectability of the Raman instability. This enables the extraction of valuable information about the plasma properties, such as the density and magnetic field distributions, through spectral analysis.

The relationship between the effective pulse duration, τ_{eff}, and the bandwidth of the cumulative scattered wave is inversely proportional. As depicted in Fig.12, it is evident that as the effective pulse duration, $\tau_{eff}\omega_M$, increases, the bandwidth of the scattered wave decreases. Specifically, when $\tau_{eff}\omega_M$ exceeds a value of 15, the bandwidth becomes less than 20% of the maximum peak shift.
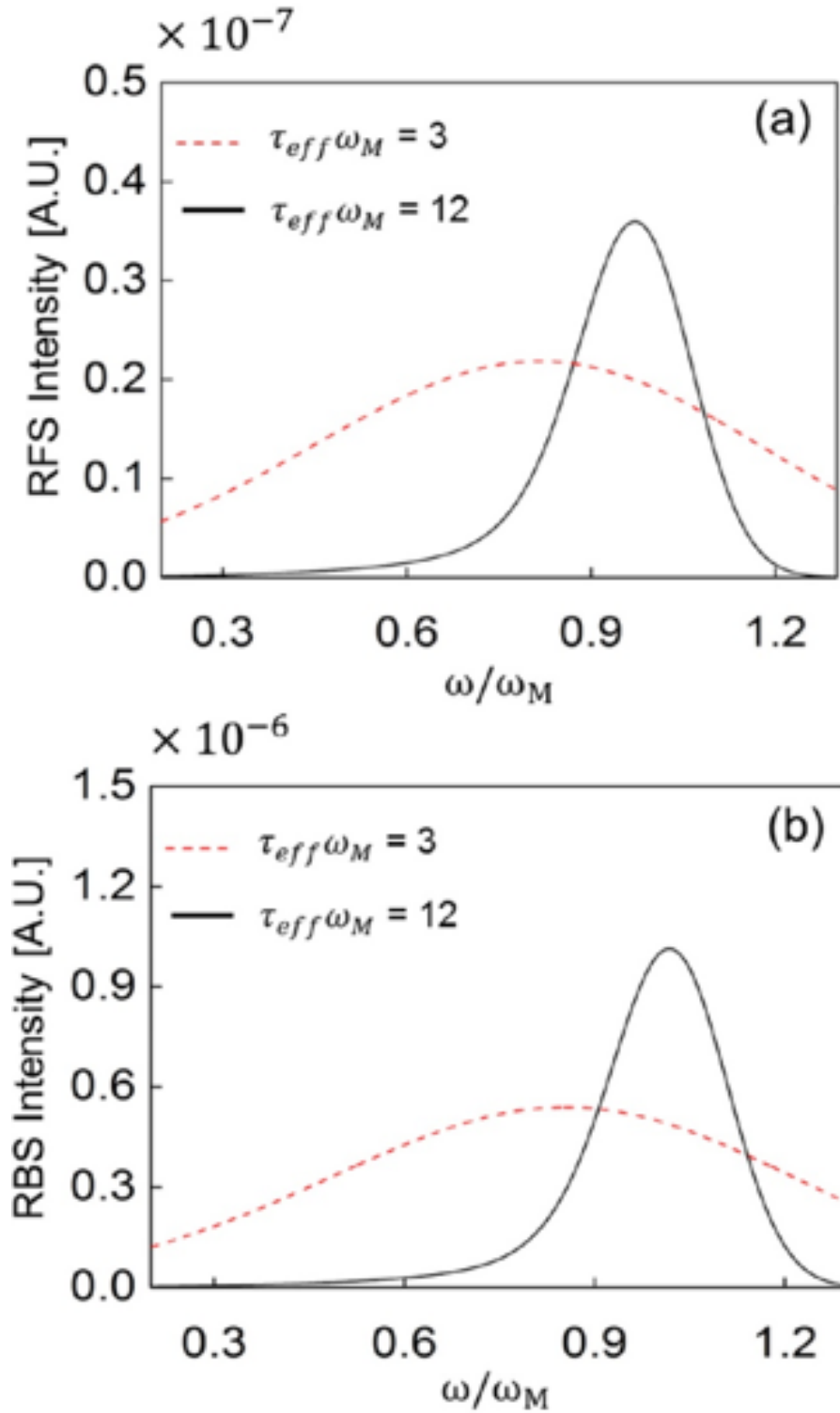
Figure 11: (a) Amplitude of RFS and (b) amplitude of RBS are plotted against the normalized frequency of the scattered wave, which is shifted by the maximum frequency at the focal point of the pump pulse with varying effective durations.
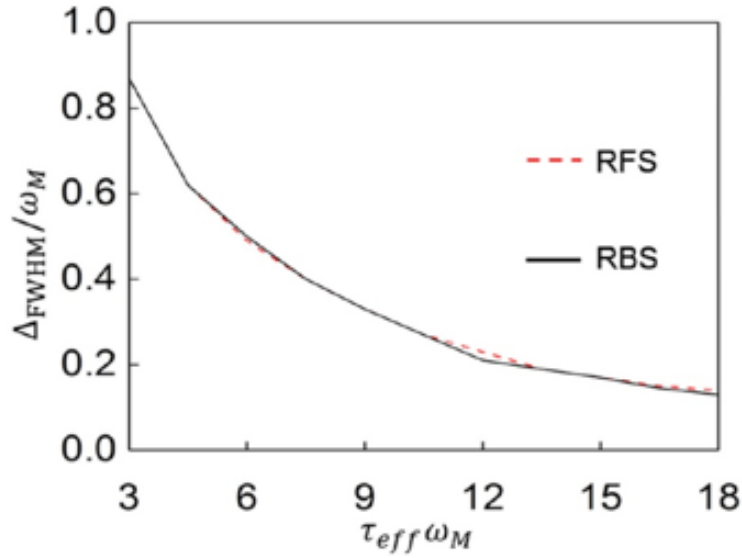
Figure 12: Bandwidth of the integrated signals of scattered waves vs effective pulse duration.

This observation is of significant importance in terms of achieving spectral accuracy in the diagnostic method based on Raman scattering. A narrower bandwidth allows for a more precise determination of the spectral peak shift, which in turn provides a more accurate measurement of the plasma properties. The advantage of longer pulses, characterized by a higher effective pulse duration, lies in their ability to reduce the bandwidth of the scattered wave. By extending the interaction time between the laser and the plasma, longer pulses facilitate the growth of the Raman instability and allow for a more precise capture of the exact values of the spectral peaks.

Therefore, when aiming for spectral accuracy and precise measurement of plasma parameters, it is beneficial to utilize longer pulses with higher effective pulse duration. This choice ensures a reduced bandwidth, resulting in a narrower spectral distribution that allows for a more reliable determination of the peak shifts and, subsequently, the plasma properties of interest.

1.8 Simulation results

After obtaining analytical results from the theoretical framework, it was discovered that Raman scattering can be employed as a diagnostic method to determine plasma density and magnetic field parameters. To validate the feasibility of this diagnostic approach, numerical simulations were conducted. For these simulations, a particle-in-cell (PIC) code was employed, coupled with a numerical dispersion-free along the x-direction (NDFX) field solver scheme [52].

The utilization of the NDFX scheme in modeling stimulated Raman scattering offers several advantages. Firstly, it eliminates the need for absorption boundaries, ensuring that the simulation accurately captures the dynamics of the scattering process without any artificial limitations. Additionally, the NDFX scheme has a null reflection rate, minimizing any unwanted reflections that could interfere with the accurate assessment of the scattered waves. Another notable advantage of the NDFX scheme is its ability to

Inhomogeneous magnetic fields
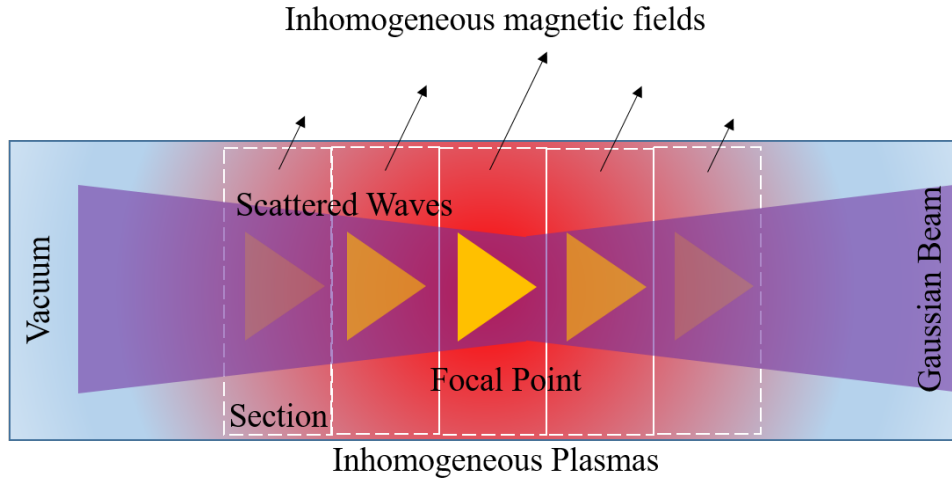
Figure 13: The SRS simulation model comprises of five sections. The laser pulse parameters for each section are determined using the Gaussian beam formula, which sets the section size to cover the pulse adequately. The scattered waves are represented by yellow triangles whose opacity corresponds to the intensity of scattered waves. Constant magnetic fields are present in each section, but there are variations along the sections.

separate the left- and right-going parts of the field, facilitating the monitoring of the backward scattered waves. This feature enhances the diagnostic capabilities and enables a comprehensive analysis of the scattering phenomenon in the simulated plasma system.

While an ideal approach would involve modeling the entire system, the computational demands associated with such simulations often impose limitations. To overcome these challenges, separated simulations were conducted to simulate jointed sections strategically positioned around the focal points of interest, taking into account the presence of inhomogeneous plasmas and magnetic fields. By selecting specific regions of interest, the simulations could capture the essential dynamics and interactions within those areas. Additionally, to facilitate a comprehensive analysis of the signal strength across different locations, certain sections were deliberately placed away from the focal point. This enabled a comparative study of the signal properties and their variations in different regions of the plasma.

The size of each section was carefully determined to be five times the pulse length corresponding to the Rayleigh length, ensuring that an adequate spatial extent was considered to capture the relevant phenomena and minimize any edge effects. This advantageous feature enables the reliable detection and analysis of the Raman scattered signals, there is no significant difference observed between launching new laser pulses in each discrete section or launching a single laser pulse across the entire simulated domain.

It is worth noting that the chosen modeling approach strikes a balance between computational feasibility and capturing the essential dynamics of the system. While some simplifications and approximations are made to accommodate computational limitations, the approach remains effective in providing meaningful results and a realistic representation of the phenomena under investigation.

In the virtual experimental setup, a CO_2 laser pulse was employed, featuring a focused spot size of 100 μm and a pulse duration of 10 ps. The parameter a_0 was determined to be 0.2, which characterizes the laser's peak normalized vector potential. Utilizing these specific parameters, important quantities such as $\tau\omega_0 \approx 1000$ ($\tau\omega_M = 30$) and $Z_R = 3.14$ mm were calculated. The value of $\tau\omega_0$ denotes the laser pulse length in units of the laser's characteristic period, providing an indication of the pulse's duration relative to its oscillation time.

In this case, the calculated value of $\tau\omega_0 \approx 1000$ suggests that the laser pulse is significantly longer than one oscillation cycle. Similarly, $\tau\omega_M$ characterizes the pulse length in relation to the plasma's characteristic period. With a value of 30, it implies that the laser pulse duration is comparable to or slightly shorter than the plasma's oscillation time, indicating a potential for strong interactions between the laser and the plasma. The parameter Z_R represents the Rayleigh range, which is a measure of the distance over which the laser beam remains approximately focused. The calculated value of $Z_R = 3.14$ mm indicates that the laser beam retains a relatively tight focus within this range. The maximum plasma density employed in the experiment is 10^{16} cm^{-3}. This density corresponds to a frequency ratio of $\omega_p/\omega_0 \approx 0.3$, where ω_p represents the plasma frequency. The chosen plasma density ensures that the plasma effects are significant and play a crucial role in the interaction with the laser.

The choice of a CO_2 laser pulse for stimulated Raman scattering (SRS) in low-density and small-length plasmas is driven by its wavelength characteristics and interaction properties. The wavelength of the CO_2 laser is well-matched to the plasma wavelength in such conditions, allowing for efficient energy exchange and growth of scattered waves. This makes it a suitable candidate for probing and diagnosing these plasma systems. However, when considering the application of SRS to Tokamak plasmas, which are significantly larger in size, certain limitations arise.

Tokamaks typically exhibit much lower plasma densities compared to the smaller-scale plasmas where the CO_2 laser is effective. The plasma density in Tokamaks can drop by several orders of magnitude, posing challenges for the successful implementation of SRS. One crucial factor to consider is the maximum growing length achievable before encountering pump depletion. In the case of the CO_2 laser, the growing length is limited to the order of meters in Tokamak plasmas. This constraint significantly restricts the diagnostic capabilities of the CO_2 laser in such large-scale plasma systems.

As a result, alternative electromagnetic sources, such as terahertz pulses, may be more advantageous for diagnosing Tokamak-sized plasmas. Terahertz pulses offer shorter wavelengths and higher frequencies, enabling interactions with the larger plasma volumes and lower densities characteristic of Tokamaks. By employing terahertz pulses, it becomes possible to overcome the limitations associated with the use of the CO_2 laser and achieve more effective diagnostics in Tokamak plasma environments.

To obtain time-varying signals and investigate different cases, virtual probes were strategically placed on the left side of the simulation domain. These probes recorded the accumulated scattered waves, allowing for the analysis of their characteristics.

The simulations were performed for multiple sections, and in each section, various parameters and conditions were considered. To analyze the recorded signals, the Fast Fourier Transform (FFT) technique was applied. This mathematical algorithm converts the time-domain signals into the frequency

domain, providing valuable spectral information. By performing FFT on the data stored in the probes, the spectrum of the stimulated Raman scattering (SRS) could be obtained. A comparison was then made between the theoretical spectral shift and the maximum peak position in the obtained spectrum.

This comparison served as a means to identify and extract information about the plasma density and magnetic field. By analyzing the spectral shift and its correlation with the known theoretical values, it was possible to infer the properties of the plasma medium, such as its density and the strength of the magnetic field.

This approach of comparing the theoretical spectral shift and maximum peak position served as a diagnostic method for extracting plasma parameters from the SRS spectrum. By accurately determining the plasma density and magnetic field information through this analysis, a deeper understanding of the plasma dynamics and characteristics could be achieved.

The inclusion of Raman backscattering (RBS) data in the analysis stems from the challenges associated with distinguishing Raman forward scattering (RFS) signals from amplified noise. This difficulty arises primarily due to the significantly slower growth rate of RFS compared to RBS. Additionally, the use of a high macro-particle-to-real-particle ratio in the simulations leads to higher plasma noise levels than what would typically be encountered in real plasma systems.

Consequently, detecting a discernible RFS signal requires certain adjustments and considerations. To improve the detectability of the RFS signal, it becomes necessary to allow the pump pulse to propagate through a more uniform and longer plasma region. By increasing the length of the plasma and achieving a more homogeneous distribution, the RFS signal can be enhanced.

Similarly, increasing the number of simulated particles, if feasible within the available computational resources, can also contribute to reducing the noise level and improving the detectability of the RFS signal. While these adjustments were feasible in the previous one-dimensional analysis, the computational limitations prevented their full realization in the two-dimensional simulations.

Nonetheless, despite these limitations, the effectiveness of local measurements performed using a focused pump pulse is still demonstrated well in the context of RBS scenarios. The RBS data obtained from the simulations provide valuable insights into the scattering processes and contribute to a better understanding of the overall dynamics of the plasma system under investigation.

By subjecting the on-axis signal from each segment to Fourier transformation and collating the results, I generated Figure 9, which displays the data obtained from three distinct focal positions. This approach allowed me to examine the spectral characteristics of the scattered waves at different locations along the focal axis.

The analysis involved measuring the spectral bandwidth using the full-width at half-maximum (FWHM) criterion, denoted as $\Delta\omega_{\mathrm{FWHM}}/\omega_M$, where ω_M represents the maximum frequency present in the spectrum. The measurements were performed at the front, center, and rear focal points of the simulation. The obtained values of $\Delta\omega_{\mathrm{FWHM}}/\omega_M$ were 0.2, 0.27, and 0.16 for the front, center, and rear focal points, respectively.

These values indicate that the spectral width of the scattered waves was relatively narrow across the different focal positions. The narrow spectral width is beneficial as it allows for the clear differentiation
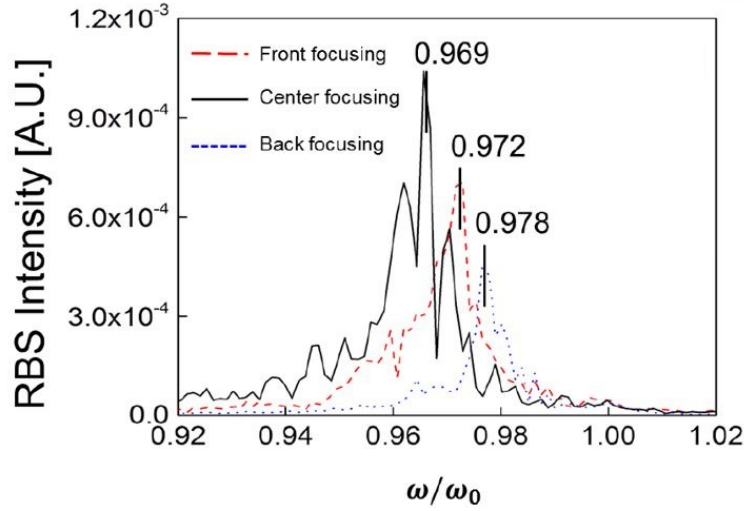
Figure 14: RBS intensity spectrum depending on the focus points. Frequencies difference between laser frequency and plasma frequency are depicted by the lines

of peak shifts across the focal positions. This characteristic is crucial for accurately identifying and analyzing the plasma density and magnetic field information contained within the spectral shifts.

The distinct values of $\Delta\omega_{\text{FWHM}}/\omega_M$ at different focal points indicate that the interaction between the laser pulse and the plasma medium varies across the focal axis, leading to observable differences in the scattered wave spectra. By examining the spectral width at different focal positions, we gain valuable insights into the spatial distribution of the plasma parameters. The variations in the spectral width can be attributed to the local plasma conditions, such as density gradients and magnetic field variations, that influence the growth of the scattered waves. Analyzing these variations and their relationship to the focal position provides valuable information for diagnosing and understanding the plasma properties.

The investigation of the Raman spectral peak shift in relation to the corresponding ω_h values, which are derived from the plasma density and magnetic field at each focal location, revealed a strong correlation. This correlation demonstrates the sensitivity of the scattered wave spectrum to the underlying plasma parameters and validates the diagnostic potential of stimulated Raman scattering (SRS). In order to explore the effects of a highly magnetized plasma, we conducted additional investigations with a magnetic field strength of $B = 50$ T, resulting in a cyclotron frequency-to-plasma frequency ratio of $\omega_c/\omega_p = 1.78$. This elevated magnetic field intensity is often encountered in scenarios involving the interaction of high-density lasers with plasmas. While the back-focusing scenario was not as prominent as in previous experiments, the observed peak shifts in the spectrum still exhibited alignment with the estimated values. Figure 15 visually presents the comparison between the measured peak shifts and the corresponding ω_h values in the highly magnetized plasma scenario.

The alignment of the observed peak shifts with the estimated values in the presence of a high magnetic field not only demonstrates the robustness and reliability of the diagnostic method based on Raman spectral analysis but also underscores the effectiveness of this technique in extracting valuable information about the plasma density and magnetic field. The presence of a high magnetic field introduces
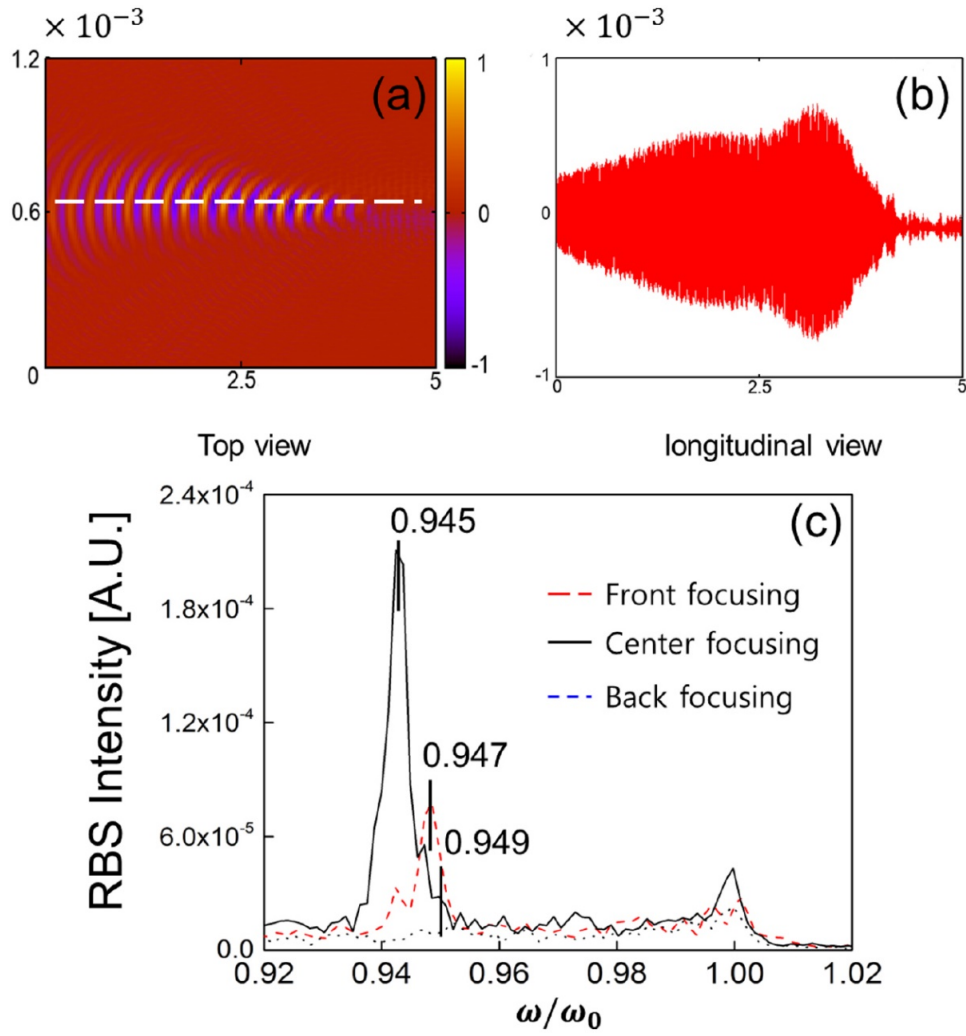
Figure 15: (a) Top view of the left going field, (b) longitudinal image of the left going field, and (c) RBS intensity spectrum. Vertical black lines represent the theoretical values of the shifted frequencies.

additional complexities to the plasma dynamics and wave interactions. The interplay between the magnetic field and the plasma particles can significantly affect the scattering processes and the behavior of the scattered waves. Despite these complexities, the diagnostic technique based on Raman spectral analysis remains effective in capturing and characterizing the underlying plasma parameters. The alignment between the observed peak shifts and the estimated values in the highly magnetized plasma scenario highlights the capability of the diagnostic method to accurately extract information about the plasma density and magnetic field. This alignment suggests that the Raman scattering process is influenced by the interplay between the laser pulse, the plasma, and the magnetic field, and it provides a reliable means of probing and studying these interactions. The ability to diagnose plasma density and magnetic field in the presence of a high magnetic field is of great significance in various research areas. For example, in fusion energy research, where high magnetic fields are used to confine and control the plasma, accurate knowledge of the plasma parameters is crucial for optimizing the performance and stability of fusion devices. Similarly, in astrophysics, where highly magnetized plasmas are prevalent in various astrophysical objects such as neutron stars and accretion disks, understanding the plasma properties is essential for unraveling the complex astrophysical phenomena.

In my simulations, I made the assumption of a cold plasma for simplicity. However, it is important to explore the possibility of a heated plasma and evaluate the impact of thermal noise on the scattered signals. In various plasma systems, such as tokamaks or high-density laser-plasma interactions, plasmas can reach temperatures in the range of hundreds of keV, which is well-documented in the field. When considering a heated plasma, it is necessary to assess the intensity of the thermal field and compare it to the scattered signals. In my case, for an assumed electron density of $n_e = 10^{16}$ cm^{-3}, the thermal field is expected to be much lower than GV m^{-1}. This is due to the relatively low thermal energy compared to the energy associated with the scattered waves. However, as observed in figures 14 and 15, the intensity of the scattered field is on the order of GV m^{-1}, indicating that Raman scattering, despite being a minor effect in the plasma, can generate signals that are strong enough compared to thermal noise. This highlights the sensitivity and selectivity of the Raman scattering diagnostic method in the presence of thermal effects. The ability of Raman scattering to produce detectable signals even in the presence of thermal noise is of significant importance. It allows for the extraction of valuable information about the plasma parameters, such as density and magnetic field, even in plasma systems with high temperatures. This demonstrates the robustness and reliability of the Raman scattering diagnostic technique, making it a promising tool for plasma diagnostics in various high-temperature plasma environments. It is worth noting that in realistic scenarios, additional noise sources, such as shot noise or electronic noise, may also be present. These noise sources should be carefully considered and their effects evaluated to ensure accurate interpretation of the scattered signals. However, the fact that the scattered signals can still be distinguished from the thermal noise suggests that the Raman scattering method has the potential to provide valuable diagnostic information even in the presence of various noise sources.

In addition to the investigations conducted in our simulations, we explored scenarios where the cyclotron frequency $\omega_c = \frac{eB}{m}$ is comparable to the plasma frequency ω_p. This situation can be realized in a wide range of plasma systems, including magnetically confined plasmas such as tokamaks. For example,

the KSTAR Tokamak, which operates at a core density of $26 \times 10^{16} \mathrm{cm}^{-3}$ and a magnetic field of 23T, exhibits a ratio of ω_c / ω_p of the order of unity. This demonstrates that the conditions for the interaction between the plasma and the magnetic field are comparable, and the effects of the magnetic field cannot be neglected. Similarly, in high-density laser-plasma interactions, where electron densities exceed $10^{18} \mathrm{cm}^{-3}$, a relativistic electron current can generate a large transient magnetic field. In such cases, the interplay between the plasma density and the magnetic field becomes significant, and the coupling between electromagnetic waves and plasma waves is influenced by the magnetic field dynamics. Considering these scenarios with comparable values of ω_c and ω_p, the analysis and diagnostic techniques based on Raman scattering provide valuable insights into the plasma behavior. By analyzing the spectral shifts and comparing them with the estimated values based on plasma density and magnetic field parameters, we can gain a deeper understanding of the plasma dynamics in magnetically confined plasmas and high-density laser-plasma interactions. The Rayleigh length is a fundamental parameter that plays a critical role in determining the focal spot size of a pump laser pulse. It represents the distance over which the beam diameter increases by a factor of $\sqrt{2}$ and is determined by the wavelength of the laser. For a typical laser wavelength of 1 μm, the Rayleigh length is usually on the order of a few microns to tens of microns. The small size of the focal spot is advantageous in many plasma applications, such as laser wakefield acceleration (LWFA) or laser-plasma radiation sources, where precise control and manipulation of the laser interaction with the plasma is crucial. The focused laser pulse can create strong electric and magnetic fields, initiate plasma waves, and drive various plasma phenomena.

In the context of this study, the proposed Raman forward scattering (RFS) diagnostic method is particularly well-suited for plasma diagnostics in different length scales. It can effectively diagnose plasmas ranging from a few centimeters to several centimeters in length, which are commonly encountered in LWFA experiments. This diagnostic method takes advantage of the interaction between the pump laser and the plasma to extract valuable information about the plasma parameters, including density and magnetic field. The compact size of the focal spot allows for precise localization of the diagnostic region within the plasma, enabling detailed characterization of plasma properties at specific locations. This is especially important in LWFA, where the plasma undergoes dynamic changes during the acceleration process. By utilizing the Raman diagnostic method, researchers can gain insights into the plasma behavior, track its evolution, and optimize the acceleration process. It relies on the scattering of the pump laser by plasma waves, without significantly altering the plasma dynamics. In conclusion, the proposed Raman diagnostic method based on the small focal spot size of the pump laser offers significant advantages for plasma diagnostics in various length scales. Its applicability to plasmas ranging from a few centimeters to several centimeters in length, such as those encountered in LWFA, makes it a versatile tool for in-depth plasma characterization. By leveraging the interaction between the pump laser and the plasma, researchers can obtain valuable insights into plasma properties, leading to improved understanding and optimization of plasma-based applications.

1.9   Conclusion

In my comprehensive research study [53], I embarked on a thorough investigation into the exciting potential of utilizing Raman scattering as an effective diagnostic tool for accurately measuring the local density and magnetic field of inhomogeneous plasmas. This research aimed to push the boundaries of plasma diagnostics and contribute to the development of advanced techniques for understanding and characterizing complex plasma systems. The focal point of my research was centered around the utilization of a focused laser pulse and its interaction with the inhomogeneous plasma. By carefully examining the Raman scattering phenomenon, I aimed to harness its unique capabilities in extracting valuable information about the plasma density and magnetic field. To achieve this, I employed a meticulous experimental setup that involved directing a precisely focused laser pulse onto the plasma sample of interest. By carefully analyzing the scattered light resulting from the interaction between the laser and the plasma, I sought to extract crucial insights into the local plasma properties. Throughout my research, I extensively investigated various aspects that play a pivotal role in the accuracy and reliability of the diagnostic method. This encompassed studying the effects of pulse duration, pulse amplitude, laser wavelength, and spot size on the spectral characteristics of the scattered light. By systematically varying these parameters, I aimed to identify optimal conditions that would yield the most precise and reliable measurements of the plasma density and magnetic field. Furthermore, I conducted in-depth theoretical analyses and numerical simulations to complement and validate the experimental findings. These computational investigations allowed for a more comprehensive understanding of the underlying physical mechanisms governing Raman scattering in inhomogeneous plasmas and provided valuable insights into the interplay between the laser pulse characteristics and the resulting spectral shifts. The results of my research, as presented in [53], demonstrated the feasibility and potential of utilizing Raman scattering as an effective diagnostic technique for determining the local density and magnetic field of inhomogeneous plasmas.

Through a meticulous theoretical estimation and analysis of the spectral bandwidth of the scattered signal, a noteworthy finding emerged in my research. It became evident that the duration of the pump pulse, a fundamental parameter in the experimental setup, played a pivotal role in determining the achievable bandwidth of the scattered signal. This particular aspect proved to be of paramount importance in accurately distinguishing between the different frequency shifts associated with various focal positions within the plasma. By carefully considering the interaction between the pump pulse and the plasma, I quantitatively assessed the relationship between the pulse duration and the resulting spectral bandwidth. Through theoretical calculations and simulations, I systematically varied the pulse duration while keeping other parameters constant, such as the pump pulse amplitude, laser wavelength, and spot size. This allowed me to isolate the impact of the pulse duration on the bandwidth of the scattered signal. The results of my analysis demonstrated a clear inverse relationship between the pulse duration and the spectral bandwidth. As the pulse duration increased, the bandwidth of the scattered signal decreased, thus enabling a more accurate distinction between the different frequency shifts associated with different focal positions. This finding was particularly significant as it highlighted the importance of employing

longer pulse duration in order to achieve a narrower bandwidth and consequently enhance the precision of the diagnostic method. The narrower bandwidth obtained with longer pulse duration offered several advantages. Firstly, it allowed for a more precise determination of the exact frequency shifts corresponding to specific focal positions within the plasma. This enabled a more accurate characterization of the local plasma density and magnetic field. Secondly, the reduced spectral overlap between adjacent frequency components resulted in improved spectral resolution, facilitating a more detailed analysis of the scattered signal and enhancing the reliability of the diagnostic method.

The fundamental premise underlying the viability of my proposed approach lies in the requirement that the scale length of the plasma non-uniformity exceeds the Rayleigh length. Extensive theoretical analyses, coupled with Particle-in-Cell (PIC) simulations, have consistently demonstrated the remarkable alignment between the peak shift of the Raman spectrum and the corresponding values of ω_p or ω_h at the focal site. This remarkable convergence is achieved when the pulse duration of the pump laser matches the specific condition dictated by the system. The robustness and applicability of this diagnostic method extend across a wide range of plasma densities, encompassing diverse plasma regimes from magnetically restricted fusion to high-density laser-plasmas. This versatility opens up a myriad of potential applications in various fields, spanning fundamental plasma physics research to practical technological advancements. By leveraging the insights garnered from this research, we can embark on a transformative journey towards a deeper understanding of plasma physics and its intricate dynamics. The ability to simultaneously measure plasma density and magnetic fields in a non-intrusive manner holds immense promise for unraveling the complexities of plasma behavior and elucidating the underlying physical mechanisms governing plasma phenomena. In the realm of magnetically restricted fusion, where precise knowledge of plasma density and magnetic field distributions is of paramount importance, this diagnostic technique offers a valuable tool for in-depth plasma characterization and optimization of fusion confinement devices. The ability to accurately determine the spatial distribution of plasma density and magnetic fields within the fusion plasma enables scientists and engineers to fine-tune experimental parameters and design more efficient and stable fusion devices. Furthermore, in the context of high-density laser-plasma interactions, where ultra-intense lasers are employed to generate extreme plasma conditions, the proposed approach presents an invaluable means of diagnosing and understanding the complex interplay between laser and plasma dynamics. By obtaining precise measurements of plasma density and magnetic fields at various focal positions, researchers can gain critical insights into the intricate processes underlying laser-plasma interactions. This, in turn, can pave the way for advancements in laser-driven particle acceleration, plasma-based radiation sources, and other cutting-edge applications. In conclusion, my research, which culminated in the development of a diagnostic method based on Raman scattering, holds immense promise for a wide range of plasma systems. By accurately determining plasma density and magnetic fields simultaneously, we can transcend the boundaries of our current understanding and unlock new frontiers in plasma physics. The potential applications span diverse fields, from fusion energy research to laser-driven plasma physics, with the ultimate goal of advancing our scientific knowledge and fueling technological progress.
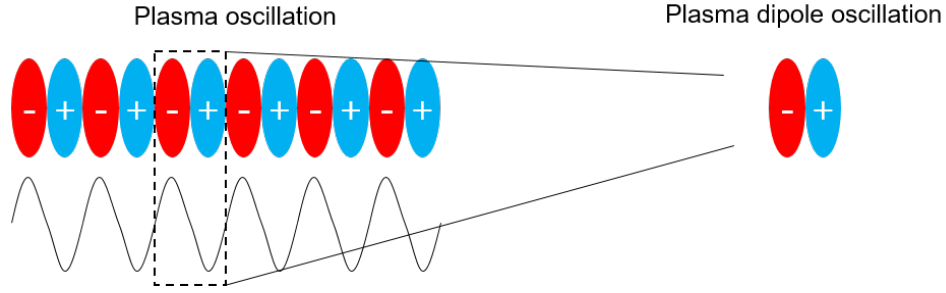
Figure 16: plasma oscillation (continuously distributed) vs plasma dipole oscillation (spatially local-ized).

II Plasma dipole oscillation

2.1 Introduction

Plasma oscillation, also known as plasma waves or collective modes, refers to the collective motion of charged particles in a plasma. A plasma is a state of matter consisting of a gas-like mixture of positively and negatively charged particles, such as ions and electrons. These charged particles interact with each other through electromagnetic forces, giving rise to collective behaviors that can be described by wave-like phenomena. Plasma oscillations occur when the charged particles in a plasma collectively respond to an external perturbation or disturbance.

The motion of the charged particles can be visualized as oscillations around their equilibrium posi-tions, similar to the way particles in a solid undergo vibrational motion. However, in a plasma, the col-lective nature of the motion leads to coherent oscillations that propagate through the plasma as waves. The fundamental plasma oscillation, known as the plasma frequency, is a characteristic frequency that depends on the plasma's properties, such as its density and the mass of the charged particles.

The plasma frequency can be derived from basic principles of plasma physics and is given by: $\omega_p = \sqrt{\frac{n_e e^2}{m_e \varepsilon_0}}$ where ω_p is the plasma frequency, n_e is the electron density, e is the elementary charge, m_e is the electron mass, and ε_0 is the vacuum permittivity. When an external perturbation, such as an electromagnetic wave or an electric field, interacts with a plasma, it can excite plasma oscillations. The plasma oscillations manifest as waves propagating through the plasma, carrying energy and momentum. The properties of these waves, such as their frequency, and propagation speed, are determined by the characteristics of the plasma, including its density, temperature, and magnetic field.

Plasma oscillations in laser plasmas are of particular interest in the field of laser-plasma interactions. When an intense laser pulse interacts with a plasma, it can drive strong oscillations of the plasma's charged particles. These oscillations are known as laser-induced plasma oscillations or laser-driven plasma waves. During the interaction, the laser pulse exerts a strong electric field on the plasma electrons, causing them to be displaced from their equilibrium positions. This displacement leads to a restoration force that pulls the electrons back towards their equilibrium, resulting in collective oscillatory motion.

The wake field in laser plasma refers to the phenomenon where an intense laser pulse propagating

through a plasma creates a trailing wake of electromagnetic fields and accelerated charged particles. This wake field is generated due to the interaction between the laser pulse and the plasma, leading to the transfer of energy from the laser to the plasma. When a high-intensity laser pulse enters a plasma, it ionizes the atoms or molecules, creating a plasma medium consisting of free electrons and positively charged ions.

The laser pulse exerts a strong electromagnetic force on the free electrons, causing them to be displaced from their equilibrium positions. As the laser pulse passes through the plasma, it pushes the free electrons forward, creating a region of depleted electron density behind the laser pulse and a region of enhanced electron density in front of it. This variation in electron density sets up a strong electric field, known as the wake field, which trails behind the laser pulse. The wake field can be thought of as a wake generated by a boat moving through water, where the boat displaces the water and creates a trailing wave.

Similarly, the laser pulse displaces the plasma electrons and creates a trailing electric field. The wake field has several important characteristics. Firstly, it can be highly nonlinear, with the electric field amplitude reaching orders of magnitude higher than the electric field of the incident laser pulse. This provides an opportunity to accelerate charged particles, such as electrons or ions, to high energies within the wake field. Secondly, the wake field can support plasma waves, such as electron plasma waves or ion acoustic waves, which can couple with the laser pulse and affect its propagation properties.

If electrons in a plasma deviate from a uniform distribution of ions, electric fields are generated to reestablish plasma neutrality by attracting the electrons back to their original positions [54]. However, due to their inertia, the electrons will oscillate at a high frequency, known as the plasma frequency, around their equilibrium positions. The massive ions are unable to respond to the rapidly oscillating field and can be treated as stationary. The charge bunching created from this oscillation results in a spatially periodic electric field that aims to restore the electrons to their neutral positions. That is the plasma oscillation. Plasma oscillation has a periodic structure. On the other hand, plasma dipole oscillation has a localized charge separation.

Non-trapping plasma dipole oscillation (PDO) has emerged as a promising technique for generating strong THz radiation. By utilizing the near-resonant beat wave excitation of an electron plasma wave (EPW), researchers have been able to generate trains of few-femtosecond electromagnetic (EM) pulses in rarefied plasmas. The unique characteristic of this approach is that the current generated by the EPW is sustained for a considerable duration even after the driving laser pulses have passed. The excitation of the EPW leads to the formation of a comoving index grating within the plasma. This grating induces a phase modulation in the laser pulses at the difference frequency, resulting in the generation of the desired electromagnetic pulses. These pulses exhibit a few-femtosecond duration and are characterized by their high intensity in the THz frequency range.

2.2 Trapping PDO

When exposed to a high-intensity laser driver, the behavior of charged particles in a plasma can undergo significant changes, particularly when they reach relativistic velocities. At such velocities, the particles become less responsive to the rapid oscillations of the driver's phase and tend to break away from the driver's path. Instead of following the oscillatory motion of the driver, these particles experience a net force known as the ponderomotive force, which pushes them away from the intense regions of the laser field. This phenomenon is commonly referred to as particle trapping in the ponderomotive potential.

However, the dynamics of a plasma system can become even more intricate when multiple laser pulses collide. In the case of pulse collisions, the interplay between the individual pulses adds an extra layer of complexity to the particle dynamics. The interaction between the pulses can lead to various effects, such as interference patterns, energy exchange, and even the creation of new plasma structures. The collision of laser pulses introduces additional degrees of freedom and can result in intricate particle trajectories and energy redistribution. The complex interplay of the pulses' electric and magnetic fields, as well as the collective response of the plasma, contributes to the overall dynamics of the system. This can include phenomena such as wave breaking, self-focusing, and the formation of localized structures.

Electromagnetic fields play a crucial role in shaping the behavior of charged particles, and understanding wave-particle interactions is essential for studying the dynamics of these particles in such fields. Let's delve into the behavior of electrons in the presence of an electric field generated by a sinusoidal traveling wave. Consider an electric field given by the equation $E = \hat{E}\sin(kx - \omega t)$, where E represents the electric field strength, $\hat{E}$ is the amplitude of the field, k is the wave number, x denotes the spatial coordinate, ω is the angular frequency, and t represents time. In this case, we assume that the wave is traveling in the positive x direction.

When an electron is subjected to this electric field, it experiences a force given by the equation $F = qE$, where F is the force on the electron and q is the charge of the electron. In this scenario, the force acting on the electron is directly proportional to the strength of the electric field. As the electron moves within the field, its motion is influenced by the varying strength and direction of the force it experiences. The motion of the electron can be described by the equation of motion, which takes into account the force acting on the electron, as well as other factors such as its initial conditions and any external influences. The behavior of the electron in the electric field depends on various factors, including the amplitude of the field ($\hat{E}$), the wave number (k), and the angular frequency (ω). These factors determine the strength, spatial extent, and temporal variation of the electric field, which in turn influence the motion of the electron.

Assuming a constant field amplitude $\hat{E}$ and neglecting the self-consistency considerations of $E(x,t)$, the equation of motion for an electron in this electric field can be described by the following equation:

$$k\frac{d^2x_0(t)}{dt^2} + \frac{e}{m}\hat{E}\sin[kx_0(t)] = 0 \tag{61}$$

where m represents the mass of the electron, x is the position of the electron along the spatial coordinate x, t denotes time, q is the charge of the electron, $\hat{E}$ is the amplitude of the electric field, k is the wave number, and ω is the angular frequency.

This equation of motion describes the acceleration experienced by the electron due to the electric field. The term on the right-hand side represents the force acting on the electron, which is given by $q\hat{E}\sin(kx - \omega t)$. Here, $q\hat{E}$ represents the magnitude of the force, and the sinusoidal term $\sin(kx - \omega t)$ accounts for the spatial and temporal variation of the electric field. Solving this equation of motion allows us to determine the trajectory and behavior of the electron in the given electric field. However, it's important to note that this simplified equation assumes a constant field amplitude and disregards the self-consistency considerations, which means that the equation does not take into account the feedback between the electron's motion and the electric field it generates.

However, when the field amplitude is finite, the displacement of the electron relative to the wave frame becomes a crucial factor in analyzing wave-particle interactions. To account for this, the concept of trapping time scale, denoted as τ_{tr} or bounce frequency ω_B, is introduced. The trapping time scale represents the frequency at which electrons bounce back and forth between the potential well created by the wave. The trapping time scale is determined by the time it takes for an electron to become trapped in the wave or escape from its influence.

It depends on various factors such as the field amplitude, the electron's initial conditions, and the wave characteristics. When the electron's motion is in resonance with the wave, meaning its natural frequency matches the frequency of the wave, it becomes more likely to be trapped and experience significant energy exchange with the wave. During the trapping process, the electron undergoes oscillatory motion within the potential well created by the wave. As the electron moves towards the regions of higher electric field, it gains energy and accelerates, reaching maximum displacement before being decelerated and moving back towards regions of lower field.

This oscillatory behavior leads to the concept of the bounce frequency ω_B, which characterizes the frequency at which electrons bounce back and forth within the wave potential. The trapping time scale τ_{tr} is related to the bounce frequency ω_B through the equation $\omega_B = \frac{2\pi}{\tau_{tr}}$. It represents the characteristic time scale at which electrons interact with the wave, exchanging energy and momentum. Understanding the trapping time scale is crucial in studying phenomena such as electron acceleration, particle trapping, and energy transfer in plasma and laser physics.

$$\tau_{tr} \equiv \omega_B^{-1} \equiv \left(\frac{m}{ek\hat{E}}\right)^{1/2} \tag{62}$$

The trapping of electrons in the potential well created by the wave leads to their periodic motion within the wave frame. As the electron reflects off the potential well boundaries, it undergoes oscillatory motion. This trapping behavior is characterized by a range of energies in which the electron can be trapped. Specifically, the range of trapping for electrons is bounded by $-e\hat{E}/k < W < e\hat{E}/k$, where W represents the electron's energy. When an electron becomes trapped, it continuously reflects off the potential well boundaries and undergoes periodic motion.

This behavior gives rise to nonlinear orbits, which arise due to the finite amplitude of the wave. These nonlinear orbits are not accounted for in conventional treatments of Landau damping, which are based on linearized Vlasov-Poisson equations. Thus, considering the nonlinear effects is important for a

comprehensive understanding of wave-particle interactions. In the case where the electron's initial position satisfies $kx_0 \approx 0, \pm 2\pi, \dots$ and its energy is approximately $W \approx -e\hat{E}/k$, the angular frequency of the periodic motion is given by $\omega_B = \left(ek\hat{E}/m\right)^{1/2}$. This frequency represents the characteristic frequency at which the trapped electron oscillates within the potential well. It is important to note that this frequency depends on the amplitude of the electric field $\hat{E}$, the wave vector k, and the mass of the electron m.

An untrapped electron with an energy $W > e\hat{E}/k$ experiences a different behavior when compared to a trapped electron. As the untrapped electron traverses the potential created by the wave, it undergoes acceleration and deceleration. However, unlike the trapped electron, its initial direction of motion is not reversed. When the field amplitude $\hat{E}$ is slowly varying in time, the particle orbits can still be determined using the equation $\frac{m}{2}\left(\frac{dx_0}{dt}\right)^2 - e\phi(x_0) = const$, which remains valid for multiple bounce periods. This equation describes the conservation of mechanical energy for the untrapped electron. The term $\frac{m}{2}\left(\frac{dx_0}{dt}\right)^2$ represents the kinetic energy, and $e\phi(x_0)$ corresponds to the electric potential energy. For particles that are trapped near the bottom of the potential well of the wave, the condition for the validity of the aforementioned equation can be expressed as:

$$\left|\frac{1}{E_0}\frac{dE_0}{dt}\right| \ll \omega_B \tag{63}$$

This condition ensures that the field amplitude $\hat{E}$ changes slowly enough for the equation to accurately describe the particle orbits over many bounce periods. It implies that the time variation of the field amplitude should be much slower than the inverse of the bounce frequency $\omega_B/2\pi$.

In the case where laser pulses are used to generate Plasma Dipole Oscillation (PDO), the condition for the validity of the equation describing the particle motion may be modified due to the presence of frequency detuning between the pulses. When two laser pulses with frequency detuning are overlapped, they no longer form standing waves, but rather create a beating pattern in the electric field. The electric field generated by the detuned laser pulses can be described by a modified equation, taking into account the frequency detuning $\Delta\omega$:

$$E = \hat{E}\sin(\Delta k x)\cos(\Delta\omega t) \tag{64}$$

where $\hat{E}$ is the field amplitudes of the respective pulses, $\Delta\omega$ and Δk are beat frequency and wave-number. Then equation of motion is

$$\frac{d^2x}{dt^2} + \frac{e}{m}\hat{E}\sin(\Delta k x)\cos(\Delta\omega t) = 0 \tag{65}$$

I set the solution of this equation as following

$$x = x_0\cos\Delta\omega t \tag{66}$$

Insert equation of motion, envelop equation is obtained.

$$\frac{d^2x_0}{dt^2} - \Delta\omega^2 x_0 + \frac{e}{m}E_0\sin(\Delta k x_0\cos\Delta\omega t) = 0 \tag{67}$$

For the coherent oscillation, $|\Delta k x_0\cos(\Delta\omega t)|$ needs to be small. $|x_0| \ll \frac{1}{\Delta k}$. Then equation becomes

$$\frac{d^2x_0}{dt^2} + \left(e/m\hat{E}\Delta k\cos\Delta\omega t - \Delta\omega^2\right)x_0 = 0 \tag{68}$$
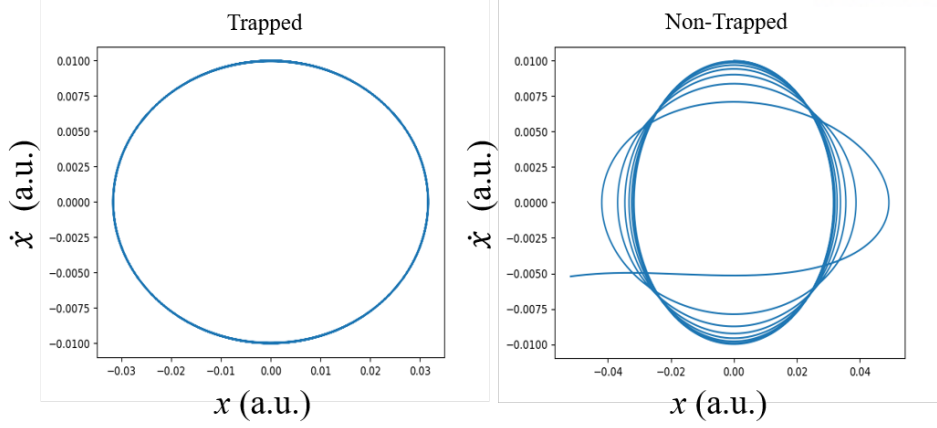
Figure 17: Result of particle paths driven by external electromagnetic waves. Upper limit value is 0.7 (a.u.). Phase velocities of beat waves are 0.089 (Trapped) and 0.716 (Non-trapped) respectively.

x_0 is the envelop of the electron oscillation path. If the x_0 becomes large, particle escapes from the driving fields. The condition for particle trapping in the collision of laser pulses becomes

$$e/m\hat{E}\Delta k - \Delta\omega^2 \geq 0 \tag{69}$$

Applying $\Delta k = |k - (-k)| = 2k$ and normalization of electric field with phase velocity of beat wave $v_{beat} = \Delta\omega/\Delta k$. The beat wave condition, which is based on the detuning of two laser pulses, for particle trapping is

$$a_0 \geq 2\beta_{beat}^2 \tag{70}$$

When electrons are exposed to a beat wave, resulting from the interference of two laser pulses with a frequency detuning, they experience oscillations that can lead to the phenomenon of particle trapping within the plasma wave. The conditions for particle trapping in the beat wave differ from those associated with relativistic particle trapping, making it a distinct mechanism with its own set of characteristics. Fig. 17 presents numerical results that demonstrate the beat wave condition and its influence on electron oscillations within the plasma wave. In this context, the parameter β_{beat} plays a crucial role as it determines the phase speed of the beat wave. Typically, β_{beat} assumes a small value, causing $2\beta_{beat}^2$ to gradually decrease below 1. This indicates that the required pulse amplitudes to achieve particle trapping in the plasma wave are relatively smaller compared to other trapping conditions such as relativistic particle trapping.

One of the fascinating aspects of the beat wave trapping mechanism is the strong dependence on the detuning of the two laser pulses. The frequency difference between the two pulses plays a crucial role in determining the strength and characteristics of the generated beat wave. To achieve efficient particle trapping in the plasma wave, the detuning must be precisely controlled within a specific range. By carefully adjusting the detuning, researchers can tailor the properties of the beat wave to meet their experimental requirements. A detuning that is too small may result in weak beat wave interactions, leading to ineffective particle trapping. On the other hand, a detuning that is too large can hinder the

formation of a coherent beat wave, diminishing the trapping efficiency. In addition to detuning, the amplitude of the laser pulses is another important parameter to consider. Optimizing the pulse amplitude is crucial to ensure efficient particle trapping without causing undesirable effects in the plasma. The amplitude should be chosen such that it provides sufficient energy to induce significant oscillations and trapping of the particles, while avoiding excessive perturbations or disruptions to the plasma.

Once the laser pulses collide and pass through each other, the resulting beat waves start propagating in a particular direction, determined by the sign of the detuning difference. As the beat wave travels, it exerts ponderomotive forces on the trapped particles, causing them to be dragged along with the wave motion. This phenomenon of particle trapping and dragging by the beat wave can lead to intriguing dynamics and fascinating effects. One noteworthy aspect of this process is the mixing of particle phases during the dragging processes. As the particles are trapped and dragged by the beat wave, their individual phases become entangled and intertwined.

The mixing of phases occurs due to the complex interplay between the particle motion, the beat wave dynamics, and the collective electromagnetic fields generated by the trapped particles themselves. This phase mixing phenomenon has significant implications for the behavior and interactions of the trapped particles. It can lead to the emergence of collective behaviors and cooperative effects among the trapped particles. The mixing of particle phases can result in synchronization phenomena, where the particles oscillate in unison or exhibit coordinated motion.

This synchronization can give rise to enhanced particle acceleration, improved energy transfer, and the formation of highly structured particle distributions. The phase mixing also contributes to the efficient energy exchange between the beat wave and the trapped particles. The particles gain energy from the beat wave through the ponderomotive forces, while at the same time, their motion influences the dynamics of the beat wave itself. This intricate interplay between the particles and the wave leads to the transfer of energy back and forth, ultimately contributing to the sustained trapping and dragging of the particles by the beat wave.

The figure 18 presented in the study illustrates the electron motion during different stages of the laser pulse interaction. The upper row of plots focuses on the electron motion while the laser pulses are overlapping, whereas the lower row depicts the electron motion after the pulses have passed through each other. By examining these plots, it becomes possible to analyze and compare the behavior of the electrons under these different conditions. The results displayed in the figure were obtained through a two-dimensional Particle-in-Cell (PIC) simulation.

Various parameters were considered in the simulation, including the laser pulse parameters (a_0, τ, σ, λ_1, and λ_2) and the plasma density (n_0). These parameters play a crucial role in determining the characteristics of the electron motion and the dynamics of the plasma system. In the upper row of plots, which corresponds to the overlap of the laser pulses, the electron motion is influenced by the combined fields generated by the pulses. The plots provide insights into the electron's behavior, such as its velocity components in the x and y directions represented by $\gamma v_x/c$ and $\gamma v_y/c$, respectively.

These plots are presented as phase portraits, where the electron's relativistic gamma factor γ is multiplied by its velocity components and normalized to the speed of light (c). The electron's motion is
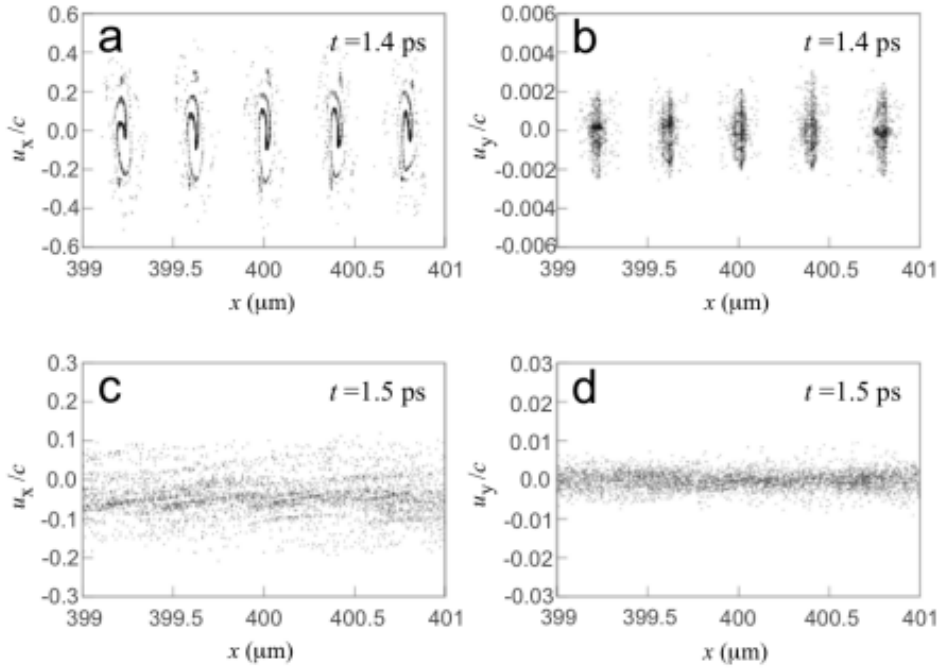
Figure 18: Electron distributions in the phase space during the formation of plasma dipole block

observed within a specific region near the dipole center at $x = 400\,\mu$m. Moving to the lower row of plots, which represents the electron motion after the pulses have passed through each other, different characteristics emerge. The electron dynamics undergo a transition due to the changes in the electromagnetic fields as the pulses separate.

This transition in the electron motion can reveal valuable information about the interplay between the laser pulses and the plasma. Notably, the length of the dipole, representing the region where the electron motion is influenced by the overlapping laser pulses, is comparable to the pulse width. This suggests that the electron motion is closely connected to the temporal profile and spatial extent of the laser pulses. By considering the details of the electron motion within this confined region, researchers can gain insights into the intricate dynamics and the interplay between the particles and the laser fields.

2.3 Radiation Mechanism

The oscillation of the localized plasma block causes radiation emission from PDO. For electromagnetic waves, this radiation is linearly polarized, and its frequency is equal to the frequency of the plasma block. The plasma oscillation involves all of the charged particles in the plasma, whereas the bunched electrons near the collisional site relevant to dipole field.

The dispersion relation of plasma oscillation shows that there is no cross point with the dispersion relation of vacuum light, indicating that plasma oscillation does not emit radiation. One characteristic of plasma is its ability to act as a frequency-dependent medium, blocking or attenuating external radiation at frequencies close to its plasma frequency. This phenomenon, known as the cut-off. However, PDO is an exception to this rule. It has been observed that PDO can emit radiation. This can be demonstrated by

41
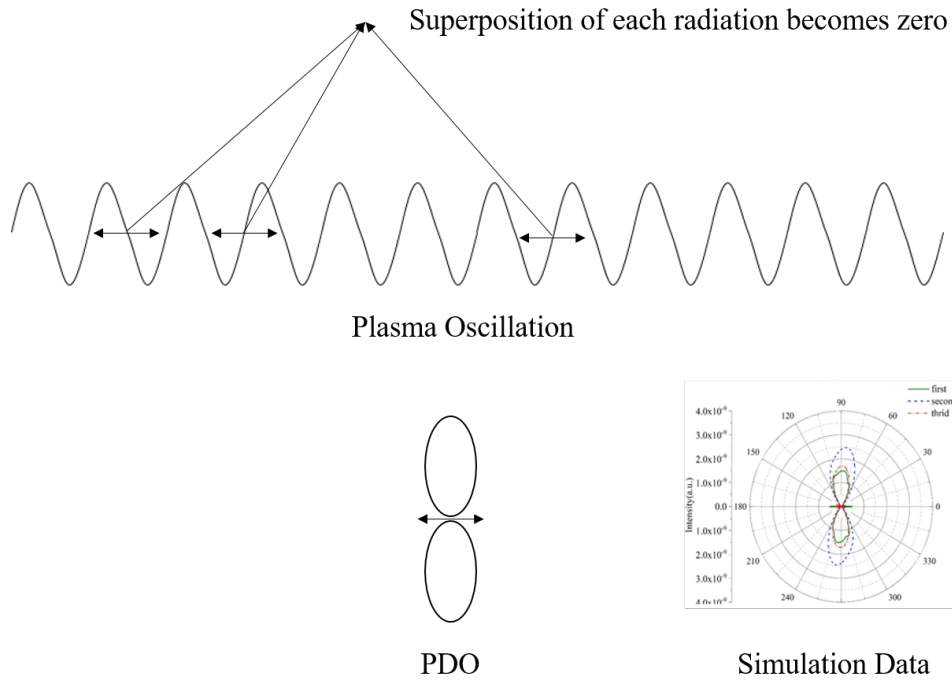
Figure 19: Schematic diagram of interference of radiation from plasma oscillation and PDO. Angular intensity of PDO's radiation also provided, which is calculated by PIC data.

the interference of radiation from each oscillator in the PDO.

Plasma waves are often considered to consist of an infinite number of oscillators, all oscillating at the same frequency. At points outside the plasma wave, when integrating the radiation from each individual oscillator, the interference effects lead to a net-zero result. This interference arises due to the phase differences and cancellations between the radiation emitted by different oscillators, resulting in a suppression of the overall radiation.

This interference-based explanation aligns with the conclusion that there is no crossing point in the dispersion relation. The absence of a crossing point signifies that the plasma wave and electromagnetic waves do not exhibit resonance or overlap at the plasma frequency. As a result, the propagation of radiation at this frequency range is significantly hindered or completely blocked.

However, it is important to note that the PDO does not consist of an infinite number of oscillators uniformly distributed throughout space. Instead, it can be localized within a specific region or exhibit spatially varying characteristics. In such cases, the integration of radiation from individual oscillators does not lead to complete cancellation or a net-zero result.

The localized nature of the plasma wave allows for the radiation to interact with a limited number of oscillators, leading to non-zero contributions from specific regions. As a result, the behavior of radiation inside the plasma, particularly when the source of radiation is located within the plasma, can deviate from the traditional cut-off phenomenon. Instead of complete attenuation, the radiation may exhibit modified propagation characteristics, such as dispersion, refraction, or resonant interactions with localized plasma structures.
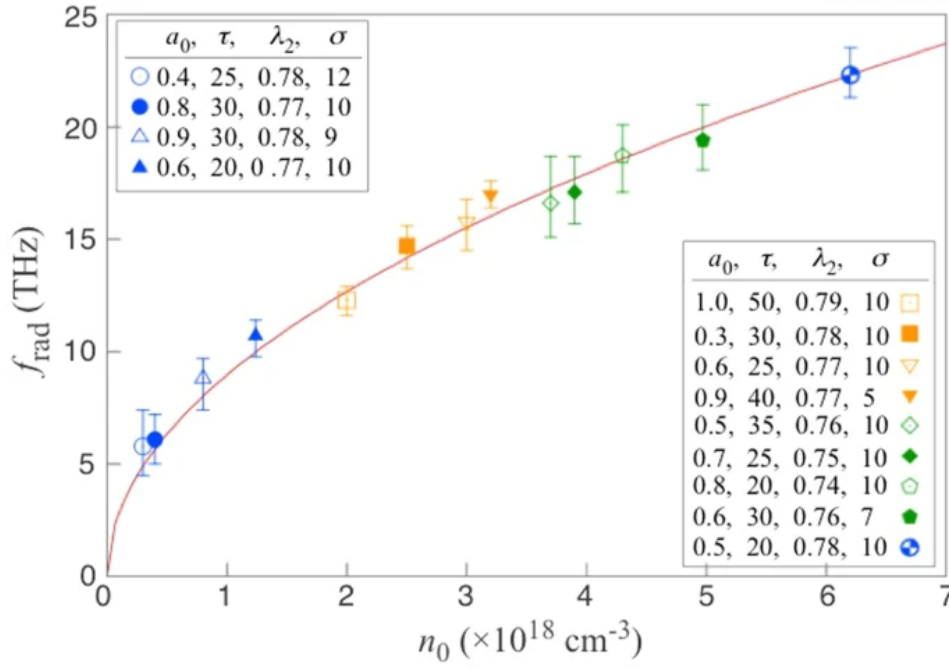
Figure 20: PDO spectra data and theoretical spectra curve with various plasma and laser parameters.

PDO spectrum displays a prominent peak at the plasma frequency (ω_p), which coincides with the frequency of plasma oscillation. The spectral peak of the PDO can be primarily attributed to the bunching of electrons within the beat ponderomotive potential [55]. This beat wave leads to the formation of electron bunches, where groups of electrons cluster together within the PDO structure.

The formation of these bunches is a consequence of the phase mixing between the individual electron. The electron bunching within the PDO results in the spectral peak at the plasma frequency ω_p. The bunches of electrons collectively contribute to the emission of radiation at this frequency. The emitted radiation carries the imprint of the PDO's oscillatory motion and exhibits the same frequency as that of the underlying oscillator. To comprehensively explore the spectral characteristics of Plasma Dipole Oscillation (PDO), Particle-in-Cell (PIC) code is employed.

The simulation results consistently demonstrated that the PDO spectrum exhibits a prominent peak precisely at the plasma frequency ω_p, which aligns with the theoretical expectations. This agreement between theory and simulation confirms the robustness and accuracy of the modeling techniques employed. The observed peak at ω_p indicates the dominant oscillatory behavior of the PDO, with the plasma frequency serving as a natural resonance frequency for the collective plasma motion.

In addition to investigating the PDO spectrum, the simulations also focused on the radiation emitted from the PDO itself. Remarkably, the analysis of the emitted radiation revealed that its spectral characteristics matched those of the PDO, with a dominant frequency at ω_p. This observation provided further evidence of the close relationship between the PDO and its radiation emission.

Efficient energy conversion is a critical factor in assessing the performance of Plasma Dipole Oscillation (PDO) as a radiation source. To gain insights into the energy conversion process, one-dimensional (1D) theoretical analyses are performed. By employing this approach, the performance of the PDO is
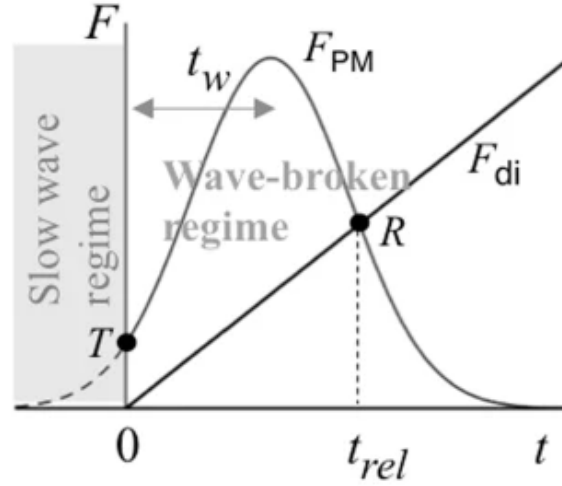
Figure 21: Force balance model, restoring force and beat wave dragging

optimized as a efficient radiation emitter. In the theoretical framework, several assumptions are made to simplify the analysis. First, it is assumed that the release point of the dipole coincides with the peak of the driving ponderomotive force. This positioning ensures that the dipole field reaches its maximum strength for the given intensity of the laser pulses. By maximizing the dipole field, the potential for efficient energy conversion is enhanced. Next, the slope of the dipole growth is determined by considering the amplitude and duration of the driving laser pulses. These parameters play a crucial role in shaping the temporal evolution of the dipole field.

At the release point, a delicate balance between the electric force exerted on an electron by the dipole field (E_{di}) and the ponderomotive force is achieved. This balance ensures that the two forces counteract each other, resulting in the theoretical maximum efficiency of energy conversion. This point of equilibrium represents an optimal condition for achieving efficient energy transfer from the driving laser pulses to the PDO and subsequent radiation emission.

$$eE_{di} = e\alpha S\tau = \alpha e^2 n_0 c\beta\phi\tau = \frac{\alpha\eta mc\omega a_0^2}{\sqrt{1+a_0^2/2}} \approx \alpha\eta mc\omega a_0^2 \tag{71}$$

$$\bar{E}_{di} = \frac{\alpha\omega_p^2}{\omega}\beta_\phi\tau = \alpha\eta a_0^2 \tag{72}$$

where $\beta_\phi = \frac{v_\phi}{c} = \frac{\Delta\omega}{2ck}$, $\bar{E}_{di} = eE_{di}/(mc\omega)$ (i.e. the normalized velocity of the ponderomotive potential train), α is the fraction of the trapped electrons and η is the ensemble-average factor. In the cases where the dimensionless laser pulse parameter a_0 is less than or equal to 1, the energy conversion efficiency of the Plasma Dipole Oscillation (PDO) can be quantified. By considering the energy of the driving pulse per unit transverse area, denoted as $a_0^2 c\tau$, and the dipole field energy per unit transverse area, represented by $\bar{E}_{di}^2 c\tau$, researchers can analyze the efficiency of energy conversion.

The energy conversion efficiency, denoted by ζ, represents the rate at which the dipole field energy U_{di} is converted into radiation energy U_{rad}. It is defined as the ratio of the radiation energy to the dipole

field energy. Mathematically, it can be expressed as:

$$\zeta = \frac{U_{rad}}{U_{di}} \tag{73}$$

The energy of the driving pulse per unit transverse area, $a_0^2 c\tau$, represents the initial energy available for the system. On the other hand, the dipole field energy per unit transverse area, $\overline{E}_{di}^2 c\tau$, represents the energy stored in the dipole field.

The energy conversion efficiency, ζ, quantifies the fraction of the dipole field energy that is effectively converted into radiation energy. The value of ζ depends on various factors, including the characteristics of the driving laser pulse, the properties of the plasma, and the specific conditions of the experimental setup. By carefully designing and optimizing these parameters, researchers can enhance the energy conversion efficiency and maximize the radiation output from the PDO. Then the final form of energy conversion efficiency from the laser to radiation is

$$\varepsilon = \frac{\zeta U_{di}}{U_{laser}} = \zeta \frac{\overline{E}_{di}^2 c\tau}{a_0^2 c\tau} = \zeta^2 \alpha^2 \eta^2 a_0^2 \tag{74}$$

Eliminating a_0^2 using Eq. 72 yields

$$\varepsilon = \zeta \alpha \eta \frac{\omega_p^2}{\omega} \beta_\phi \tau \tag{75}$$

When the detuning is not very large (i.e. low $\Delta\omega$), the fraction of trapping is almost unity ($\alpha \approx 1$). The conversion rate of U_{di} to U_{rad} is approximately 0.5. The ensemble average factor is approximately 0.3. With the additional phenomenological reduction factor $R = 0.6$, Eq. 75 can be expressed as:

$$\varepsilon \simeq 0.1 \frac{\omega_p^2}{\omega} \beta_\phi \tau \tag{76}$$

According to Eq.75, increasing the velocity of the ponderomotive potential train (β_ϕ) can significantly improve the conversion efficiency.

Eq.75 suggest that the efficiency can be greatly increased by using a large conversion rate ζ. However, in practical applications, it is difficult to achieve ζ values larger than 0.1. For example, with a wavelength of $\lambda \approx 300$ THz ($\Delta x = 1$ μm), a conversion rate of $\zeta \approx 0.05$, and typical 30-fs driving pulses ($\tau \approx 30$ fs), the efficiency to generate 20 THz radiation is only around 10^{-3}. To further enhance the efficiency of energy conversion in Plasma Dipole Oscillation (PDO), one approach is to increase the pulse duration, τ. By utilizing longer pulses, a larger amount of energy can be delivered to the system, potentially leading to higher energy conversion efficiency. However, using very long pulses in exactly head-on collisions of laser pulses presents practical challenges.

One issue arises from the fact that the dipole length, which is comparable to the pulse width, becomes too large when using very long pulses. This can result in the breaking of the coherent block-like motion of the electrons within the dipole. To overcome this limitation, a solution lies in employing oblique collisions of laser pulses. By colliding laser pulses at an oblique angle, the dipole length can be effectively controlled and maintained at a smaller size, even when using very long pulses.
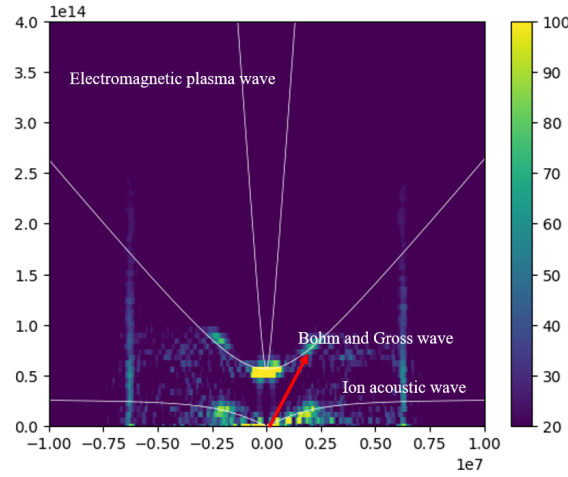
Figure 22: Dispersion curves of plasma dipole field

This control is achieved by adjusting both the collision angle and the spot size of the pulses. The oblique collision geometry ensures that the dipole length remains within a manageable range, preserving the coherent motion of electrons and preventing the degradation of the energy conversion efficiency. This approach offers several advantages. Firstly, it allows for the utilization of longer pulses, thereby increasing the energy available for conversion. Longer pulses can carry a larger amount of energy, enhancing the overall efficiency of energy transfer. Secondly, by maintaining a small dipole length, the coherent block-like motion of electrons is preserved, ensuring the sustained generation of the PDO. This contributes to the stability and reliability of the radiation source.

Potential problems that can arise in using long laser pulses include various instabilities [56] originating from the prolonged interaction between the laser and plasma, as well as ion motion, which is neglected in our analysis of the PDO. To avoid laser-plasma instabilities that may disturb the formation of the dipole, the laser path inside the plasma should be made as short as possible by controlling the launching angle of the laser pulses and the plasma profile. Thus, the time scale of ion motion may be the only limiting factor in increasing τ. Assuming a single-ionized argon plasma [57], the ratio of ion and electron plasma frequencies, $\omega_{pe}/\omega_{pi} = 270$. This means that the ions remain stationary during a few hundred cycles of the electron oscillation. For the 20 THz case, this amounts to tens of picoseconds. Assuming a much shorter pulse duration than that, for example, $\tau = 3000$ fs, the conversion efficiency can reach approximately 0.1, which is unprecedentedly high in the millijoule-order, tens-of-THz regime.

The process of plasma block formation is indeed a fascinating phenomenon with various stages and dynamics. Initially, when particles in the plasma have random phases, there is significant heat generation due to the rapid interactions between particles. However, as the beat wave dragging stage progresses, the particles in the plasma become coherently organized. They start oscillating in a synchronized manner, driven by the ponderomotive forces exerted by the beat wave.

This coherent motion of the particles leads to a explosive emission of radiation from the plasma. The emitted radiation rapidly decays after a few cycles, indicating a decrease in the energy radiated by the plasma block. At this stage, the plasma block undergoes a transition, transforming from an intense

radiation-emitting state to a thermalized state.

The heat generated initially through the phase-randomized motion of particles starts to diffuse and spread throughout the plasma. The diffusion process follows the characteristics of Bohm and Gross waves, which describe the propagation of heat in plasmas. The transition from a coherent plasma block to a thermalized state is significant, as it represents the conversion of the initially concentrated energy into a more distributed and diffused form.

2.4 Comparison of PDO generation methods

Laser frequency detuning plays a crucial role in classifying different generation schemes within certain experimental setups. When the detuning parameter, denoted as $\Delta\omega$, is less than the plasma frequency, a phenomenon known as beat wave can effectively drag trapped particles. In this scenario, where $\Delta\omega < \omega_p$, the beat wave effectively drags trapped particles with the phase velocity.

$$v_{ph} = \frac{\Delta\omega}{k_1 + k_2} \tag{77}$$

where k_1 and k_2 are wave numbers of each laser pulses.

On the other hand, when the detuning parameter is equal to the plasma frequency ($\Delta\omega = \omega_p$), a different phenomenon emerges. In this case, the phase velocity of the beat wave matches the velocity of the trapped particles, and they are no longer dragged by beat wave. Instead, a resonant interaction occurs, leading to the generation of nonlinear currents.

Different generation schemes exhibit varying efficiencies in terms of radiation emission. The radiation emission efficiency can be quantified by the scaling laws associated with each scheme. In the case of the nonlinear current scheme, the scaling law is given by a 4th power dependence on the laser input, while the particle trapping scheme follows a 2nd power dependence. The exact form of the radiation relation for the nonlinear current scheme is expressed as:

$$\frac{eE_{rad}}{mc\omega_0} = \frac{\pi}{16}\frac{\omega_c}{\omega_p}\sigma^2 k^2 a_0^4 e^{-0.084\omega_p^2\tau^2} \tag{78}$$

Here, σ represents the laser spot size, ω_c is the characteristic frequency, ω_p is the plasma frequency, k is the wave number, a_0 is the laser amplitude, and τ denotes the pulse duration. On the other hand, the exact form of the radiation relation for the particle trapping scheme is given by:

$$\frac{eE_{rad}}{mc\omega_0} = 0.21\alpha a_0^2 \tag{79}$$

In this equation, α represents the trapping rate. When considering plasma diagnostics, it is advantageous to have a low laser amplitude to minimize the perturbation of the plasma state. Additionally, higher radiation intensity is preferable for better detection capabilities. Comparing the two schemes, we find that for a laser amplitude of $a_0 = 10^{-2}$, the radiation amplitude for the nonlinear current scheme is $a_0^4 = 10^{-8}$, while for the particle trapping scheme, it is $a_0^2 = 10^{-4}$.

Therefore, the radiation from the particle trapping scheme is larger than that from the nonlinear current scheme. Consequently, the particle trapping scheme is more appropriate for plasma diagnostics,
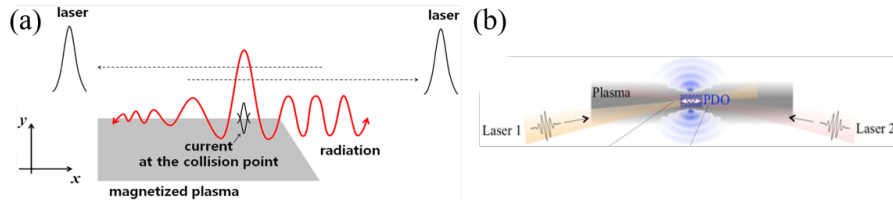
Figure 23: Nonlinear current scheme and particle trapping scheme

as it provides higher radiation intensity while maintaining a lower laser amplitude, thus minimizing the perturbations to the plasma state.

III PDO Application

3.1 Plasma Diagnostics

Overview of Plasma Diagnostics

Plasma parameters play a crucial role in determining the behavior of plasmas in various applications. The density of charge carriers, for example, determines the level of ionization and the plasma frequency. Plasma frequency, in turn, influences the absorption of electromagnetic radiation by the plasma. Plasma density also affects the plasma Debye length, which is important in determining the spatial extent of electric fields in plasmas. These parameters are critical in understanding the behavior of plasmas in fusion reactors [58], plasma thrusters [59], and plasma-based material processing [60].

Laser plasma interaction is another important area where plasma parameters are crucial. When a high-intensity laser pulse is focused on a solid target [61], a plasma is formed due to ionization of the target material. The plasma produced in this process absorbs and scatters the laser light, leading to various nonlinear effects such as harmonic generation [62], self-focusing [63], and self-phase modulation [64]. The plasma parameters such as density, temperature, and electron density distribution play a crucial role in determining the extent and nature of these nonlinear effects. Understanding these effects is crucial for developing laser-based material processing techniques, such as laser ablation, welding, and cutting.

Conventional Plasma Diagnostics

Interferometry [65] is a widely used technique in plasma diagnostics to study the behavior of plasma waves and their interactions with surrounding materials. It involves the measurement of the interference patterns produced by the superposition of two or more waves in a plasma. By analyzing these patterns, we can determine the plasma density, electron temperature, and other properties of the plasma. Interferometry is particularly useful in studying high-density plasmas such as those used in fusion research and semiconductor manufacturing.

Abel inversion [66], tomographic techniques [67], and reflectometry [68] are commonly used plasma

diagnostic techniques. Abel inversion is a mathematical method that retrieves the plasma density profile along a radial direction by measuring the refractive index or phase shift of light passing through the plasma. However, Abel inversion has limitations in cases where the plasma is not axially symmetric or where the refractive index gradient is steep. Additionally, Abel inversion requires a well-defined radial profile of the refractive index, which may be difficult to obtain experimentally.

Tomographic techniques [69], on the other hand, provide a more complete picture of the plasma density by measuring the line-integrated density along many viewing directions. Tomography algorithms reconstruct the 2D or 3D plasma density distribution from these measurements. This technique can be used to diagnose non-axisymmetric plasmas and plasmas with steep density gradients. However, tomography requires multiple lines of sight, and the accuracy of the reconstruction depends on the number and distribution of the lines of sight.

Reflectometry is a technique that measures the reflection of microwaves from a plasma. This method can provide information on the plasma density profile by measuring the frequency shift of the reflected wave. Reflectometry can be used to diagnose high-density plasmas, such as those found in fusion experiments. However, the accuracy of the technique depends on the wavelength of the microwaves and the smoothness of the density profile. Additionally, the technique is sensitive to the shape and position of the plasma relative to the probe, which can make it difficult to obtain accurate measurements.

Langmuir probe [70] is a diagnostic tool used to measure the plasma properties in a plasma reactor or a fusion device. It consists of a small electrode that is inserted into the plasma, and a voltage is applied between the electrode and the surrounding plasma. By measuring the current that flows between the electrode and the plasma, the electron temperature, density, and potential can be determined. The Langmuir probe is a simple and effective method to measure the plasma properties and is widely used in plasma research and industrial plasma processing.

Thomson scattering method is a diagnostic tool used to measure the temperature and density of a plasma. It involves shining a laser beam into the plasma and measuring the scattered light that is produced. The scattered light provides information about the plasma's temperature and density. The Thomson scattering method is non-intrusive and can be used to measure the properties of a plasma in real-time. It is widely used in fusion research and plasma processing industries to monitor and control plasma properties.

Polarimetry [71] is a diagnostic technique used to measure the polarization properties of electromagnetic radiation. It involves measuring the changes in the polarization state of a beam of light as it passes through a plasma or a magnetic field. Polarimetry can be used to measure the magnetic field strength and direction in a plasma or to measure the properties of a plasma, such as its temperature and density. Polarimetry is a versatile and powerful diagnostic tool that is widely used in plasma research and astrophysics.

Raman scattering [72] is a spectroscopic technique that provides information about the vibrational modes of molecules. It involves shining a monochromatic light source on a sample, and analyzing the in-elastically scattered light. Raman scattering is widely used in the study of condensed matter, including the properties of solids, liquids, and gases. In plasma physics, Raman scattering is used to measure the

temperature and density of plasmas, and to study plasma wave phenomena, such as Langmuir waves and ion acoustic waves.

Stark broadening [73] is a spectroscopic effect that results from the interaction of a spectral line with an electric field. When a spectral line is broadened due to Stark effect, the electric field induces a splitting of the energy levels of the atoms or ions that emit the line. This splitting leads to a broadening of the spectral line, which can be measured and used to infer properties of the plasma, such as its temperature and density. Stark broadening is an important diagnostic tool in plasma physics and is used to study a wide range of phenomena, including plasma turbulence, laser-plasma interactions, and astrophysical plasmas.

Another important plasma diagnostic tool is the PDO. PDO is a collective behavior of electrons in plasmas that results in a dipole-like oscillation of the plasma. It is driven by the beat-wave ponderomotive force that arises when two counter-propagating laser beams interact with a plasma. PDO has important applications in magnetic field diagnostics and the generation of intense radiation. By studying the properties of PDO, we can gain insights into the behavior of plasmas under high-energy laser irradiation and develop new techniques for manipulating and controlling plasmas for a variety of applications.

3.2 Reconstruction of in-homogeneous plasma density

Reconstruction steps

The reconstruction of plasma density involves a two-step process that utilizes plasma dipole oscillation (PDO) and external probes to extract density information. In the first step, PDO is generated within the plasma, and as a result, radiation is emitted. This radiation carries valuable information about the plasma density profile. In the second step, external probes are strategically positioned to collect the emitted signals. These probes analyze the collected signals and extract density information by identifying peaks in the spectra.

By repeating these operations and scanning the plasma with laser beams, it becomes possible to reconstruct the plasma density profile. To validate this approach and assess its accuracy in capturing inhomogeneous plasma densities, three-dimensional Particle-in-Cell (PIC) simulations are considered the most reliable method. However, due to computational constraints, two-dimensional PIC simulations were utilized in this particular study.

The choice of two dimensions was made to accommodate the requirement of numerous simulation shots, which were necessary for laser scanning. Although the two-dimensional simulations do not capture the full complexity of three-dimensional behavior, they still provide valuable insights and serve as a practical compromise in the context of this study. The laser parameters used in the simulations were selected based on the typical wavelengths of Ti:sapphire lasers, which are commonly used in experimental setups. Specifically, wavelengths of 800 nm and 780 nm were employed, slightly detuned to generate the beat wave required for PDO generation.

The laser intensity, characterized by the parameter a_0, was set between 0.1 and 0.3. It is worth noting that below a certain intensity threshold, as defined by the condition for trapping, the main mechanism

for dipole generation shifts from particle trapping to the nonlinear current mechanism. In such cases, the beat ponderomotive potential generates a non-zero density perturbation associated with the second-order current. This leads to the formation of large and localized electrostatic oscillations, known as PDO.

The particle trapping technique has proven to be advantageous in achieving a high signal-to-noise ratio in the generation of plasma dipole oscillation (PDO). Compared to other methods such as the nonlinear current approach, the particle trapping method exhibits significantly higher radiation intensity. The radiation intensity of PDO generated through particle trapping is on the order of 10^{-3}, whereas the nonlinear current method yields radiation intensity on the order of 10^{-4}.

To conduct simulations and study the characteristics of PDO, a simulation domain with dimensions of $400\mu\text{m} \times 400\mu\text{m}$ is typically employed. This domain size allows for the examination of the behavior and properties of PDO over a sufficiently large spatial region. In order to ensure accurate simulations, the Courant–Friedrichs–Lewy (CFL) criterion, which governs the stability of numerical methods, is minimally satisfied. Adhering to this criterion guarantees that the time step used in the simulations is small enough to accurately capture the dynamics of the system.

In the simulation setup, the mesh size is an essential consideration. In this case, a mesh size of $\Delta x = 0.05\mu\text{m}$ and $\Delta y = 0.2\mu\text{m}$ is employed, with the x-direction mesh having better resolution. This choice is motivated by the fact that the laser pulse primarily propagates in the x-direction. By utilizing a highly anisotropic mesh, numerical dispersion, which can introduce inaccuracies in the simulation results, is minimized. The mesh resolution and its anisotropic nature contribute to obtaining more precise and reliable data regarding the characteristics of PDO.

To validate the effectiveness of the new diagnostic method, both linear and nonlinear plasma density profiles are adopted. By comparing the simulation results obtained using these profiles with known analytical solutions or experimental data, the accuracy and reliability of the diagnostic method can be established. This validation process helps to ensure that the simulated PDO behaviors and radiation characteristics are consistent with theoretical expectations and experimental observations.

Linear density

In this paper, a novel method is proposed for reconstructing the original linear density profiles of a plasma by employing intersecting laser pulses and analyzing the emitted radiation. A simulation framework is developed to validate this process and investigate its feasibility. The simulation setup involves directing laser pulses obliquely from two sides of the plasma, causing them to collide at a specific spot. The interaction of these pulses leads to the generation of a dipole within the plasma, which subsequently emits radiation.

To gather relevant data, two virtual probes are strategically placed within the simulation domain. One probe is positioned at the center of the dipole, while the other is located in the vacuum region. These probes are responsible for measuring the electric field component E_x and the magnetic field component B_z as a function of time. The obtained results from the simulation highlight some key findings. It is observed that the dipole field exhibits non-zero curl electric field components, which play a crucial role
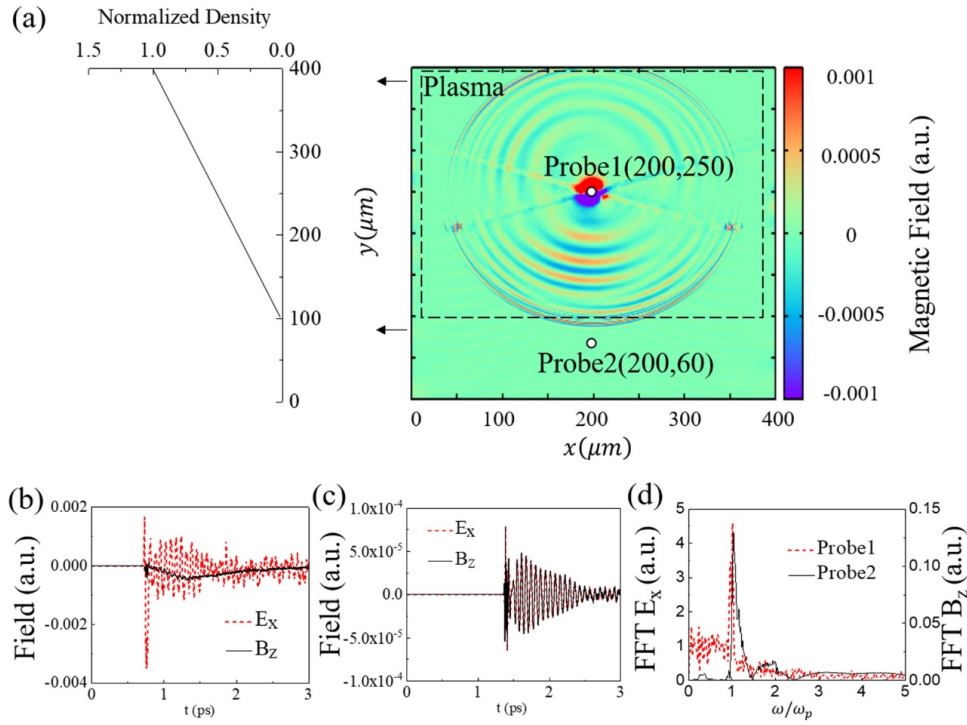
Figure 24: (a) Plasma density profile with a gradient along the x axis. The normalized density rises linearly from zero at $y = 100$ μm to $n/n_0 = 1$ at $y = 400$ μm, with n_0 equal to 4.96×10^{18} cm^{-3}. Magnetic field snapshot (b) Dipole field measured in the probe at the collisional point. (c) Radiation field measured in the probe at the vacuum. (d) FFT of signals observed in two probes.

in the radiation generation process.

The emitted radiation is found to possess a frequency that corresponds to the dipole's oscillation frequency. By intersecting laser pulses and analyzing the radiation emitted by the resulting dipole, the proposed method offers a promising avenue for recovering the original linear density profiles of a plasma. This approach leverages the unique characteristics of the dipole field and its associated radiation to infer information about the plasma density distribution. The simulation-based validation presented in this paper lays the foundation for further experimental investigations and potential applications in plasma diagnostics and characterization.

The proposed method of measuring local density in a linear plasma, as supported by the obtained results, holds great promise for reconstructing the plasma density profile. By employing laser pulse collisions and analyzing the emitted radiation, it becomes possible to replicate the density distribution throughout the plasma. This opens up avenues for scanning the laser pulse collision point and probing the radiation to reconstruct the plasma density profile. In the simulation setup, two laser pulses were projected obliquely from two sides, precisely at coordinates $(x, y) = (0 mum, 340 mum)$ and $(x, y) = (400 mum, 340 mum)$. These pulses were directed to collide at a predetermined location along the x-axis, specifically at $250 mum$. This configuration allows for the utilization of two virtual probes strategically positioned to measure the radiation emitted by the dipole generated from the pulse collision. Through careful analysis of the radiation collected by the virtual probes, valuable information about the plasma density can be extracted. The peak frequency observed in the emitted radiation corresponds to the plasma frequency, which in turn is related to the local plasma density. By accurately translating the peak frequency of the radiation into density values, the density profile of the plasma can be replicated.

To further validate the proposed method, detailed measurements of E_x and B_z were performed at Probe 1 as a function of time. These measurements aimed to demonstrate that the dipole field contains non-zero curl electric field components that are responsible for the emitted radiation. The temporal evolution of E_x and B_z was captured, allowing for a comprehensive analysis of the field dynamics during the collision and subsequent dipole oscillation. The plot of E_x or B_z as a function of time at Probe 1 revealed interesting behavior. It showed that the laser pulses reached the focal point at a specific time, precisely at $t = 7.31$ ps. This observation provides valuable insight into the temporal synchronization of the laser pulses, ensuring that their collision occurs at the desired location within the plasma. The arrival time of the pulses at the focal point serves as a critical reference for understanding the subsequent dynamics of the system. To gain a deeper understanding of the dipole field and its relationship to the emitted radiation, measurements of the amplitude and phase of the normalized electric and magnetic fields were conducted using Probe 2. These measurements were carried out to compare and correlate the resulting fields with the radiation field. The obtained data demonstrated a remarkable agreement between the observed fields and the radiation field, validating the presence of the dipole field and its role in generating the emitted radiation. In order to analyze the frequency characteristics of the signals collected by Probe 2, a Fast Fourier Transform (FFT) was employed. The frequency distributions obtained from the FFT provided valuable insights into the spectral content of the signals. Remarkably, it was discovered that the frequency of the emitted radiation matched the dipole's oscillation frequency. This correspondence
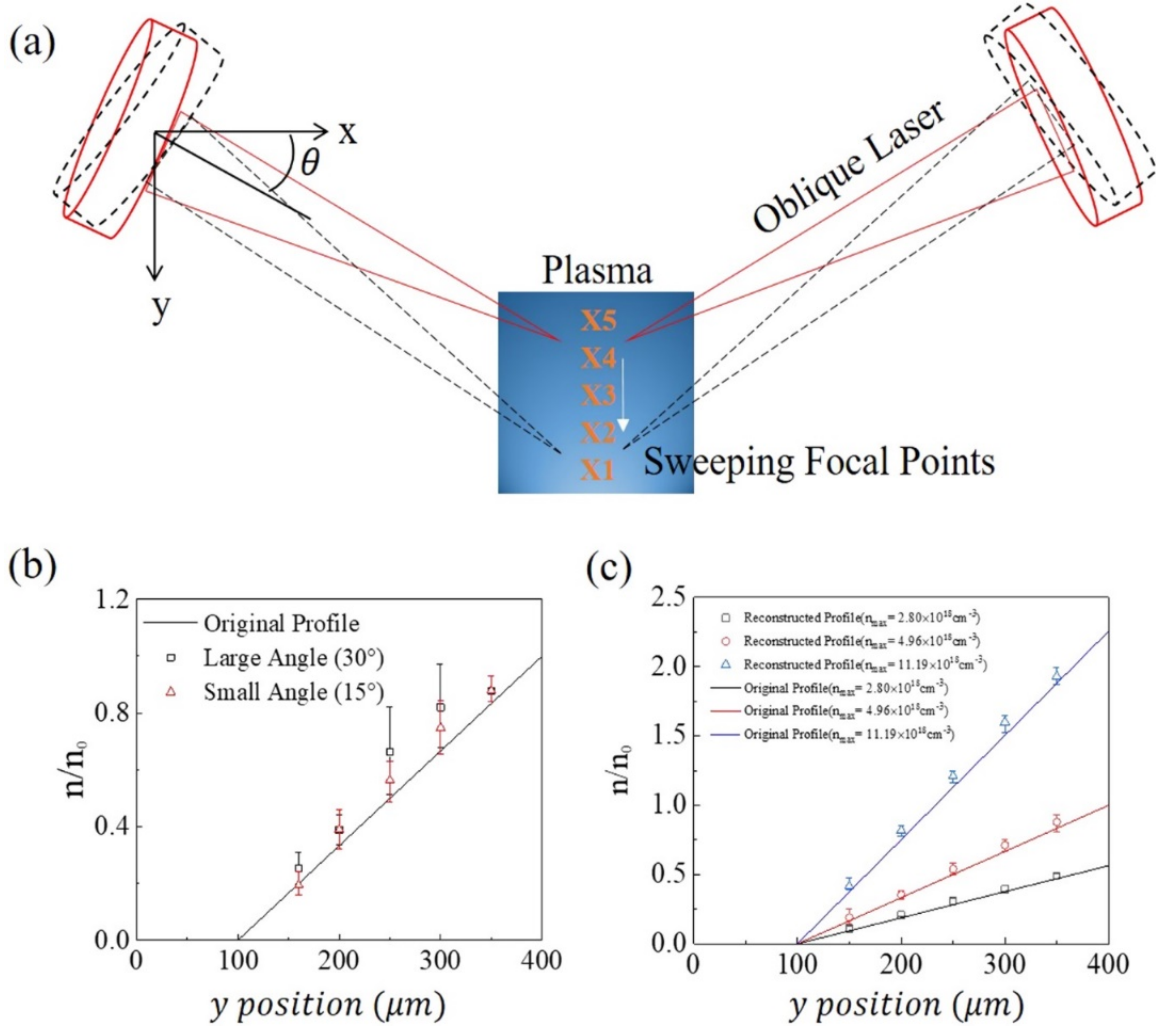
Figure 25: (a) This schematic diagram illustrates the experimental setup used to produce radiation with obliquely propagating lasers. (b) The density profile reconstruction is shown for two different collision angles: 15° and 30°. (c) By sweeping the shooting angles of the pulses at fixed launching points located far from the plasma, the density reconstruction of three distinct gradients was achieved. The greatest density at $y = 400\mu m$ is represented as n_{max} in the legend. The vertical axes in (b) and (c) show the density normalized by $n_0 = 4.96 \times 10^{18} cm^{-3}$ while the horizontal axes reflect the y-position along the gradient. The wavelengths of the laser are $\lambda_1 = 800nm$, $\lambda_2 = 780nm$, and the normalized peak amplitude is $a_0 = 0.3$.

confirms

the

fundamental

connection

between the dipole's motion and the radiation emitted from the plasma. It underscores the ability to extract density information from the radiation and utilize it to reconstruct the plasma density profile. The comprehensive measurements performed at Probe 1 and Probe 2, along with the analysis of the temporal and frequency characteristics, provide compelling evidence for the efficacy of the proposed method. The agreement between the observed fields, the radiation field, and the dipole's oscillation frequency further strengthens the confidence in the accuracy and reliability of the density reconstruction approach.

To enable the reconstruction of the plasma profile, the laser pulse collision point was systematically scanned. This scanning process involved employing counter-propagating laser pulses that collided at multiple locations along a linear density variation profile, similar to the configuration depicted in Fig. 24. By varying the collision point, it became possible to gather density information at different spatial locations within the plasma. The scanning of the collision point allowed for a comprehensive analysis of the plasma density profile. At each collision point, the radiation emitted from the dipole generated by the laser pulses was carefully measured and analyzed. The emitted radiation carried valuable information about the local density variations within the plasma. By probing the radiation and extracting relevant spectral features, researchers could extract density information associated with each collision point. The obtained density information, combined with the precise knowledge of the collision locations, formed the basis for rebuilding the plasma profile. The collected data points, representing density measurements at different positions along the linear density variation profile, were used to interpolate and reconstruct the complete plasma density profile. This reconstruction process involved employing advanced mathematical algorithms and interpolation techniques to accurately capture the variations in plasma density. By systematically scanning the laser pulse collision point and repeating the radiation measurement and analysis process, a detailed and comprehensive map of the plasma density profile could be obtained. This map provided valuable insights into the spatial distribution of plasma density, revealing regions of high and low density, as well as any gradients or irregularities in the plasma structure.

The virtual probes placed outside the plasma played a crucial role in measuring the radiation emitted from the dipole formed by the collision of the laser pulses. The collected data provided valuable insights into the spectral characteristics of the emitted radiation. In particular, the spectra exhibited distinct peaks whose positions were influenced by the specific collision location of the laser pulses. By analyzing the spectra and identifying the positions of the peaks, researchers could extract important information related to the density variations within the plasma. The peak frequency observed in the spectra was directly related to the plasma frequency ω_p, which is determined by the density of the plasma. The plasma frequency is given by the equation $\omega_p = \sqrt{\frac{e^2 n}{m \varepsilon_0}}$, where e is the elementary charge, n is the plasma density, m is the mass of the particles in the plasma, and ε_0 is the vacuum permittivity. Using the known relationship between the plasma frequency and density, researchers were able to convert the observed peak frequencies in the spectra to corresponding density values. This allowed for the reconstruction of the plasma density profile. By mapping the peak frequencies to their corresponding density values, a detailed and accurate representation of the plasma density variations could be obtained. The conversion of peak frequencies to density values enabled the creation of a density profile that accurately reflected

the underlying density distribution within the plasma. This information provided valuable insights into the spatial variations of plasma density, allowing researchers to study and understand the behavior of the plasma in greater detail.

In practical scenarios, it may not always be possible to adjust the precise entrance point of laser pulses in real-world plasma systems. However, there are alternative strategies that can be employed to effectively modify the collision position and achieve control over the resulting plasma dynamics. Colliding laser pulses obliquely offers a versatile approach to manipulating the interaction dynamics between the pulses and the plasma. By adjusting the launching angles of the laser pulses, researchers can influence not only the collision position but also the efficiency of energy transfer and the detection of local density variations. When the laser pulses are directed obliquely into the plasma, the interaction region and collision point are shifted compared to the case of head-on collisions. This provides researchers with the ability to explore different regions of the plasma and investigate the resulting effects on the emitted radiation and density profiles. By carefully selecting the launching angles, specific areas within the plasma can be targeted, allowing for the gathering of valuable information about their density variations. One advantage of oblique laser pulse collisions is the enhanced efficiency of converting the driving pulse energy to radiation energy. The oblique angle introduces an additional degree of freedom in controlling the energy transfer process. Depending on the specific geometry and characteristics of the plasma, the oblique collision can promote more efficient energy deposition and enhance the radiation emission. This can lead to a higher signal-to-noise ratio in the measurements, enabling more accurate detection and characterization of the plasma properties. Moreover, oblique collisions offer the opportunity to detect local densities within the plasma. By analyzing the radiation emitted during the oblique collision, researchers can extract information about the density variations in specific regions of interest. The emitted radiation carries signatures of the plasma properties, including the local density, and by carefully analyzing the radiation spectra, researchers can infer the density distribution within the plasma.

Although the oblique collision of laser beams offers advantages in terms of energy transfer and localized dipole formation, it is important to consider potential drawbacks that may arise when the collision angle exceeds a certain threshold. One such drawback is the induction of longitudinal and transverse motion of electrons within the plasma. When the laser pulses collide obliquely, the interaction dynamics between the laser fields and the plasma become more complex. The oblique angle introduces a component of force that can induce not only oscillatory motion but also a net momentum transfer to the electrons. This can lead to longitudinal motion along the direction of laser propagation as well as transverse motion perpendicular to the laser propagation direction. The induced longitudinal motion can result in a displacement of the electrons along the laser axis, potentially causing changes in the plasma density distribution. This displacement can affect the overall dynamics of the plasma and influence the accuracy of density measurements. Additionally, the induced transverse motion can lead to particle diffusion or even plasma expansion in the transverse direction, which may impact the stability and confinement of the plasma. The extent of these electron motions depends on various factors, including the collision angle, laser parameters, and plasma conditions. It is crucial to carefully consider and control these factors to minimize any undesirable effects on the plasma and the accuracy of density measurements. Mitigation

strategies can be employed to address these potential drawbacks. For example, adjusting the laser pulse parameters, such as pulse duration and intensity, can help optimize the energy transfer efficiency while minimizing electron motion. Additionally, employing advanced plasma confinement techniques, such as magnetic fields or tailored plasma geometries, can aid in reducing transverse expansion and improving the stability of the plasma during oblique collisions.

Indeed, the impact angle of the laser pulses in the oblique collision configuration can introduce an element of unpredictability in determining the exact location of the dipole formation. This unpredictability arises from the combined effects of the collision angle, laser intensity, plasma properties, and the overall dynamics of the interaction. When conducting measurements to evaluate local densities in plasmas using this method, it becomes crucial to carefully examine and control the impact angle. The angle should be selected based on the desired objectives and the specific characteristics of the plasma being studied. A thorough understanding of the plasma properties and the expected behavior of the laser-plasma interaction is necessary to optimize the angle and minimize any potential uncertainties in the dipole location. In the experimental setup depicted in Fig.24(a), where the laser entrance window is stationary and located far away from the plasma, it provides a reference point for establishing a consistent and well-defined collision geometry. By keeping the laser entrance window fixed and ensuring that it is sufficiently distant from the plasma region, one can minimize any unintended variations or disturbances in the laser pulse trajectories. However, it is important to note that the actual impact position of the laser pulses within the plasma can still be influenced by factors such as laser beam quality, plasma density gradients, and the presence of instabilities. These factors can introduce some level of uncertainty in determining the precise location of the dipole formation. To mitigate these uncertainties, advanced diagnostic techniques, such as interferometry or time-resolved imaging, can be employed to visualize and track the evolution of the plasma density during the laser pulse collision. These techniques can provide valuable insights into the dynamics of the dipole formation and help validate the accuracy of the density measurements.

In order to ensure accurate replication of the original density profile, careful selection of the laser launching point is essential. As shown in Fig.24(b), the crossing angle of the laser pulses was limited to less than $15°$ to minimize any potential uncertainties in the dipole formation and the subsequent measurement of local densities. By maintaining a relatively small crossing angle, the laser pulses interact within a well-defined region, allowing for a more controlled and predictable collision process. This ensures that the resulting dipole formation and the emitted radiation are influenced predominantly by the specific density distribution of the plasma. By utilizing this method and restricting the crossing angle, you were able to successfully replicate the original density profiles of various linear density gradients. This demonstrates the effectiveness of the approach in accurately capturing the density variations within the plasma.

Non-linear density

In the study of plasma systems, it is important to consider not only linear density profiles but also non-linear density gradients that are commonly observed in both confined and unbounded plasmas. While the
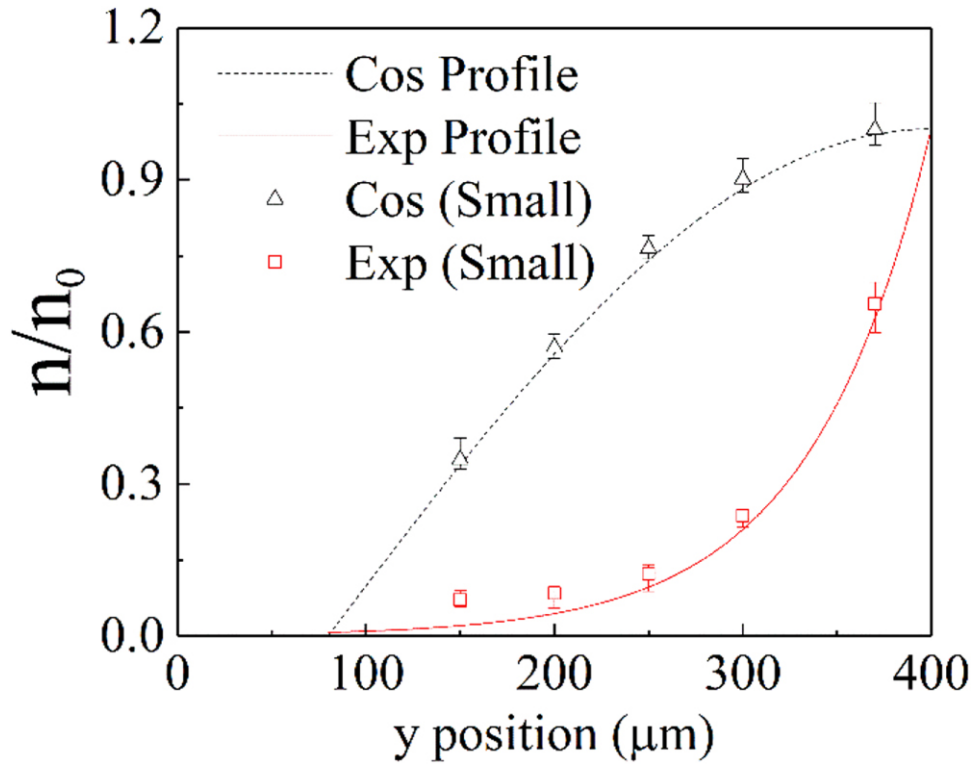
Figure 26: Density profiles including cosine and exponential. Exact forms of profiles are $n/n_0 = \cos[(y-400)/640]$ and $n/n_0 = \exp[(y-400)/100]$ with $n_0 = 4.96 \times 10^{18}$ cm^{-3}, which are represented by dashed and solid lines, respectively. Laser pulses were collided at modest angles ($< 15°$) with the same settings as Fig.25. Data points are based on the simulation dataset where laser pulses are obliquely fired.

Particle-in-Cell (PIC) simulation method coupled with the dipole technique has demonstrated success in accurately reproducing linear density profiles, it is also theoretically applicable to nonlinear profiles. To assess the effectiveness of the dipole technique in capturing nonlinear density gradients, the researcher in this study created two test cases: a trigonometric function and an exponential function. These functions were chosen due to their prevalence in plasma systems and their ability to represent different types of density distributions. The results, as depicted in Fig.26, demonstrate that the dipole technique can accurately reproduce the original density profiles for both the trigonometric and exponential functions. The reconstructed profiles exhibit minimal error bars, indicating a high level of fidelity in capturing the underlying density variations.

The observed discrepancy between the predicted and actual results in the low-density zone of the exponential density profile can be attributed to various numerical and physical factors. One possible factor is the limited number of simulation particles employed in the study. At low densities, the number of particles representing the plasma becomes insufficient, leading to higher numerical inaccuracies and potentially affecting the accuracy of the density reconstruction. Another factor that could contribute to the discrepancy is the size of the dipole compared to the wavelength of the dipole radiation. If the dipole size is significantly smaller than the wavelength, it can result in distortions in the dipole's oscillation frequency, which in turn can affect the accuracy of the density measurements. This aspect requires further investigation and validation to assess its impact on the density reconstruction process. Additionally, it is important to consider the limitations of the PDO method itself. The method may not be suitable for monitoring deep density troughs, as the radiation emitted by the PDOs within such troughs may have a frequency lower than the cutoff frequency of the denser regions in the surrounding plasma. This can make it challenging to accurately measure and reconstruct the density variations in these regions using the dipole technique.

In the presented study (Fig. 22), a monotonic density profile with a density trough spanning from $200\mu m$ to $300\mu m$ in the y-direction was successfully generated, and the density reconstruction using the dipole technique exhibited high precision within the monotonic segments of the profile ($100\mu m < y < 200\mu m$ and $300\mu m < y < 400\mu m$). However, the accuracy of the density measurements within the trough region was compromised. The observed discrepancy in the error bars within the density trough can be attributed to the presence of a density bump on the left side of the trough. The density bump acts as an obstacle for the emitted waves, selectively allowing only spectral components with frequencies higher than the plasma frequency at $y = 200\mu m$ (referred to as $\omega_p, 200\mu m$) to pass through it. Consequently, the density values derived from the emitted radiation frequencies tend to converge near the density peak of the bump, which corresponds to $y = 200\mu m$. This behavior highlights a limitation of the dipole technique in accurately measuring the density within regions obstructed by density variations. The presence of sharp density gradients or localized features, such as the density bump in this case, can significantly affect the emitted radiation and introduce complexities in the density reconstruction process. Further investigations and refinements are necessary to mitigate these challenges and improve the accuracy of density measurements in regions with density troughs and other non-monotonic density profiles.
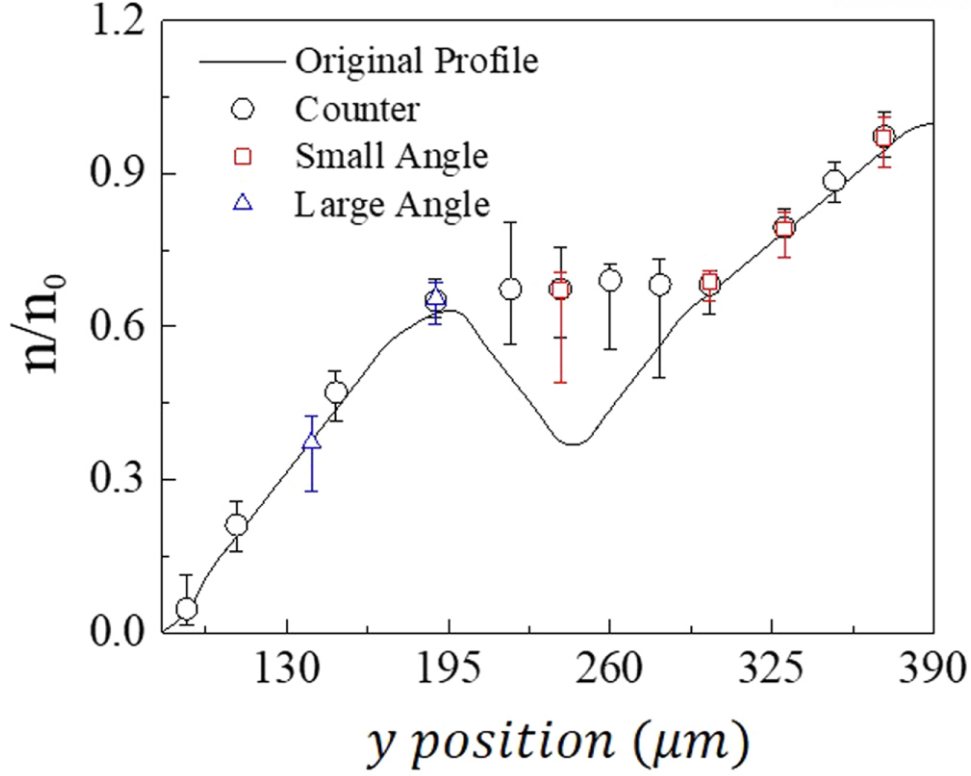
Figure 27: Reconstruction of density profiles that do not increase monotonically. The vertical axis shows the reconstructed value normalized by the maximal value $n_0 = 4.96 \times 10^{18} \text{cm}^{-3}$. The laser field's normalized peak amplitude is $a_0 = 0.3$. Figures 3 and 4 show the simulation domain with the same dimensions. The laser pulses have wavelengths of 800 and 780nm, a pulse duration of 30fs, and a spot size of 5μm.

The observed low radiation intensity within the density trough can be attributed to the high absorption of radiation energy by the ambient plasma cut-off. This absorption phenomenon causes a reduction in the overall radiation intensity originating within the density trough compared to other locations in the plasma. Additionally, the spectral power of the emitted radiation decreases with increasing frequency, leading to a lower intensity of radiation passing through the density bump. The peak in the radiation spectrum at the plasma frequency ω_p in $200\mu m$ further complicates the density measurement within the trough. This peak results in a relatively flat density measurement across the trough at $y = 200\mu m$, as the radiation passing through the density bump primarily carries information about the density peak rather than the actual density decline within the trough.

3.3 Discussion

Scaling parameters

The ratio of dipole size to radiation wavelength is a critical statistic in the scope of the PDO method. This ratio is crucial in establishing the features of the dipole-like radiation emitted. Investigating the scaling nature of this ratio might provide important insights into the PDO method's applicability across other

plasma parameter regimes. Scaling estimates enable dipole and radiation behavior to be generalized to larger or smaller systems without requiring massive amounts of computer resources or lengthy simulations. By identifying the essential components that determine dipole size and radiation wavelength, scaling rules are established that provide a simple yet effective technique for predicting the behavior of the PDO method in varied plasma systems. Scaling concepts might be extended to other plasma regimes, such as Tokamaks, to substantially reduce processing requirements and accelerate the evaluation of local density profiles. These scaling estimates provide for a better understanding of the PDO technique's projected behavior in various plasma configurations, allowing for more informed judgments concerning experimental settings and data processing.

$$R = \frac{l}{\lambda} \tag{80}$$

where l is dipole displacement and λ is radiation wavelength. Another parameter is the product of pulse amplitude and duration (D).

$$D = E_0 \tau \tag{81}$$

R parameter

The displacement of the dipole in the PDO method is determined by the phenomenon known as beat wave dragging. The beat wave, which is created by the collision of the laser pulses, propagates through the plasma at a phase velocity denoted by v_ϕ. This phase velocity can be calculated as the ratio of the frequency difference $\Delta\omega$ to the wavenumber difference Δk, i.e., $v_\phi = \Delta\omega/\Delta k$. In typical scenarios, the frequency difference $\Delta\omega$ is set to be approximately within the range of the plasma frequency ω_p, and the wavenumber difference Δk can be approximated as twice the wavevector magnitude, which is equal to $2k = 2\omega/c$, where ω is the laser frequency and c is the speed of light. The dragging time, which determines the displacement of the dipole, is approximately proportional to the duration of the laser pulse. Incorporating these factors, the dipole displacement can be expressed as $v_\phi \tau \sim \omega_p/2\omega c\tau$, where τ represents the pulse duration. The radiation wavelength associated with the dipole emission can be calculated as $\omega_p/2\pi c$, where ω_p is the plasma frequency. To characterize the radiation intensity relative to the plasma density, pulse duration, and wavelength, a scaling parameter denoted by R is introduced. The scaling parameter is given by $R \sim \omega_p^2/4\pi\omega\tau$. It serves as an index for the radiation intensity and reflects the interplay between the plasma density, laser pulse duration, and wavelength. In the case of low-density plasmas, it is necessary to adjust the laser frequency to a lower value to match the plasma properties. Additionally, longer pulse durations are preferred to achieve optimal results.

D parameter

The parameter D plays a significant role in determining the electron trapping threshold and regulating the energy deposition by external electromagnetic (EM) sources into the plasma. By adjusting the amplitude and duration of the laser pulse, or a combination of both, we can manipulate the value of D to match the requirements of different plasma systems. In normalized form, the parameter D is defined as

follows:

$$D = a_0 \omega \tau \tag{82}$$

This parameter represents the ratio of the electric field energy to the electron rest mass energy, multiplied by the square root of the ratio of the electron mass to twice the vacuum permittivity. It provides a measure of the intensity of the external EM fields relative to the electron dynamics in the plasma. By manipulating the pulse amplitude, duration, or both, we can control the value of D. Increasing the pulse amplitude or duration leads to a higher value of D, indicating a stronger interaction between the laser pulse and the plasma electrons. This can result in enhanced electron trapping and increased energy deposition. Conversely, decreasing the pulse amplitude or duration reduces the value of D, resulting in a weaker interaction between the laser pulse and the plasma electrons. This can be advantageous in scenarios where a more gentle energy deposition or a lower electron trapping threshold is desired. Assuming that the spot size of the laser beam is smaller than the diffraction threshold ($\sigma \sim \lambda$), the laser intensity can be related to the laser power. The amplitude (I) of a laser beam is defined as the power (P) per unit area (A) and can be expressed as:

$$I = \frac{P}{A} \tag{83}$$

The power of the laser beam is a measure of the total amount of energy delivered per unit time. It represents the rate at which energy is transferred to the target or the surrounding medium. On the other hand, the area of the laser beam corresponds to the spatial extent over which the power is distributed. In situations where the spot size of the laser beam is smaller than the diffraction limit, we can approximate the area by considering the cross-sectional area of the laser beam. This area is roughly proportional to the square of the spot size. Thus, the laser intensity, which is defined as the power per unit area, can be expressed using this relationship.

$$I \propto \frac{P}{\sigma^2} \tag{84}$$

where σ represents the spot size of the laser beam, and P denotes the laser power. This relationship implies that as the laser power increases while keeping the spot size constant, the laser intensity will also increase. Conversely, reducing the laser power while maintaining the same spot size will result in a decrease in laser intensity. Finally, relation between laser amplitude and power is

$$a_0 \sim \sqrt{\frac{P[W]}{3 \times 10^5}} \tag{85}$$

Application scaling parameters for each plasma system

In order to tailor our simulations for fusion plasma in a Tokamak, such as in the case of a Tokamak fusion reactor, adjustments would be necessary for the values of parameters R and D. These parameters play a crucial role in determining the characteristics of the laser pulses used in our diagnostic technique. Based on predicted values derived from R and D, we can estimate the required duration and power for probing a plasma with a density of 10^{14}cm^{-3} and a wavelength of $10\mu\text{m}$. In this scenario, the estimated

duration is around 10 picoseconds (ps), and the power required is in the range of megawatts (MW). Remarkably, these values can be readily achieved using CO_2 lasers, which makes our diagnostic technique well-suited for practical application in fusion research.

In the realm of plasma physics, the properties and behavior of plasmas can vary significantly depending on their density. High-density plasmas, characterized by a large number of charged particles per unit volume, often require intense pulse power to initiate and sustain their unique state. However, when dealing with lower density plasmas, the pulse power requirements are generally relaxed. One common method for generating low-temperature plasmas (LTP) involves the application of a voltage differential between two electrodes immersed in a gas or liquid medium. This technique, known as electrode discharge, effectively induces ionization and creates a plasma. By adjusting the parameters of this setup, particularly the distance between the electrodes (referred to as D), researchers can achieve the desired plasma density and other relevant properties. One notable advantage of working with lower density plasmas is the reduced pulse power necessary for their production and maintenance. Compared to high-density plasmas, which often demand substantial energy inputs, low-density plasmas can be sustained with lower levels of pulse power. By properly optimizing the value of D, it becomes possible to reach the critical threshold for electron trapping, a phenomenon crucial for plasma formation, with significantly reduced pulse power.

Collision Impact on PDO in low density plasma

The sustained operation of plasma discharge oscillators (PDOs) is of utmost importance for their practical applications. However, like other cross-beam methods such as plasma photonic crystal and plasma holography, PDOs can be susceptible to disruption due to collisional events. These collisions hinder the sustainability and effectiveness of PDOs in fulfilling their intended functions. Collisional events in PDOs primarily involve interactions between electrons and neutrals, as well as interactions between electrons and ions. These collisions can impede the smooth operation of PDOs and hinder their stability. Understanding and mitigating these collisional effects is crucial for optimizing the performance and longevity of PDO-based systems. One specific type of collision that occurs in PDOs is electron-neutral collisions. In plasmas, the frequency of these collisions is often assumed to follow a Maxwellian distribution. The Maxwellian distribution describes the statistical behavior of particles within the plasma and provides insights into their collisional interactions. By considering the Maxwellian distribution, researchers can analyze and model the collisional effects in PDOs, aiding in the development of strategies to mitigate their impact. In addition to electron-neutral collisions, collisions between electrons and ions also play a significant role in the disruption of PDO operation. These collisions can result in energy transfer, momentum exchange, and changes in the overall plasma dynamics. Managing and controlling these collisions are crucial for maintaining the stability and sustained operation of PDOs. The challenges posed by collisional events are not unique to PDOs but are also encountered in other cross-beam methods such as plasma photonic crystal and plasma holography. These techniques, despite their unique characteristics and potential applications, share the common hurdle of collision-induced disruptions. Researchers

in these fields are actively investigating methods to overcome these challenges and improve the sustainability and performance of their respective technologies.

$$v_{en}[s^{-1}] \sim 2 \times 10^{-7} n_n [cm^{-3}] (T_e [eV])^{1/2} \tag{86}$$

When considering low-temperature plasmas (LTP), such as inductive coupled plasmas (ICPs), the collision frequency is often negligible compared to the plasma frequency. In the case of ICPs, which typically operate within a pressure range of 0.3 to 1000 mTorr, the collision frequency can be estimated based on the neutral density (n_n) and the electron temperature range. For instance, assuming a neutral density of 10^{13} cm^{-3} and an electron temperature spanning from 1.8 eV to 11 eV, the maximum collision frequency can be calculated. However, it is important to note that collision frequencies vary with the specific conditions of the plasma and the interaction cross-sections between particles. Considering the given parameters, the collision frequency can be estimated to be approximately 1 MHz. Meanwhile, the plasma frequency, which characterizes the collective oscillations of charged particles in the plasma, typically covers a range from a few to several hundred GHz for plasma densities on the order of 10^{11} to 10^{12} cm^{-3}. The significant disparity between the collision frequency and the plasma frequency highlights the dominance of collective plasma phenomena over collisional events in LTPs. This implies that, in many cases, the effects of individual particle collisions can be overshadowed by the overall behavior of the plasma, driven by collective interactions and wave phenomena. Expanding on this concept can help in understanding the dynamics and properties of LTPs, as well as designing plasma-based systems and technologies. By focusing on the collective behavior of the plasma, researchers can exploit phenomena such as plasma waves, resonances, and mode coupling, which play critical roles in many plasma applications.

The operational conditions for plasma discharge oscillators (PDOs) appear to be favorable in the scrape-off layer (SOL) or edge plasma of a Tokamak fusion reactor. In this region, characterized by a temperature of approximately 1 keV, the neutral density is relatively low. Even in regions close to the divertor target, where the neutral density reaches a maximum value of 10^{14} cm^{-3}, the frequency of electron-neutral collisions remains lower than the plasma frequency, which typically lies around 1 GHz. Consequently, the impact of electron-neutral collisions on the emission of PDOs in various plasma sources, including Tokamaks, may not be significant. The SOL, located at the periphery of a Tokamak plasma, serves as a transition region between the confined plasma in the core and the material surfaces of the reactor vessel. With a temperature of approximately 1 keV, the SOL provides conditions conducive to PDO operation. The relatively high electron temperature promotes ionization and sustains the plasma state necessary for PDO emission. Although the neutral density in the SOL is low, even near the divertor target where the neutral density is at its highest, it remains below 10^{14} cm^{-3}. Consequently, the frequency of electron-neutral collisions in this region remains lower than the plasma frequency. As a result, the impact of these collisions on the emission of PDOs is expected to be negligible. This favorable scenario in the SOL or edge plasma of Tokamaks implies that PDOs can effectively operate without significant disruption caused by electron-neutral collisions. It allows for the exploration and utilization of PDO-based techniques for various applications within Tokamaks, including plasma diagnostics, heat-

ing, and control. It is worth noting that while electron-neutral collisions may not significantly affect PDO emission in most plasma sources, other factors such as electron-electron collisions, plasma instabilities, and wave-particle interactions can still influence the performance of PDOs. Therefore, a comprehensive understanding of the plasma environment and its associated phenomena is crucial for optimizing the design and implementation of PDO-based systems in Tokamaks and other plasma devices.

Collision Impact on PDO in high density plasma

In fully ionized and high-density plasmas, often generated by lasers, the oscillation of plasma discharge oscillators (PDOs) can be susceptible to disruption caused by electron-ion collisions. Unlike the previously mentioned low-temperature plasmas, where electron-neutral collisions were of primary concern, in high-density plasmas, electron-ion collisions play a significant role in affecting the behavior of PDOs. The frequency of electron-ion collisions can be estimated based on the properties of the plasma. However, it is important to note that the collision frequency depends on various factors, including the plasma density, electron temperature, and ion species present in the plasma. To further delve into the details, a thorough understanding of the electron-ion collision frequency is necessary. This frequency quantifies the rate at which electrons and ions collide within the plasma. Its precise determination requires consideration of factors such as the interaction cross-sections, the energy distribution of particles, and the species-dependent collision frequencies. In high-density plasmas produced by lasers, the plasma is often fully ionized, meaning that the vast majority of atoms are ionized, leaving only free electrons and ions. In such scenarios, electron-ion collisions can significantly impact the behavior of PDO oscillations. The collision frequency resulting from electron-ion collisions can influence various aspects of PDO operation, such as the energy transfer between particles, momentum exchange, and the overall plasma dynamics. These collisions can modify the electron distribution function and affect the plasma's ability to sustain the necessary conditions for PDO emission. While electron-ion collisions can introduce disruptions to PDO oscillations, researchers and engineers strive to mitigate their adverse effects through careful experimental design and optimization. This includes considering the plasma parameters, such as density and temperature, as well as the choice of ion species and their corresponding cross-sections for collisional interactions.

$$v_{ei}[s^{-1}] \sim 3 \times 10^{-5} n_e \text{cm}^{-3} T_e^{-3/2} \tag{87}$$

According to the frequency analysis, in order to ensure that the collision frequency between electrons and ions (v_{ei}) remains less than 10% of the plasma frequency (f_p) in a high-density plasma with $n_e \sim 10^{18} \text{cm}^{-3}$ (as used in this study), the electron temperature (T_e) needs to be greater than 1-2 eV [74]. Fortunately, many laser-plasma interactions satisfy this requirement by having electron temperatures exceeding the specified threshold. Furthermore, in the context of plasma dipoles, the electron bunch inherent in the dipole structure tends to have a high temperature. This arises due to the formation of the plasma dipole through trapped electrons in the ponderomotive potential train, which is caused by phase-mixing processes. These processes often lead to electron heating, resulting in a hot electron bunch. The thermal velocity of the electron bunch within the plasma dipole is on the order of $\beta = v/c \sim 0.01$,

corresponding to an electron temperature of approximately 50 eV. This temperature is sufficiently high to render the collision frequency between electrons and ions (ν_{ei}) insignificant. Thus, even though the particle-in-cell (PIC) code used in the study does not incorporate collisional processes, the results remain accurate because electron-ion collisions do not significantly impact the disruption of PDOs at such high temperatures. The absence of electron-ion collisions as a disruptive factor in PDO operation at high temperatures simplifies the analysis and interpretation of the results obtained from the PIC simulations. By focusing on the dominant processes and effects driving the PDO behavior, researchers can confidently rely on the accuracy and reliability of the simulation outcomes.

PDO radiation emission

The intensity of plasma discharge oscillator (PDO) emission plays a crucial role in the detectability of the emitted signal. It directly influences the number of photons emitted per unit time, thereby impacting the signal-to-noise ratio of the detector. A higher intensity of emission translates to a stronger signal, improving the detectability and overall quality of the measurement. The intensity of PDO emission is directly proportional to the square of the amplitude of the dipole oscillation. As discussed earlier, the amplitude is determined by the parameters R and D, which characterize the dimensions and properties of the plasma dipole. By controlling these parameters, researchers can manipulate the intensity of the emitted radiation. The field strength of PDO radiation can be approximated using the expression $E = E_0 \sigma_{di}/r$, where E represents the electric field strength, E_0 is a constant, σ_{di} denotes the dipole cross-section, and r is the distance from the source. This approximation provides an understanding of the relationship between the emitted field strength and the relevant parameters. By adjusting the parameters R and D, researchers can effectively modulate the intensity of PDO emission. Increasing the dipole dimensions or altering the characteristics of the plasma dipole can lead to a higher amplitude of oscillation and, consequently, a stronger emitted signal. This has significant implications for the detectability and sensitivity of PDO-based detection systems.

To assess the detectability of plasma discharge oscillator (PDO) emission, power calculations can be performed, taking into account the transverse width of the dipole (σ_{di}) and the field strength at its transverse position (E_0). In laser-produced plasmas, which are often employed in PDO studies, the typical spot size of the laser pulse (σ) is comparable to the plasma wavelength ($\lambda_p = 2\pi c/\omega_p$), where ω_p is the plasma frequency. At a distance r from the emission source, which is typically chosen as $r \sim N\lambda_p$, with $N \sim 100$, the field strength E can be approximated as E_0/N. This consideration allows us to estimate the field strength at a measurable location based on the known parameters. For the plasma conditions considered in this study, the field strength at the dipole transverse position, E_0, is estimated to be approximately 1 GV/m. Consequently, at the measuring location, the field strength E is on the order of 10 MV/m, which is a significant and powerful signal. Such a field strength is well above the detection threshold of many measurement techniques commonly used in experimental setups. It is typically easily detectable by various detection systems, including probes, antennas, or other suitable receivers. The strong field strength enhances the likelihood of capturing and measuring the emitted signal accurately,

66

further contributing to the reliability of PDO-based measurements. Furthermore, the selected distance ($r \sim N\lambda_p$) takes advantage of the favorable properties of plasma waves and radiation propagation. By positioning the measuring location at a multiple of the plasma wavelength, the emitted radiation experiences constructive interference and optimal signal transmission. This positioning ensures that the measured field strength is maximized, further aiding in its detectability.

In the context of nuclear fusion or low-temperature plasmas, the plasma wavelength (λ_p) tends to be larger compared to laser-produced plasmas. For instance, at a density of $n_e \sim 10^{14}$ cm^{-3}, the plasma wavelength can be approximately 1 mm. In such scenarios, it may be advantageous to position the detection equipment at a distance of 1 m, using $N \sim 1000$ as a suitable multiple of the plasma wavelength. Considering a field strength E_0 that is proportional to the plasma density (n_e) and assuming E_0 to be on the order of 10^5 V/m, the calculated field strength at 1 m from the dipole would be of the order of a few hundred V/m. Despite being smaller than in laser-produced plasmas, this field strength remains quite strong and easily measurable. A few hundred V/m is well above the noise floor of typical detection systems used in nuclear fusion or low-temperature plasma experiments. Measurement techniques such as probes, antennas, or other appropriate receivers can effectively capture and measure signals of this magnitude. Furthermore, it is important to note that the specific field strength values provided here are approximate and depend on various factors, including the plasma density, dipole parameters, and the specific experimental setup. These values serve as examples to demonstrate the detectability of PDO emission in different plasma conditions.

Temperature effect on the formation of PDO

In high-temperature plasmas, such as those found in fusion research devices like Tokamaks, the formation and detection of dipoles can be significantly influenced by the plasma's elevated temperature. In these hot plasmas, ensuring a high signal-to-noise ratio (SNR) is of paramount importance for accurate measurements, as the desired signal arises from the dipole field while the noise originates from thermal fluctuations within the plasma. The SNR is a crucial factor in any measurement or detection system, representing the ratio of the desired signal to the background noise. In the context of PDOs, it is essential to maximize the SNR to extract meaningful information from the dipole field and minimize the impact of thermal noise on the measurement accuracy. Hot plasmas pose challenges to achieving a high SNR due to the elevated thermal energy levels within the system. Thermal fluctuations in the plasma generate random noise that can obscure the dipole signal, making it more difficult to discern the desired signal amidst the background noise. Therefore, careful consideration and design of measurement techniques are necessary to optimize the SNR in these high-temperature plasma environments.

To investigate the influence of electron temperature (T_e) on dipole formation, a series of 1D simulations were conducted, employing standard parameters as used in this study. The simulations were performed for different T_e values, and the results obtained for T_e values of 1 keV and 10 keV are presented in Figure 28. The simulations, based on particle-in-cell (PIC) techniques, provide valuable insights into the behavior of the plasma system under varying T_e conditions. Remarkably, the results reveal that even at a

relatively high T_e of 10 keV, dipole oscillations can still be observed. This finding suggests that the dipole approach holds promise for measuring the density of the core plasma in fusion research devices, including Tokamaks. The ability to observe dipole oscillations at elevated T_e values is significant for fusion research, as it indicates that the dipole method remains viable in capturing important plasma characteristics, such as core plasma density. This capability opens up possibilities for utilizing the dipole approach in Tokamaks and other fusion devices, where accurately measuring the density of the core plasma is of utmost importance.

It is worth noting that the simulations presented in the study may underestimate the signal-to-noise ratio (SNR) due to the inherent thermal noise present in the system. In these simulations, thermal noise can be amplified due to Poisson sampling, and the particles in the simulation represent macro-particles. However, by increasing the number of simulation particles, the numerical-thermal noise is significantly reduced, resulting in a more accurate representation of the dipole oscillation and making it easier to detect. In Fig. 28(b), the red line represents the dipole oscillation obtained with a higher number of simulation particles, showcasing a more pronounced and easily detectable signal. This demonstrates the importance of utilizing a sufficiently large number of particles in the simulations to minimize the impact of numerical-thermal noise and obtain reliable results. Furthermore, the dipole oscillation becomes even more evident at higher driving pulse intensities, as shown by the blue line in Fig. 28(b). This indicates that increasing the intensity of the driving pulse can enhance the detectability of the dipole signal, further emphasizing the need to carefully consider the experimental parameters to optimize the SNR. For future research focusing on 2D radiation simulations, it is essential to incorporate a large number of simulation particles to accurately capture the noise level and reproduce realistic experimental conditions. However, it is important to acknowledge that utilizing a larger number of particles requires significant computational resources, highlighting the computational challenges associated with such simulations.

The nature of the dipole oscillation in plasma optical dipole emission (PDO) is distinct, as it is primarily an intrinsic oscillation rather than a propagating wave. At the generation points, electrons within the PDO exhibit a high level of thermal energy, leading to the generation of Langmuir waves that follow the Bohm-Gross dispersion relation. However, during the radiation emission process, the influence of Langmuir waves can be disregarded due to the relatively short time period involved. Consequently, the PDO field remains unaffected by thermal noise and retains its integrity. Therefore, whether the plasmas are initially thermal or cold does not significantly impact the behavior of the PDO. The large field strength of the PDO ensures its stability and insensitivity to thermal noise, making it a reliable diagnostic tool for various plasma conditions. In contrast, the presence of a magnetic field has a considerable influence on the frequency and direction of the dipole oscillation. Magnetic fields can significantly alter the dynamics of the PDO and introduce additional complexities to its behavior. The dipole method's sensitivity to magnetic fields presents an exciting opportunity for measuring the strength and direction of highly magnetized plasmas, commonly encountered in fusion experiments and other magnetized plasma systems. By exploiting the sensitivity of the dipole method to magnetic fields, researchers can gain valuable insights into the characteristics of magnetized plasmas, including their strength and directional properties. This feature makes the dipole method a promising tool for studying and understanding the
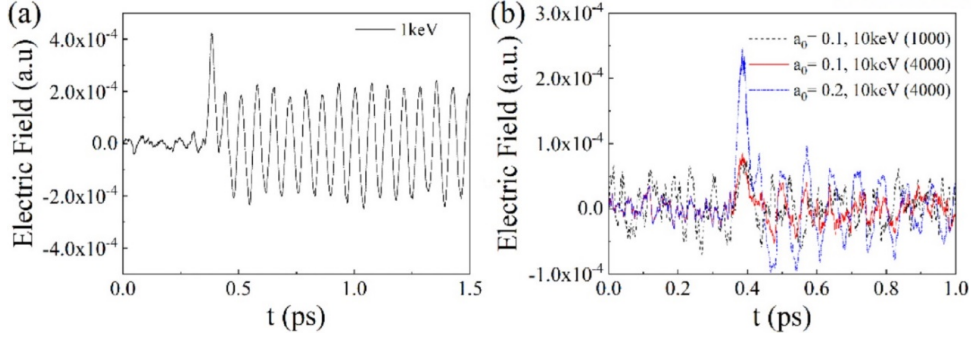
Figure 28: Thermal effect on the PDO formation at (a) 1 keV and (b) 10 keV. Field intensities are $a_0 = 0.1$ for 1keV and $a_0 = 0.1$ and 0.2 for 10keV. By increasing the number of particles, simulations were monitored to suppress the noise.

behavior of highly magnetized plasmas in fusion experiments and other relevant research endeavors.

In the course of my investigation, I have focused on studying the size of plasma optical dipole emission (PDO), which is determined by the parameters of the driving pulse. The pulse spot radius, denoted by σ, along with its duration, characterized by $c\tau$, play crucial roles in defining the dimensions of the PDO. It is important to note that these dimensions are typically smaller than the density gradient of the plasma, represented by $L_{grad} = n/\nabla n$. The small size of the PDO relative to the density gradient holds significant implications for plasma diagnostics. In such a scenario, the quasi-narrowband spectra of the PDO radiation can serve as a powerful tool for accurately pinpointing the local density of the plasma. By analyzing the characteristics of the emitted radiation, researchers can extract valuable information about the density distribution within the plasma. The ability to accurately determine local density through PDO radiation is of great importance in various plasma research applications. It provides insights into the spatial variation of plasma density, which is crucial for understanding plasma dynamics, identifying instabilities, and optimizing plasma parameters for desired outcomes. The quasi-narrowband spectra of the PDO radiation enable precise mapping of density variations, allowing for detailed analysis and control of plasma behavior.

The ability to obtain localized density measurements through plasma optical dipole emission (PDO) and its quasi-narrowband spectra offers researchers valuable tools for diagnosing plasma properties and gaining a deeper understanding of plasma phenomena. This capability has the potential to revolutionize plasma research, particularly in the context of fusion experiments, where achieving stable and efficient plasma confinement is of utmost importance. In fusion experiments, such as those conducted in Tokamaks, precise knowledge of the plasma density distribution is crucial for maintaining the desired plasma conditions. The ability to accurately diagnose and map the density variations within the plasma enables researchers to optimize the plasma confinement and stability. By analyzing the quasi-narrowband spectra of PDO radiation, researchers can obtain localized density measurements, which provide critical information for controlling and adjusting plasma parameters to enhance performance and mitigate instabilities. The application of PDO in fusion research extends beyond density diagnostics. The localized density measurements obtained through PDO can be utilized to study plasma turbulence, particle

transport, and the interaction between the plasma and magnetic fields. Understanding these fundamental processes is vital for improving the efficiency and sustainability of fusion reactions. Moreover, the precise characterization of plasma density through PDO opens up new avenues for advanced plasma control techniques. By utilizing the localized density information, researchers can develop feedback control systems to actively adjust plasma parameters in real-time, ensuring stable and optimized plasma conditions. This dynamic control capability has the potential to enhance plasma confinement, increase fusion reaction rates, and improve overall experimental outcomes. Furthermore, the application of PDO and its quasi-narrowband spectra is not limited to fusion experiments alone. It finds relevance in various plasma research areas, such as astrophysics, plasma diagnostics in industrial applications, and laboratory plasma experiments. The ability to accurately diagnose and map plasma density variations provides valuable insights into the behavior of plasmas in diverse settings, facilitating the development of improved plasma sources, plasma-based technologies, and advanced plasma processing techniques.

When the plasma density gradient aligns with the necessary conditions, it enables the density within the laser spot, where the induced plasma optical dipole oscillation (PDO) occurs, to become quasi-homogeneous. In this scenario, the plasma density exhibits relatively uniform characteristics within the laser spot region, facilitating efficient dipole oscillation in a homogeneous plasma environment. This quasi-homogeneity is essential for maintaining a well-defined oscillation mode and achieving monochromatic radiation from the PDO. However, when the plasma density exhibits significant variations compared to the size of the laser spot or the pulse duration, the situation becomes more complex. In such cases, the local density variations within the laser spot can lead to the generation of multiple oscillation modes that may overlap or interact with each other. This mixing of oscillation modes can result in uncertainties in the PDO's oscillation frequency and a reduction in radiation monochromaticity. The presence of significant density variations within the plasma introduces additional complexity to the dynamics of the PDO. Different regions of the laser spot experience different local densities, which can lead to the generation of multiple oscillation modes associated with the respective local densities. These oscillation modes can interfere with each other, causing frequency mixing and broadening of the radiation spectrum. The uncertainty in the PDO's oscillation frequency arises from the superposition of different oscillation modes with distinct frequencies originating from the local density variations within the laser spot. The resulting radiation spectrum becomes broader, encompassing a range of frequencies rather than a single well-defined frequency. This reduction in radiation monochromaticity poses challenges for precise frequency characterization and can affect the accuracy of density measurements based on the PDO. To mitigate the effects of density variations on the PDO's oscillation frequency and radiation monochromaticity, efforts can be made to minimize the density gradients within the plasma or tailor the laser parameters to match the plasma density profile. By optimizing the experimental setup and adjusting the laser parameters, it is possible to achieve a better balance between the plasma density variations and the size/duration of the laser spot, thereby enhancing the monochromaticity of the emitted radiation.

In the context of plasma diagnostics using plasma optical dipole emission (PDO), the tolerance of the dipole oscillation to high-density gradients is a critical factor in determining the highest measurable density gradient. This investigation is crucial for understanding the limitations and optimizing the diag-

nostic utility of the PDO approach. One key parameter that affects the dipole oscillation's tolerance to density gradients is the size of the laser spot, characterized by the spot radius σ. When the density gradient across the dipole dimension becomes significant, with fluctuations exceeding 10% of the average density, the spectral broadening of the PDO emission becomes prominent. This broadening can greatly diminish the diagnostic utility of the PDO approach, as it leads to an overlap of different oscillation modes and reduces the ability to precisely measure the density distribution. Additionally, the pulse duration $c\tau$ of the laser pulse plays a crucial role in determining the dipole oscillation's tolerance to density gradients. The ratio of $c\tau$ to the density gradient length scale L_{grad} serves as an indicator of the relative importance of the pulse duration compared to the density variation. When $c\tau/L_{grad}$ exceeds 0.1, it signifies a significant density fluctuation across the dipole dimension. In such cases, the spectral broadening of the PDO emission becomes especially significant, further diminishing the diagnostic accuracy. To determine the highest measurable density gradient and derive a precise expression for it, a thorough investigation is required. This investigation involves conducting detailed simulations and experimental studies to explore the behavior of the dipole oscillation under different density gradient conditions. By systematically varying the density gradient, laser spot size, and pulse duration, researchers can analyze the resulting PDO emission spectra and quantify the spectral broadening effects. The outcome of this investigation will provide insights into the dipole oscillation's tolerance to high-density gradients and help determine the maximum measurable density gradient within the constraints of maintaining acceptable spectral broadening. The precise expression derived from this study will serve as a valuable tool for plasma researchers and diagnostic practitioners, guiding them in optimizing the experimental parameters to achieve the most accurate and reliable density measurements using PDO.

In the context of PDO, it is important to note that the approach may encounter limitations when applied to plasma density profiles characterized by density bumps or convex shapes, as depicted in Figure 28. In such cases, the radiation generated by the PDO approach tends to experience cutoff effects in front of the convex region or in the center of the density bump. This can significantly impact the accuracy and reliability of the density measurements obtained using the PDO technique. One possible alternative to address this issue is the exploration of second harmonics in the PDO emission. It has been observed that second harmonics, which have higher frequencies, may have better penetration capabilities through density bumps or convex profiles compared to the fundamental harmonic. This suggests that by inducing nonlinear PDO oscillations and generating second harmonics, it may be possible to partially mitigate the limitations posed by density bumps or convex density profiles. To generate second harmonics in the PDO emission, stronger laser pulses are typically required. Nonlinear PDO oscillations can be induced by increasing the intensity of the laser pulses, thereby promoting nonlinear interactions within the plasma and facilitating the production of second harmonics. Several simulations have demonstrated the occurrence of second harmonic generation in the PDO emission. The mechanisms underlying this phenomenon are still the subject of ongoing research. One proposed explanation for second harmonic production involves the reversal of two plasmons decay, where the nonlinear interactions within the plasma lead to the conversion of energy from the fundamental harmonic to the second harmonic. Another possibility is the generation of a nonlinear current through the overlapping of non-symmetric laser pulses, resulting in the

production of higher harmonics in the PDO emission. However, the specific mechanisms responsible for second harmonic generation in PDO emission are still not fully understood and require further investigation. In summary, the PDO approach may encounter limitations when applied to density profiles characterized by bumps or convex shapes. The radiation generated by PDO can experience cutoff effects in front of convex regions or within density bumps. One potential solution to partially address this issue is to explore the generation of second harmonics in the PDO emission. By inducing nonlinear PDO oscillations and promoting the production of higher harmonics, it may be possible to mitigate the limitations posed by density bumps or convex density profiles. However, the mechanisms underlying second harmonic generation in PDO emission are still under investigation, and further research is needed to fully understand and exploit this phenomenon.

3.4 Summary

In my previous research, presented in a study by Kylychbekov et al. [75], I introduced an innovative diagnostic technique aimed at sensing local plasma densities and reconstructing irregular density profiles using simulations. This technique leverages the unique properties of the local Plasma Density Oscillation (PDO) and its emission of electromagnetic (EM) radiation at frequencies close to the plasma frequency. The proposed approach involves the collision of two detuned electromagnetic pulses within the plasma. These pulses can be launched at various angles and positions, either in a head-on configuration or obliquely. The collision of these pulses generates the local PDO, which can be observed and studied in simulations. By carefully varying the launching angle and collision position of the pulses, it becomes possible to reconstruct non-uniform density profiles in two-dimensional Particle-in-Cell (PIC) simulations. This technique has primarily been applied to laser-produced plasmas, as documented in the work by Harilal et al. [76]. However, it holds the potential for extension to low-temperature, collisional plasmas used in plasma processing applications, as well as fusion plasma monitoring. Furthermore, through one-dimensional simulations, I have observed that the dipole oscillation of the PDO remains stable even in very hot plasmas. This finding suggests that the proposed diagnostic approach can also be applied to high-temperature plasma diagnostics, such as those encountered in fusion research. Overall, the technique introduced in my research offers a promising avenue for accurately sensing local plasma densities and reconstructing irregular density profiles. By utilizing the local PDO and its associated emission of EM radiation, this approach can provide valuable insights into plasma properties, making it applicable to a range of plasma systems, including laser-produced plasmas, low-temperature plasmas, and high-temperature fusion plasmas.

IV Magnetic effect on PDO

4.1 Introduction

Plasma dipole oscillation is indeed a novel diagnostic method that holds significant potential for studying density profiles of plasmas in laser plasma experiments. This unique diagnostic technique provides

valuable insights into the behavior and characteristics of plasmas by observing the dipole oscillation mode.

In a plasma dipole oscillation, the plasma density exhibits an oscillatory behavior akin to the dipole moment of a physical dipole. This oscillation is typically induced by an external perturbation or an intrinsic instability within the plasma. By analyzing the properties of the dipole oscillation, researchers can gain valuable information about the density distribution and profile of the plasma.

One of the advantages of plasma dipole oscillation as a diagnostic method is its sensitivity to changes in plasma density. By measuring the frequency of the radiation from the dipole oscillation, researchers can obtain information about the spatial variations in plasma density. This is particularly useful for studying density gradients, plasma boundaries, and the effects of plasma instabilities on the density profile.

The application of the plasma dipole oscillation method extends beyond laser plasmas to Tokamaks, which are magnetic fusion devices used for creating and confining high-temperature plasmas. The unique diagnostic capabilities of the plasma dipole oscillation method can provide valuable insights into the behavior and characteristics of plasmas within Tokamaks. In a Tokamak, the plasma dipole oscillation method can be employed to study the density profiles and fluctuations within the confined plasma. By observing and analyzing the dipole oscillation mode in the Tokamak, researchers can gain valuable information about the spatial distribution of plasma density, which is crucial for understanding plasma stability, confinement, and performance.

The plasma dipole oscillation method can be particularly useful in Tokamaks for characterizing the edge plasma region. The edge plasma, which is located near the plasma boundary, plays a crucial role in the overall plasma behavior and confinement. By studying the density profiles in the edge plasma using the dipole oscillation method, researchers can gain insights into phenomena such as edge localized modes (ELMs), plasma instabilities, and plasma-material interactions.

The diagnostic technique involves detecting and analyzing the dipole oscillation in the Tokamak plasma using various diagnostic tools and techniques. This can include magnetic probes, Langmuir probes, or other diagnostic instruments capable of measuring the perturbations in plasma density. Advanced data analysis methods are employed to extract the relevant parameters and deduce information about the plasma density profiles.

Overall, the magnetic properties associated with the plasma dipole oscillation offer exciting prospects for the creation of new diagnostic methods. Expanding our understanding of the PDO and its relation-
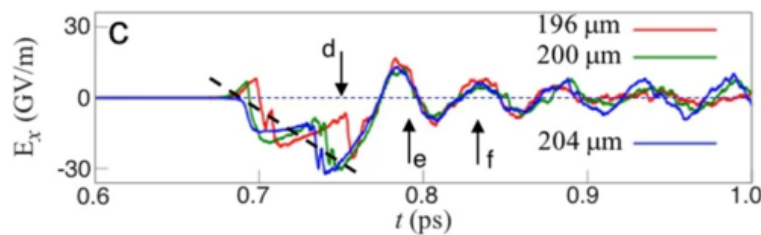

Figure 29: The electric field probed at three different positions inside the dipole

ship with magnetic fields could open up opportunities for more comprehensive and insightful plasma diagnostics. Understanding the magnetic properties of the PDO can pave the way for the development of new diagnostic methods in plasma physics. By leveraging the magnetic properties associated with the PDO, researchers can explore additional avenues for characterizing and studying plasmas in different settings.

One potential direction is to develop a magnetic field diagnostic based on the PDO. Traditional magnetic field measurements in plasmas often rely on techniques such as magnetic probes or Faraday rotation.

Magnetic probes, also known as magnetic field probes or magnetic sensors, are devices used to measure the strength and direction of magnetic fields. They play a crucial role in studying and characterizing magnetic fields in various scientific and technological applications, including plasma physics, magnetohydrodynamics (MHD), electrical engineering, and materials science.

The basic principle behind magnetic probes involves exploiting the interaction between a magnetic field and a sensing element to generate an electrical signal that can be measured and analyzed. There are different types of magnetic probes, each utilizing specific sensing principles to detect and quantify magnetic fields. Here are a few common types:

- Hall Effect Probes: Hall effect probes are based on the Hall effect, which is the generation of a voltage difference across a conductor when it is subjected to a perpendicular magnetic field and an electric current. Hall effect probes typically consist of a semiconductor material with a current-carrying conductor and a voltage-measuring element. The applied magnetic field causes a deflection of charge carriers, resulting in a measurable voltage that is proportional to the magnetic field strength.

- Fluxgate Probes: Fluxgate probes utilize the magnetic core saturation principle. They consist of a ferromagnetic core that undergoes cyclic magnetic saturation when exposed to an alternating current. The core's saturation level is influenced by the external magnetic field being measured. By measuring the changes in the core's magnetic properties, such as permeability or inductance, the magnetic field strength can be determined.

- Magnetoresistive Probes: Magnetoresistive probes employ the magnetoresistive effect, which is the change in the electrical resistance of a material in response to an applied magnetic field. Magnetoresistive materials exhibit a resistance that depends on the orientation and strength of the external magnetic field. These probes typically use materials like permalloy or giant magnetoresistive (GMR) materials, and they measure the change in resistance to determine the magnetic field strength.

- SQUID Probes: Superconducting Quantum Interference Device (SQUID) probes are highly sensitive magnetic field detectors. They operate based on the superconducting properties of certain materials at very low temperatures. SQUIDs can detect extremely weak magnetic fields by utilizing the quantum interference between two superconducting loops. The minute changes in the

magnetic field induce changes in the SQUID's electrical properties, allowing for highly sensitive measurements.

Magnetic probes can vary in terms of their sensitivity, measurement range, frequency response, and spatial resolution, depending on the specific application requirements. They are commonly used in scientific research, industrial applications, medical imaging (e.g., magnetic resonance imaging), and various other fields where precise magnetic field measurements are essential.

In plasma physics, magnetic probes are crucial for characterizing and studying the magnetic fields in plasma confinement devices like Tokamaks or stellarators. They enable researchers to analyze the behavior, stability, and dynamics of the magnetic fields within the plasma, helping to understand and optimize plasma performance.

Faraday rotation is a phenomenon in which the plane of polarization of an electromagnetic wave changes as it passes through a medium in the presence of a magnetic field. It is named after Michael Faraday, who first observed and described this effect. When an electromagnetic wave, such as light or radio waves, interacts with a medium that contains free charged particles (e.g., electrons) and a magnetic field, the wave's polarization plane rotates. The amount of rotation is proportional to the strength of the magnetic field, the frequency of the wave, and the number of charged particles in the medium.

The rotation occurs because the charged particles in the medium, under the influence of the magnetic field, experience a force that causes them to spiral around the field lines. As the wave propagates through the medium, the spiraling motion of the charged particles affects the wave's polarization. The rotation is in the same direction as the magnetic field for one polarization, and in the opposite direction for the other polarization. Faraday rotation is a fundamental phenomenon that provides valuable insights into the interaction between light and magnetic fields.

However, these methods may have limitations in certain environments or when dealing with complex plasma structures. By exploiting the magnetic response of the PDO, it may be possible to design a novel diagnostic tool that provides complementary information about the magnetic field properties within the plasma.

It is important to note that the development of a magnetic field diagnostic based on the PDO would require careful experimental design, theoretical modeling, and validation. Researchers would need to understand the relationship between the PDO characteristics and the magnetic field properties in different plasma environments. Additionally, efforts would be required to optimize the sensitivity, accuracy, and spatial resolution of the diagnostic technique.

The plasma frequency represents the natural frequency at which electrons in a plasma can collectively oscillate back and forth. At frequencies below the plasma frequency, electromagnetic waves cannot propagate through the plasma as free oscillations are quickly damped. However, at frequencies above the plasma frequency, the plasma becomes transparent to the electromagnetic waves, and they can propagate through it.

Radio bursts, on the other hand, are brief and intense bursts of radio waves that are observed in various astrophysical contexts. They can originate from a variety of sources, including pulsars, magnetars,

active galactic nuclei, and fast radio bursts (FRBs). The exact mechanisms responsible for generating radio bursts are still a subject of ongoing research.

In relation to the plasma frequency, radio bursts often occur at frequencies below the plasma frequency of the surrounding plasma medium. This is because radio waves with frequencies lower than the plasma frequency cannot penetrate the plasma but are reflected or absorbed by it. However, there can be exceptions or modifications to this general behavior depending on the specific properties and dynamics of the plasma and the source of the radio burst.

For example, some radio bursts may involve mechanisms such as electron cyclotron maser instability or plasma instabilities, which can generate radio waves within the plasma itself or at frequencies above the plasma frequency. In these cases, specific interactions between particles and fields in the plasma result in the emission of coherent or incoherent radiation at radio frequencies.

High brightness radio bursts and coherent plasma behavior are interconnected phenomena that involve the emission of intense and coherent radio waves from plasma systems.

High brightness radio bursts refer to bursts of radio waves with exceptionally high intensity or brightness. These bursts are often observed in astrophysical sources such as pulsars, magnetars, and fast radio bursts (FRBs). They are characterized by their short duration, typically lasting milliseconds, and their high peak luminosities, which can be orders of magnitude greater than the average radio emission from these sources.

The coherent plasma behavior is a key factor in the generation of high brightness radio bursts. Coherence in this context refers to the synchronization and collective behavior of charged particles in a plasma, which leads to the emission of coherent radiation. Coherent plasma behavior can arise due to a variety of physical processes, including plasma instabilities, plasma waves, and electromagnetic interactions.

One prominent mechanism that can produce coherent plasma behavior and contribute to high brightness radio bursts is the electron cyclotron maser instability (ECMI). In this process, energetic electrons in a plasma interact with a magnetic field that has a frequency close to the electron cyclotron frequency. The interaction leads to the amplification and coherent emission of electromagnetic waves at the cyclotron frequency or its harmonics. This can result in intense radio emission that is highly directional and coherent.

Another mechanism that can contribute to high brightness radio bursts is plasma turbulence. In regions of plasma turbulence, interactions between particles and waves can produce coherent plasma structures and enhance the emission of intense radio waves. These turbulent plasma regions can occur in various astrophysical environments, such as magnetized plasmas surrounding compact objects or in the vicinity of shock waves.

Understanding the connection between high brightness radio bursts and coherent plasma behavior requires detailed observations, theoretical modeling, and simulations. Researchers study the properties and characteristics of these bursts to unravel the physical processes responsible for their generation. By examining the coherence, polarization, temporal structure, and frequency properties of the radio emission, valuable insights into the underlying plasma dynamics and emission mechanisms can be gained.

In the field of laser plasma interactions, numerous experiments have been conducted to study radio

bursts and their generation mechanisms. These experiments aim to understand the fundamental physics of plasma dynamics, high-energy particle acceleration, and the emission of electromagnetic waves in the radio frequency range. Here are a few examples of such experiments:

- Coherent Radiation Emission: The enhanced electron beams, in the presence of a magnetic field, can undergo various instabilities and generate coherent radiation. These emissions may manifest as radio bursts and provide insights into the interplay between the magnetic field, plasma dynamics, and high-energy particle acceleration.

- Plasma Instabilities and Emission: The instabilities present in laser-produced plasmas can generate coherent plasma waves, electron beams, and plasma turbulence. These in turn can emit intense radio waves through processes like gyroresonance emission or plasma wave interactions.

- Radio Burst Characterization: Experimental setups involving antennas, spectrometers, and amplifiers are utilized to measure and analyze the emitted radio waves. The observed characteristics of the radio bursts help understand the properties of plasma turbulence and the associated wave-particle interactions.

The conversion of electromagnetic waves from a coherent plasma structure is a complex and intricate process that involves the transformation of plasma oscillations into detectable electromagnetic radiation. It encompasses a range of physical phenomena and mechanisms that arise from the collective behavior of charged particles in a plasma environment.

One of the key processes in this conversion is the generation of Langmuir waves. Langmuir waves are collective oscillations of electrons in a plasma that occur when the electrons are perturbed from their equilibrium positions. These waves can interact with energetic particles, such as high-energy electrons, resulting in wave-particle interactions. Through these interactions, energy and momentum are transferred between the Langmuir waves and the particles, leading to the generation of electromagnetic waves. Additionally, nonlinear effects such as wave breaking or wave decay can further contribute to the conversion of Langmuir waves into electromagnetic waves. These nonlinear processes redistribute the energy of the Langmuir waves, resulting in the emission of radiation at harmonics or in different frequency ranges.

The coherent structures of Langmuir waves play a crucial role in the generation of high brightness temperature radiation in plasma environments. Langmuir waves, which are collective oscillations of electrons in a plasma, can exhibit coherent behavior and form localized structures within the plasma. These coherent structures can arise from various plasma instabilities or wave-wave interactions and are characterized by their distinct spatial and temporal properties.

The presence of coherent Langmuir wave structures is essential for the efficient conversion of plasma energy into high brightness temperature radiation. The coherent nature of these structures allows for the constructive interference of the emitted radiation, resulting in enhanced intensity and brightness. This is particularly important in understanding astrophysical phenomena such as radio bursts, where

observations often reveal extremely high brightness temperatures that cannot be easily explained by incoherent emission mechanisms alone.

In regions of the plasma where the Langmuir waves are highly organized and coherent, the electron density and electric field fluctuations are concentrated within these structures. As a result, the acceleration and oscillation of electrons occur in a synchronized manner, leading to enhanced radiation emission. The coherence of Langmuir waves ensures that the emitted radiation is concentrated within a narrow angular range, further contributing to the high brightness temperature observed.

The generation of high brightness temperature radiation from coherent Langmuir wave structures is facilitated by the interplay between the plasma dynamics, wave-particle interactions, and the surrounding plasma environment. The plasma parameters, such as electron density, temperature, and magnetic field strength, influence the formation and stability of the coherent structures. The presence of other plasma waves, instabilities, or turbulence can also affect the properties and evolution of these structures, ultimately influencing the characteristics of the emitted radiation.

While the generation of high brightness temperature radiation from coherent Langmuir wave structures is an intriguing phenomenon, it is important to acknowledge certain limitations associated with this process. These limitations arise from various factors that can affect the efficiency and characteristics of the radiation emission.

The generation of coherent Langmuir wave structures and their subsequent conversion into high brightness temperature radiation strongly depends on the plasma conditions. Inhomogeneities in plasma parameters, such as electron density, temperature, and magnetic field strength, can affect the formation and stability of these structures. Non-uniform plasma conditions can lead to mode coupling, wave dispersion, and energy dissipation, reducing the coherence and efficiency of the radiation generation process.

The interaction between Langmuir waves and particles within the plasma can influence the conversion efficiency and properties of the emitted radiation. Wave-particle interactions, such as scattering, Landau damping, and wave-breaking, can dissipate energy from the coherent Langmuir waves, reducing the overall intensity and coherence of the generated radiation.

Nonlinear processes can significantly impact the generation of high brightness temperature radiation from coherent Langmuir wave structures. Nonlinear wave-wave interactions, such as harmonic generation or wave steepening, can redistribute the energy of the Langmuir waves, leading to the emission of radiation at different frequencies or harmonics. While nonlinear effects can enhance the complexity and richness of the radiation spectrum, they can also reduce the coherence and intensity of the emitted radiation.

The generation of high brightness temperature radiation from coherent Langmuir wave structures is typically confined to specific frequency ranges. The coherent radiation is often observed in the radio or microwave frequency regimes. Generating coherent radiation at higher frequencies, such as visible or X-rays, faces additional challenges due to the shorter wavelength and the need for more stringent coherence requirements.

Plasma instabilities and turbulence can disrupt the coherence of Langmuir wave structures and affect

the generation of high brightness temperature radiation. In regions of plasma turbulence, wave-particle interactions become more chaotic and incoherent, leading to the incoherent emission of electromagnetic waves. Plasma instabilities can introduce additional modes and fluctuations, complicating the coherence and intensity of the emitted radiation.

Langmuir wave collapse refers to the phenomenon where Langmuir waves, which are coherent plasma oscillations driven by electron density perturbations, undergo a rapid and dramatic energy localization leading to intense electric fields and particle acceleration. This collapse occurs when the nonlinear effects within the plasma become dominant, causing the wave to become highly focused and localized in space. This localized process may lead to plasma dipole oscillation.

However, the specific connection between Langmuir wave collapse and plasma dipole oscillation has not been extensively studied or established in the scientific literature. While both phenomena involve plasma oscillations, their relationship and potential interplay have not been thoroughly investigated or documented.

Langmuir wave collapse itself is a complex phenomenon that occurs when the nonlinear effects within the plasma become significant. The intense electric fields generated during collapse can lead to particle acceleration and the production of high-energy radiation. The process of collapse results in the localization of energy and can have important implications for plasma physics, such as in the study of laser-produced plasmas or astrophysical environments.

On the other hand, plasma dipole oscillation refers to the collective oscillation of the plasma density, exhibiting a dipole-like behavior with alternating regions of high and low density. This phenomenon is distinct from Langmuir wave collapse and involves different aspects of plasma behavior and dynamics.

While there might not be a specific study on the direct connection between Langmuir wave collapse and plasma dipole oscillation, it is important to note that plasma physics is a vast and evolving field of research. New studies and discoveries continually expand our understanding of plasma phenomena, and it is possible that future investigations may uncover potential relationships or correlations between these phenomena.

To explore the potential connection between Langmuir wave collapse and plasma dipole oscillation, further simulation and theoretical studies would be required. These studies could involve detailed observations and measurements of plasma behavior, numerical simulations, and theoretical modeling. By delving into these areas of research, scientists may gain valuable insights into the complex dynamics of plasmas and potentially reveal new connections between different plasma oscillations and instabilities.

Before embarking on the study of the potential connection between Langmuir wave collapse and plasma dipole oscillation, it is crucial to establish that the Plasma Dipole Oscillation (PDO) is indeed generated in astrophysical plasmas. The PDO is a penitential candidate for a strong radiator in various astrophysical contexts, including but not limited to solar flares, magnetospheric phenomena, and stellar atmospheres. Such interconnectedness provides a rich landscape for investigating the potential implications and interests of exploring the connection between these phenomena.

The primary interest of this paper is to unravel the underlying physics and mechanisms governing plasma dipole oscillation in astrophysical plasmas characterized by the presence of a strong magnetic

field. In astrophysical environments, such as magnetars, pulsars, or magnetospheres, the magnetic field plays a crucial role in shaping the behavior and dynamics of plasmas. Therefore, understanding how plasma dipole oscillations manifest and interact within the context of strong magnetic fields is of significant interest and importance.

One of the central objectives is to investigate how the presence of a strong magnetic field influences the generation of plasma dipole oscillations. The magnetic field, with its associated forces and constraints, can impose additional effects and constraints on the behavior of plasmas. It is crucial to comprehend how these magnetic field-induced modifications impact the characteristics and dynamics of plasma dipole oscillations, such as their amplitude, frequency, and spatial distribution.

Another key focus is to explore the coupling between plasma dipole oscillations and the magnetic field itself. The strong magnetic field can exert a profound influence on plasma behavior. Investigating how plasma dipole oscillations interact and couple with the magnetic field can provide insights into the interplay between plasma dynamics and magnetic forces, contributing to our understanding of astrophysical plasma phenomena.

Furthermore, the study aims to elucidate the consequences and implications of plasma dipole oscillations in the presence of a strong magnetic field. The interplay between plasma oscillations and the magnetic field can give rise to various effects, including the generation of intense electromagnetic radiation and the formation of localized plasma structures. Exploring these consequences can shed light on the role of plasma dipole oscillations in astrophysical processes such as magnetar flares, pulsar emissions, or the dynamics of magnetospheric plasmas.

To investigate these phenomena, a combination of theoretical modeling and numerical simulations is employed. Theoretical frameworks are developed to describe the behavior of plasmas under the influence of strong magnetic fields and to formulate equations governing plasma dipole oscillations in these environments. Numerical simulations provide a means to explore the complex interactions and dynamics of plasma dipole oscillations within realistic astrophysical scenarios.

4.2 Displacement of plasma block

In the case of a non-magnetic field configuration, build-up process of dipole field was investigated. Under these conditions, the dragging phase occurs, where the plasma block experiences a linear displacement with the phase velocity of the beat wave, denoted as v_ϕ. The rapid oscillation observed at the bounce frequency $\omega_b = 2\omega a_0$ during the linear growth phase confirms that the field growth is primarily caused by trapped electrons, which generate an electrostatic dipole. Subsequently, following the collision of pulses, the dipole block enters a relaxation-oscillation phase at the plasma frequency (observed for $t > 0.75$ in Fig.29). During this relaxation-oscillation period, the micro-bunches of electrons within the dipole block merge together to form a single super-bunch, exhibiting collective behavior.

On the other hand, in the case of a homogeneous magnetic field, the dynamics of the dipole block show notable differences. The presence of the magnetic field introduces additional constraints and influences on the motion of the electrons. The dipole block now exhibits a more complex behavior, with the
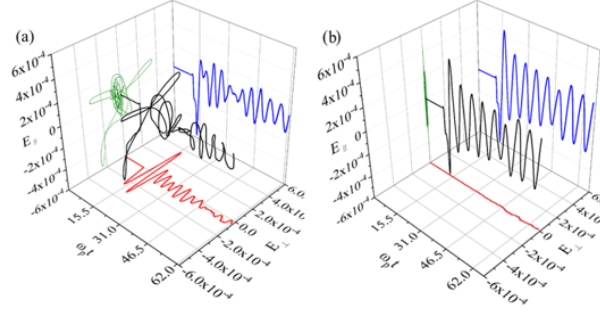
Figure 30: The electric fields probed at the dipole center (a) magnetic field is 120T and (b) is 0T respectively.

electron trajectories being modified by the Lorentz force. This leads to a deviation from the previously observed linear displacement and results in a curved trajectory for the dipole block.

Moreover, the magnetic field affects the relaxation-oscillation process of the dipole block. The merging of micro-bunches to form a super-bunch is still observed, but the presence of the magnetic field alters the dynamics of this process. Dragging phase in the magnetic field becomes different due to the magnetic force. Magnetic force bends linear averaged path of plasma block. (a) in Fig.30 depicts the dipole field variation in the presence of a magnetic field. As expected, the magnetic force causes the dipole block to deviate from its linear path, resulting in a bent trajectory. This bending effect alters the dynamics of the dipole block and leads to a modified relaxation-oscillation behavior compared to the non-magnetic field case.

Based on the detailed observation of the dipole field variation, an interesting interpretation emerges regarding the motion of the plasma block. In the absence of a magnetic field, the plasma block undergoes a linear displacement during the dragging phase, with a velocity proportional to the beat wave phase velocity (v_ϕ). However, when a magnetic field is introduced, the motion of the plasma block transforms from a linear trajectory to a rotational motion. This intriguing behavior is depicted in Figure 31, where the different motion patterns are illustrated.

When the plasma block is displaced from its original position due to the bending effect caused by the magnetic field, a charge separation occurs within the block. This charge separation leads to the application of restoring forces on the plasma block, causing it to undergo a reverse displacement following the previous bending path. To capture this behavior, I propose a model where the displacement of the plasma block can be described as a circular displacement, denoted as $r\phi$, where r represents the radial distance and ϕ represents the angular position.

By considering the circular displacement, we can construct a harmonic oscillator equation to describe the dynamics of the plasma block. This equation incorporates the restoring forces that act on the block due to the charge separation and the influence of the magnetic field. The harmonic oscillator equation allows us to analyze the periodic oscillations and determine the amplitude and frequency of the motion.

81

$$\frac{\partial^2}{\partial t^2}\delta(r\phi) + \omega_p^2\delta(r\phi) = 0 \tag{88}$$

If the system's axis follows the $r\phi$ direction, resulting in a reduction in the degree of freedom, the frequency of the PDO aligns with the plasma frequency. In this simplified scenario, the motion is confined to a single path, and the PDO primarily occur along the $r\phi$ direction. As a result, the frequency of the PDO coincides with the plasma frequency.

However, in situations where the system exhibits full freedom in all three dimensions, the frequencies associated with PDO can deviate from the plasma frequency. This is due to the additional degrees of freedom departing $r\phi$ by the motion in the radial r and azimuths angle ϕ directions. In such cases, the PDO can manifest at frequencies different from the plasma frequency, as the oscillations involve a more complex interplay between the different spatial dimensions.

By adopting these approaches, experimenters can effectively handle signals in three dimensions and discern the diverse frequencies associated with plasma dipole oscillations. This allows for a comprehensive understanding of the complex dynamics and behavior of plasmas, leading to insights into the underlying physics, energy transfer mechanisms, and potential applications in various astrophysical and laboratory plasma settings.

Applying time derivative to equation of motion, I obtain the following equation.

$$\delta\ddot{r}\delta\phi + 2\delta\dot{r}\delta\dot{\phi} + \delta r\delta\ddot{\phi} + \omega_p^2\delta(r\phi) = 0 \tag{89}$$

The derived equation of motion incorporates terms influenced by the magnetic force, restoring forces due to charge separation, and inertial forces acting on the plasma block. However, accurately determining the constraint of angular motion poses challenges due to the plasma block not being a perfect rigid body. Consequently, the form of the current, typically expressed as $\rho\frac{d\delta(r\phi)}{dt}$, is not a straightforward representation in this case. To address this complexity, I introduce an unknown factor to account for the specific characteristics of the plasma block and its angular motion. In order to further explore the rotational dynamics of the plasma block, I propose an ad-hoc relation between the angular factor and known parameters. This relation aims to capture the interdependence between the angular displacement and other variables involved in the equation of motion. While this introduces some level of approximation, it allows for a more comprehensive understanding of the system and its behavior. By incorporating this unknown factor and establishing a relation with relevant parameters, we can better analyze and predict the rotational motion of the plasma block. This approach enables us to account for the inherent complexities arising from the plasma block's non-rigid nature and provides a means to refine our understanding of its angular dynamics.

In the context of determining the constraint of angular motion in the rotational dynamics of the plasma block, an ad-hoc relation can be inferred based on the magnetization properties. The magnetization of the plasma block plays a crucial role in the interaction with the magnetic field and the resulting rotational behavior. By considering the magnetization effects, we can establish a relation between the angular factor and the known parameters, thereby enhancing our understanding of the system's angular dynamics.
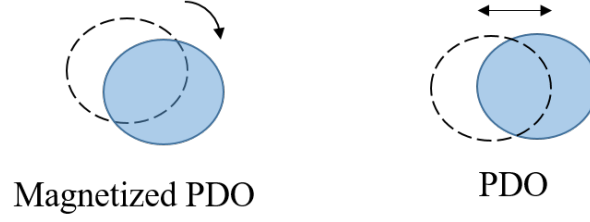
Figure 31: The schematic diagram of dipole field change comparing non-magnetic field and magnetic field cases

$$M \equiv \frac{mv_\perp^2}{2B} = \frac{qr^2\dot{\phi}^2}{2\omega_c} \tag{90}$$

To account for these magnetization effects and incorporate them into the equation of motion, an ad-hoc relation is proposed. This relation establishes a connection between the unknown factor representing the angular motion and the relevant parameters, considering the magnetization properties of the plasma block. By including this relation, we can gain insights into how the magnetization influences the rotational behavior and further refine our understanding of the system. I model angular factor γ by ω_p and ω_c, representing electric and magnetic forces respectively.

$$\delta\dot{\phi} \sim \pm\sqrt{\frac{2M\omega_c}{qr^2}} = \pm\gamma(\omega_p, \omega_c)\delta\phi \tag{91}$$

By inserting $\delta\dot{\phi}$ into the equation, I obtain a modified expression that explicitly includes the time derivative of the angular displacement. Rearranging the terms in this equation allows me to isolate and analyze the contributions of the angular factor to the overall rotational dynamics of the plasma block.

$$\delta\ddot{r} \pm 2\gamma(\omega_p, \omega_c)\delta\dot{r} + \left(\omega_p^2 - \gamma^2(\omega_p, \omega_c)\right)\delta r = 0 \tag{92}$$

It is important to note that the ad-hoc relation based on magnetization is an approximation and may require further validation through experimental studies and numerical simulations. By conducting detailed measurements and modeling efforts, we can assess the accuracy and limitations of the proposed relation and gain a more comprehensive understanding of the intricate interplay between magnetization and the rotational dynamics of the plasma block. Applying harmonics to Eq.92, auxiliary equation can be obtained.

$$\omega^2 \pm 2i\gamma(\omega_p, \omega_c)\omega + \left(\omega_p^2 - \gamma^2(\omega_p, \omega_c)\right) = 0 \tag{93}$$

The use of harmonics in the analysis of the auxiliary equation allows us to identify dominant modes of oscillation and examine their contributions to the overall radial motion. This analysis aids in understanding the behavior of the plasma block over time and provides a framework for predicting and controlling its radial dynamics. The solution of this auxiliary equation shows the frequency of magnetized plasma dipole oscillation.
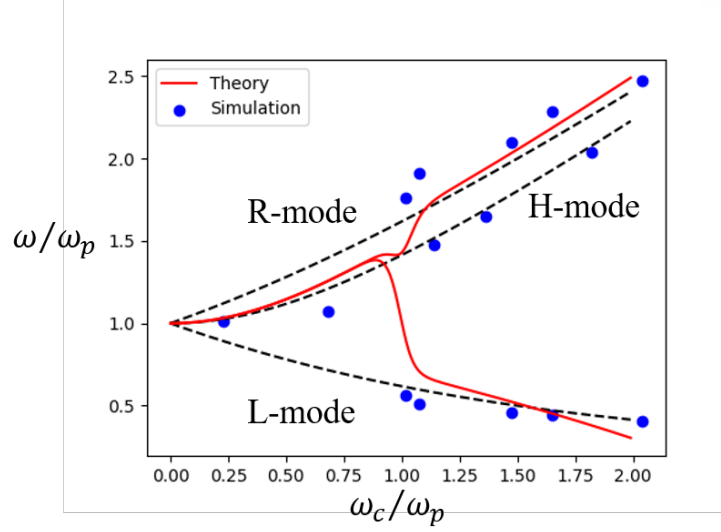
Figure 32: Spectral peaks of magnetized PDO, dashed lines represent H-mode and X-modes, red lines are calculated by theory and point data is obtained from the simulations

$$\omega = \pm i\gamma + \frac{\sqrt{4\omega_p^2 + 5\gamma^2}}{2} \tag{94}$$

I investigate spectrum of magnetized PDO using the PIC code. This computational approach allowed me to fit the ad-hoc relation. By performing numerical simulations, I obtained the spectrum of the magnetized PDOs. This spectrum shows the regime of the mode variation depending on the magnetic fields.

The fitting results for the circular factors, as determined from the analysis, indeed exhibit a notable similarity, differing only in one parameter in exponent. For the right circular factor, denoted as R, the equation is:

$$\gamma_R = (1 - \frac{1}{1 + e^{-32(x-1)}} - \frac{i}{2}\frac{1}{1 + e^{-32(x-1)}})\omega_c \tag{95}$$

Similarly, for the left circular factor, denoted as L, the equation takes the form:

$$\gamma_L = (1 - \frac{1}{1 + e^{-32(x-1)}} - \frac{i}{\sqrt{15}}\frac{1}{1 + e^{-32(x-1)}})\omega_c \tag{96}$$

By incorporating these circular factors into the frequency equation and eliminating the imaginary component, I conducted an extended analysis that yielded the curves illustrated in Figure 32. Notably, even after applying this approach, certain data points persist in the H-mode. Consequently, the unexplained characteristics of the bending path model remain unresolved. The H-mode phenomenon continues to present challenges and complexities that require further investigation and understanding.

The analysis of the spectral peaks curve reveals an intriguing feature: the H-mode splits into X-modes at a specific point, approximately around $\omega_c \sim \omega_p$. This critical point signifies the transition to fully magnetized electron plasma. I classify the regimes of magnetized PDO by this critical points. $\omega_c \ll \omega_p$ is weak field regime and $\omega_c \geq \omega_p$ is strong field regime.
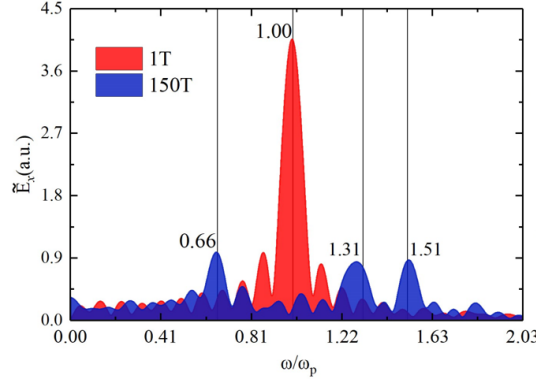
Figure 33: Spectrum of PDO in the magnetic fields, 1T and 150T

4.3 Interpretation of spectral characteristics of the plasma block motion in the dipole field

In the preceding section, an intriguing observation was made regarding the behavior of the H-mode and X-modes in relation to the critical magnetic field point. Despite exceeding the critical point, the H-mode persists while the presence of X-modes becomes apparent in the spectrum of the PDO. Based on the variation in spectral peak amplitudes, it can be argued that the H-mode appears to split into X-modes. The black lines depicted in Figure 33 represent the frequency positions of both the H-mode and X-modes.

In the case of a 1T magnetic field, only a single peak corresponding to the H-mode is observed. However, in the 150T case, three peaks are evident, representing the H-mode and the two X-modes. A notable difference between the amplitudes of the spectral peaks in the H-mode is observed when comparing the 1T and 150T cases. The peak amplitude in the 1T case is significantly higher than that in the 150T case. In contrast, the X-modes in the 150T case exhibit larger amplitudes compared to the H-mode.

This intriguing phenomenon suggests that as the magnetic field strength increases beyond the critical point, there is a redistribution of the spectral energy between the H-mode and the newly emerged X-modes. The reduced amplitude of the H-mode peak in the 150T case indicates a decrease in the energy associated with the traditional H-mode behavior. Meanwhile, the amplification of the X-mode peaks suggests an enhanced presence and energy allocation to these modes in the 150T case.

H-mode is known that longitudinal mode of plasma wave. During the PDO formation, initial stage of beat wave dragging enforces the longitudinal motion to generate H-mode. However, after disappearance of beat wave, rotational motion becomes dominant with the main drivers are restoring force and magnetic force. Averaged motions of electrons in dipole field are calculated for the nonmagnetic and magnetic cases.

The H-mode is widely recognized as a longitudinal mode of plasma wave, characterized by specific behaviors and dynamics. During the formation of the PDO, the initial stage involves the beat wave dragging, which enforces the longitudinal motion and gives rise to the H-mode. However, as the beat
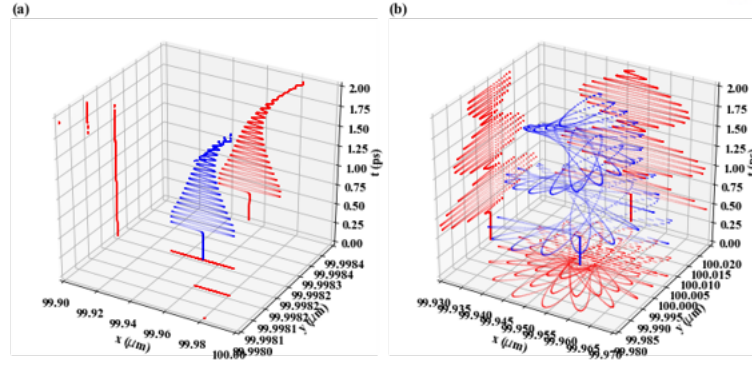
Figure 34: Averaged motion of electrons in the dipole field with magnetic fields, 0T and 120T

wave dissipates, the dominant motion transitions to a rotational nature, with the main drivers being the restoring force and the magnetic force.

To gain further insights into the average motions of electrons in dipole fields, calculations are performed for both nonmagnetic and magnetic cases. In the nonmagnetic case, the trajectory of electrons in a dipole field exhibits a notable characteristic: linear motion is conserved after their release. Once set in motion, the electrons continue along a straight path, maintaining their initial velocity and direction. This linear motion is a consequence of the absence of magnetic forces that could alter the trajectory of the electrons. As a result, they undergo unhindered motion, following a straight line in the dipole field.

In contrast, the presence of a magnetic field introduces a significant change in the behavior of electrons. When PDO is released in a beat wave, the trajectory of electrons undergoes a transition from linear to rotational motion. This shift occurs due to the disappearance of PM force of beat wave and interaction between the magnetic field and the charged particles. The magnetic force causes the electrons to follow a curved or rotational path.

In order to investigate the mode transition from H-mode to X-modes more closely, wavelet transforms were applied using various wavelet functions such as the Mexican hat, Gaussian, and Morlet. The choice of wavelet function plays a crucial role in determining the spectral resolution of the analysis. However, despite employing different wavelet functions, it proved challenging to resolve the spectral transition from the H-mode to the X-modes in a clear and distinct manner.

4.4   Radiation characteristics from the magnetized PDO

In weak field regimes, the behavior of the dipole field spectrum is predominantly characterized by the H-mode, whereas the radiation spectral peaks appear at the X-modes (See Fig. 35). The absence of the H-mode in the radiation spectrum can be understood by considering its nature as a resonance mode.

The H-mode refers to a specific mode of oscillation in the plasma that occurs when the driving frequency matches the natural frequency of the plasma column. It is essentially a resonant response of the plasma to the applied field. In weak field regimes, where the influence of external magnetic fields is not as pronounced, the dominant mode of oscillation is the H-mode. Consequently, the dipole field spectrum primarily exhibits the H-mode.
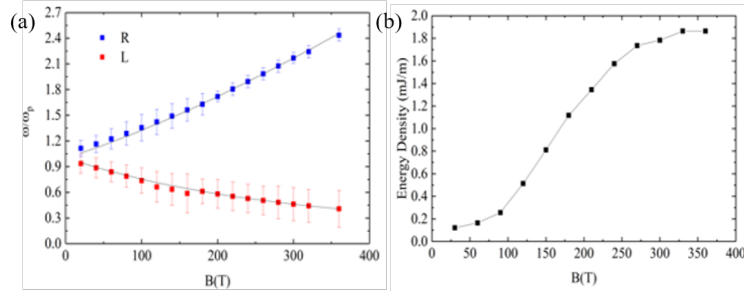
Figure 35: (a) Radiation spectrum, (b) Averaged Radiation power from the magnetized PDO

On the other hand, when radiation is emitted from the plasma, the spectral peaks appear at the X-modes. The X-mode refers to a mode of oscillation in which the electromagnetic waves propagate. Unlike the H-mode, the X-mode does not rely on a resonance condition. It is a more general mode of wave propagation in plasmas and is capable of carrying energy away from the plasma.

The existence of X-modes dominates the behavior of the dipole field spectrum in the strong field domain, which is characterized by a large effect of the external magnetic field. X-modes become the dominating mode of oscillation in the plasma, contributing a significant amount of the spectral intensity in the dipole field spectrum. This pattern is consistent with the discovery that the radiation's spectral peaks also show at the X-modes.

This behavior can be understood by considering the characteristics of the X-mode compared to other modes. Unlike the H-mode, which relies on resonance with the plasma's natural frequency, the X-mode is not limited by resonance conditions. It can propagate across the magnetic field lines and effectively carry energy away from the plasma even in the presence of strong external magnetic fields. Therefore, in the strong field regime, where the external magnetic field plays a significant role, the X-mode becomes the dominant mode for both the dipole field spectrum and the radiation spectral peaks.

It is important to note that the absence of the H-mode in the radiation spectrum does not imply the absence of radiation altogether. Rather, it signifies that the resonant mode of oscillation associated with the H-mode does not contribute significantly to the energy radiated from the plasma. Instead, the X-modes, which are not resonance modes, become more prominent in carrying away the energy in the form of radiation.

X-modes, which are observed in the strong field regime, encompass two distinct components: right circular and left circular modes. These modes arise due to the alternating rotational motion of plasma particles within the magnetic field. These dynamic plasma motions give rise to characteristic changes in the spatial distribution of electromagnetic fields, leading to an alteration in the radiation pattern from the typical dipole radiation to a more complex structure consisting of two crossed tilted figure eight shapes.

The right circular mode corresponds to the case where the plasma particles rotate in a clockwise direction when viewed along the direction of propagation, while the left circular mode corresponds to counterclockwise rotation. The rotation of plasma particles in these modes introduces a new characteristic to the radiation pattern, resulting in distinct changes in the spatial distribution of electromagnetic fields.
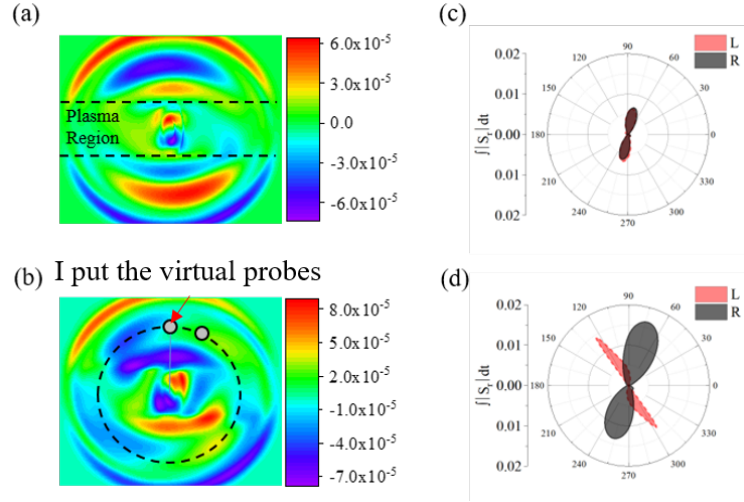
Figure 36: (a) Radiation distribution of PDO, (b) Radiation distribution of magnetized PDO, (c) angular distribution of radiation from PDO and (d) angular distribution of radiation from magnetized PDO

The alternating rotational motion of plasma particles and the resulting right and left circular modes have a profound impact on the radiation pattern emitted from the plasma. Instead of the simple dipole radiation pattern observed in weaker field regimes, the X-modes give rise to two crossed tilted figure eight shapes in the radiation pattern. These crossed tilted figure eight shapes represent the distribution of the electric and magnetic fields in space. The rotation of plasma particles in the right and left circular modes introduces an asymmetry in the radiation pattern, leading to the crossing of the figure eight shapes. The tilt of these shapes arises from the angle diversions caused by the rotational motion of plasma particles. Angular distributions of radiation are calculated fields on the dashed circle depicted in Fig. 36 (b). Virtual probes on the circle is used for calculating radiation power in Fig. 35 (b).

In summary, the presence of a magnetic field plays a significant role in changing the characteristics of PDO. The magnetic field interacts with the plasma, resulting in the bending of the PDO displacement and causing characteristic changes. The intensity of the magnetic field determines the rotational characteristics of the plasma block, influencing the modes of oscillation observed.

In the weak field regime, where the magnetic field influence is less pronounced, a magnetized PDO exhibits the upper-hybrid mode. This mode arises due to the interaction between the magnetic field and the plasma, leading to the formation of oscillations at frequencies corresponding to the upper-hybrid resonance.

In the strong field regime, the magnetic field intensity becomes significant, impacting the plasma dynamics and resulting in the presence of both upper-hybrid and X-modes in the magnetized PDO. The upper-hybrid mode persists, while the X-mode, which corresponds to the propagation of waves across the magnetic field lines, becomes more prominent. The strong magnetic field influences the rotational motion of plasma particles and facilitates the efficient transfer of energy via X-modes, ultimately leading to changes in the dipole field spectrum and the appearance of spectral peaks in the radiation at X-modes.

V PDO mechanism for the radio bursts

5.1 Brief overview of radio bursts in astrophysics

Radio bursts play a pivotal role in astrophysical research, offering profound insights into the workings of the universe [77]. These bursts, characterized by intense emissions of radio waves [78], provide a unique window into various celestial phenomena, spanning a wide range of cosmic sources and environments. Their significance lies in the wealth of information they provide about the physical mechanisms, dynamics, and properties of astrophysical systems.

One key aspect of radio bursts is their ability to unveil the underlying physical processes occurring within celestial objects. By studying the emission of radio waves, scientists can delve into the dynamics of energetic events such as solar flares [79] and coronal mass ejections [80]. Solar radio bursts, originating from the Sun, provide invaluable information about the Sun's magnetic activity, plasma instabilities, and magnetic reconnection processes [81]. These bursts allow us to probe the Sun's dynamic atmosphere and gain insights into the mechanisms responsible for releasing vast amounts of energy into space.

In addition to solar radio bursts, other types of radio bursts contribute to our understanding of cosmic phenomena. Fast Radio Bursts (FRBs) are an enigmatic class of bursts originating from extragalactic sources [82]. The study of FRBs has the potential to revolutionize our understanding of the Universe. These millisecond-duration bursts, with their intense and coherent radio emission [83], carry information about extreme astrophysical environments, such as neutron stars, magnetars, and possibly even cosmological events such as compact object mergers. The detection and analysis of FRBs provide a unique opportunity to probe the interstellar and intergalactic medium, offering insights into the distribution of matter and magnetic fields on cosmological scales.

the importance of radio bursts extends beyond individual objects. The study of radio bursts provides insights into fundamental physical processes such as synchrotron radiation, plasma instabilities, and magnetic reconnection. These processes are common in astrophysical plasmas and occur in various contexts, including accretion disks around black holes, active galactic nuclei, and pulsar magnetospheres. By analyzing radio bursts, researchers can test and refine theoretical models, advancing our understanding of the underlying physical mechanisms that govern the behavior of cosmic objects.

Furthermore, radio bursts offer a unique opportunity for multi-wavelength studies. By correlating radio observations with data from other wavelengths, such as X-rays, gamma rays, and optical, scientists can gain a comprehensive view of astrophysical phenomena. The synergy between different wavelengths allows for a more complete understanding of the physical processes, energy transfer mechanisms, and interactions between different components of astrophysical systems.

To fully exploit the potential of radio bursts, ongoing technological advancements are essential. The development of sensitive radio telescopes, array configurations, and sophisticated data analysis techniques has greatly enhanced our ability to detect and characterize these bursts. The increased sensitivity and higher time and frequency resolution enable researchers to explore a broader parameter space, uncovering previously unknown phenomena and improving our understanding of known sources.

5.2 Solar Radio Bursts

Eruptions on the Sun, such as solar flares and coronal mass ejections (CMEs), are known to generate intense radio emission, giving rise to solar radio bursts. These bursts are of significant importance in astrophysics as they provide valuable insights into the dynamic and energetic processes occurring in the Sun's atmosphere.

Solar flares are sudden releases of magnetic energy stored in the Sun's atmosphere. When the magnetic field lines in the solar atmosphere become twisted and distorted, they can undergo a process called magnetic reconnection. This process leads to the rapid release of a tremendous amount of energy, causing the eruption of plasma and the emission of high-energy particles, electromagnetic radiation, and radio waves. The accelerated particles, particularly electrons, interact with the plasma and magnetic fields in the solar corona, producing intense radio emissions across a broad range of frequencies.

The energy released during a solar flare is equivalent to millions of atomic bombs exploding simultaneously. The majority of the energy is emitted in the form of X-rays and extreme ultraviolet (EUV) radiation, although flares also emit significant amounts of gamma rays, visible light, and radio waves. X-rays and EUV radiation are absorbed in Earth's atmosphere and can affect the ionosphere, causing disturbances in the propagation of radio waves.

Solar flares are classified based on their X-ray emission, with the classification ranging from A-class (weakest) to X-class (strongest). X-class flares are the most powerful, and their effects can be significant. The energy released during a flare can heat the surrounding plasma to tens of millions of degrees Celsius, accelerating charged particles, particularly electrons, to near the speed of light. These high-energy particles can escape the Sun's gravitational pull and travel through space, sometimes reaching Earth and causing space weather effects.

One of the notable consequences of solar flares is the generation of coronal mass ejections (CMEs). CMEs are massive eruptions of plasma and magnetic fields from the Sun's corona. When a flare occurs, it can trigger a CME by rapidly expelling a large amount of magnetized plasma into space. These CMEs can travel at speeds ranging from a few hundred to several thousand kilometers per second and have the potential to cause geomagnetic storms when they interact with Earth's magnetic field.

Understanding coronal mass ejections (CMEs) and unraveling the intricate triggers behind their initiation is of utmost importance in solar physics and space weather research. CMEs, which are colossal eruptions of plasma and magnetic fields from the Sun's corona, represent some of the most energetic and dynamic events in the Sun-Earth system. Despite extensive study, the precise mechanisms responsible for initiating CMEs continue to be a subject of ongoing scientific investigation and debate.

Various theories have been proposed to explain the trigger mechanisms for CME initiation. One prominent hypothesis suggests that CMEs result from the sudden release of stored magnetic energy in the Sun's corona. Magnetic instabilities, such as the kink instability or the torus instability, can cause the magnetic field lines to become highly twisted and stressed [84]. When the magnetic energy exceeds a critical threshold, a CME may be initiated, leading to the expulsion of a significant amount of plasma and magnetic flux into the interplanetary space.

Another potential trigger mechanism involves the destabilization of filament structures [85] within the Sun's atmosphere. Filaments, also known as prominences, are dense and cool plasma structures that are suspended in the Sun's magnetic field. When the equilibrium of a filament becomes disrupted, either through magnetic forces or external disturbances, it can rapidly erupt, giving rise to a CME.

Additionally, the interaction between different magnetic structures, such as magnetic reconnection, has been proposed as a trigger mechanism for CME initiation. Magnetic reconnection occurs when opposing magnetic field lines come into contact, allowing the magnetic energy to be rapidly converted into kinetic energy and thermal energy. This process can lead to the destabilization and eruption of the overlying magnetic field, initiating a CME.

Advancing our understanding of the triggers for CME initiation is crucial for several reasons. First, CMEs are capable of releasing vast amounts of energy and matter into space, influencing the space weather conditions in the heliosphere and affecting the near-Earth environment. CMEs can produce intense geomagnetic storms, which can disrupt satellite communications, power grids, and navigation systems, highlighting the need for accurate forecasting and prediction.

Furthermore, CMEs play a significant role in shaping the structure and dynamics of the solar wind, a stream of charged particles emitted by the Sun. As CMEs propagate through the interplanetary medium, they interact with the ambient plasma and magnetic field, modifying their configurations and introducing disturbances. Understanding the triggers behind CME initiation helps in elucidating the fundamental processes governing the dynamics of the solar wind and the interplanetary magnetic field (IMF) in the vicinity of Earth.

Coronal mass ejections (CMEs) and solar radio bursts are intimately linked phenomena that occur in the Sun's atmosphere. Solar radio bursts are sudden increases in radio emission observed across a wide range of frequencies, ranging from a few megahertz to several gigahertz. These bursts are often associated with the eruption and expansion of CMEs.

During a CME event, the release of immense amounts of energy and magnetic fields from the Sun's corona generates shock waves and accelerates charged particles. These energetic particles can interact with the ambient plasma and magnetic field in the solar atmosphere, giving rise to radio emissions. The acceleration of electrons in the CME-driven shock fronts and the subsequent interaction of these electrons with the ambient plasma produce radio waves through a process called gyrosynchrotron radiation.

Radiation from an accelerated charge is described by the relativistic Larmor formula, which provides insights into the power emitted by the charge. The formula is given as:

$$P = \frac{2q^2}{3c^3}\gamma^4(a_\perp^2 + a_\parallel^2) = \frac{2q^2}{3c^3}\gamma^2 a_\perp^2 \tag{97}$$

In this equation, P represents the power radiated, q is the charge of the particle, c is the speed of light, γ is the relativistic factor, and $a_\perp$ and $a_\parallel$ represent the perpendicular and parallel components of acceleration, respectively. Gyromagnetic radiation specifically occurs due to the acceleration experienced by an electron as it gyrates in a magnetic field, influenced by the Lorentz force. The power radiated in this scenario can be expressed as:

$$P = \frac{2q^2}{3c^3}\gamma^4\omega_B^2 v_\perp^2 \tag{98}$$

Here, ω_B represents the gyrofrequency, which is equal to the cyclotron frequency (ω_c) divided by the relativistic factor (γ). The perpendicular velocity of the electron is denoted by $v_\perp$. When considering the motion of a relativistic particle in a magnetic field, the angle it experiences due to the field during a short period is proportional to $\frac{2}{\gamma}$. However, taking into account time delays, the time length observed in the laboratory frame can be approximated as:

$$\Delta t \propto \frac{1}{\gamma^3 \omega_B} \tag{99}$$

Due to the relativistic nature of the particle, the power spectrum becomes sharply peaked, leading to pulsed radiation. The classification of gyromagnetic radiation types is dependent on the relativistic factor (γ). For non-relativistic or thermal conditions where $\gamma \ll 2$, the radiation is referred to as gyro-resonance or cyclotron radiation. In the mildly relativistic range where $\gamma \propto 2-6$, the radiation is known as gyrosynchrotron radiation. For ultra-relativistic conditions where $\gamma \gg 1$, the radiation is classified as synchrotron radiation. The spectral width of thermal gyroresonance radiation is exceptionally narrow and can be approximated by:

$$\frac{\Delta v}{v_c} \approx \sqrt{\frac{k_B T}{m_e c^2}} \tag{100}$$

In this equation, Δv represents the spectral width, v_c is the cyclotron frequency, k_B is the Boltzmann constant, T is the temperature, and m_e is the electron mass. The harmonic number s (e.g., $s = 1, 2, 3, ...$) is also taken into account. On the other hand, in the case of ultra-relativistic conditions, adjacent spikes in the radiation spectrum are separated in frequency by $\Delta v = \frac{v_c}{\gamma}$. Fluctuations in electron energy, magnetic field strength, or pitch angle contribute to broadening the spikes, resulting in a continuous spectrum.

Solar radio bursts can be classified into different types based on their spectral characteristics, duration, and associated phenomena. These classifications provide valuable information about the underlying physical processes and dynamics occurring in the Sun's atmosphere. Here, we will discuss some of the common types of solar radio bursts.

Type I radio bursts, also known as solar noise storms, are electromagnetic emissions observed at radio frequencies originating from the Sun. They are characterized by their narrowband, short-duration bursts of intense radio waves. These bursts occur primarily in the decimeter and meter wavelength range, corresponding to frequencies of a few tens to a few hundred megahertz. Type I radio bursts are associated with energetic processes in the solar atmosphere, particularly in the regions of the Sun's corona.

The underlying mechanism responsible for Type I radio bursts is the plasma emission process. Plasma waves are excited in the Sun's corona, where high-energy electrons interact with the magnetic field. As these electrons move along the magnetic field lines, they emit radio waves at specific harmonics of the electron gyrofrequency. The fundamental harmonic produces the Type I radio bursts, and higher harmonics are also observed in some cases.

Type I radio bursts can occur as isolated bursts or as a series of bursts. They typically exhibit rapid frequency drifts, starting from higher frequencies and drifting towards lower frequencies over time. The frequency drifts are attributed to the dispersion of plasma waves in the solar corona. The electron density along the path of the radio waves causes a frequency-dependent delay, resulting in the observed drift pattern.

These bursts are associated with solar flares and coronal mass ejections (CMEs), which are powerful eruptions of magnetic energy from the Sun. Solar flares release enormous amounts of energy across the electromagnetic spectrum, including radio waves. The Type I radio bursts provide valuable information about the acceleration and propagation of energetic electrons during solar flares and CMEs.

Observing and studying Type I radio bursts is essential for understanding the dynamic processes occurring in the Sun's atmosphere. They help in investigating the generation and propagation of solar energetic particles and the mechanisms responsible for energy release during solar flares. By analyzing the properties of these bursts, scientists can gain insights into the structure and dynamics of the Sun's corona and improve our knowledge of space weather phenomena that impact Earth and our technological infrastructure.

Type II radio bursts are another type of solar radio emission that provides valuable insights into solar eruptive events and their effects on space weather. These bursts are characterized by their wide-band, long-duration spectral features and are typically observed at frequencies ranging from a few tens of megahertz to a few hundred kilohertz. Type II bursts are associated with shock waves propagating through the solar corona and interplanetary space.

The generation of Type II radio bursts is closely tied to coronal mass ejections (CMEs), which are massive eruptions of plasma and magnetic fields from the Sun. As a CME travels outward from the Sun, it drives a shock wave through the surrounding solar corona and interplanetary medium. This shock wave, often referred to as a shock front, can accelerate electrons to high energies, producing intense radio emissions.

The emission mechanism responsible for Type II radio bursts is known as electron cyclotron maser instability (CMI). When the shock wave interacts with the ambient plasma, it causes the electrons to gyrate around the magnetic field lines. Under certain conditions, the interaction between the shock wave and the electron population can lead to the amplification of radio waves through the CMI process. This amplification results in the observed Type II burst signals.

Type II radio bursts exhibit a characteristic feature known as a frequency drift. Unlike Type I bursts, which drift from high to low frequencies, Type II bursts show a drift from low to high frequencies over time. This drift pattern is a consequence of the shock wave's outward propagation through the interplanetary medium, compressing and accelerating the plasma and causing a decrease in the plasma frequency. As a result, the observed radio waves experience a frequency increase as they move away from the Sun.

Studying Type II radio bursts is crucial for understanding the dynamics of solar eruptive events and their influence on space weather. These bursts provide information about the properties of CMEs, such as their speed, acceleration, and kinematics. By analyzing the frequency drift rates of Type II

bursts, scientists can estimate the shock wave's speed and the density gradient of the ambient plasma. This information is essential for predicting the arrival time and potential impact of CMEs on Earth's magnetosphere, ionosphere, and technological systems.

Furthermore, Type II radio bursts can serve as a diagnostic tool for characterizing the ambient solar wind and interplanetary medium. By examining the properties of these bursts, such as their spectral profiles and polarization characteristics, researchers can infer important parameters of the solar wind, such as its density, magnetic field strength, and electron density. This knowledge contributes to our understanding of space weather conditions and aids in the development of improved forecasting models to mitigate potential adverse effects on space-based assets and terrestrial infrastructure.

Type III radio bursts are a distinct class of solar radio emissions that provide valuable information about the release and propagation of high-energy electrons in the Sun's atmosphere. These bursts are characterized by their rapidly drifting spectral features and are observed at frequencies ranging from a few hundred megahertz to a few kilohertz. Type III bursts are closely associated with solar flares and are considered one of the most common types of solar radio bursts.

The underlying mechanism responsible for Type III radio bursts is the electron beam emission process. During a solar flare, energetic electrons are accelerated and injected into the Sun's corona along magnetic field lines. As these high-energy electrons propagate away from the flare site, they emit radio waves through a process called coherent plasma emission. The emitted radio waves are observed as Type III bursts.

One of the distinguishing features of Type III radio bursts is their frequency drift pattern. These bursts exhibit a rapid and continuous decrease in frequency over time. The drift pattern is a consequence of the decreasing density of electrons along the magnetic field lines as the electrons move away from the Sun. The lower electron density causes a reduction in the plasma frequency, resulting in the observed frequency drift.

Type III bursts are often observed as a series of discrete frequency bands, known as lanes or striae, that drift in parallel. The number of lanes and their separation provide information about the characteristics of the electron beam, such as its energy spectrum and the magnetic field configuration through which it propagates. By analyzing the drift rates and other properties of these lanes, scientists can infer the conditions of the solar flare, including the location and strength of the magnetic field and the distribution of the accelerated electrons.

Studying Type III radio bursts plays a crucial role in understanding the dynamics of solar flares and the processes involved in the acceleration of high-energy particles. These bursts help scientists investigate the interaction between energetic electrons and the ambient plasma in the solar corona. By analyzing the properties of Type III bursts, researchers can determine the energy content and distribution of the accelerated electrons, which provides valuable insights into the physical processes occurring during solar flares.

Type IV radio bursts are a class of solar radio emissions that are characterized by their long-duration and continuous spectral features. These bursts occur across a wide range of frequencies, from a few hundred megahertz to a few kilohertz, and are associated with intense eruptive events on the Sun, such

as coronal mass ejections (CMEs) and flares. Type IV bursts are considered the longest-lasting type of solar radio bursts and can persist for hours or even days.

The generation mechanism for Type IV radio bursts is related to the interaction between accelerated electrons and plasma in the solar corona. During eruptive events, energetic particles, particularly electrons, are accelerated to high energies. These high-energy electrons interact with the ambient plasma and emit radio waves through various mechanisms, including gyrosynchrotron radiation and plasma emission processes.

Type IV bursts are typically observed as slowly varying or drifting emissions in the radio spectrum. The spectral features of these bursts can exhibit both frequency drifts and intensity variations over time. The frequency drifts are often associated with the movement of the source region of the burst in the solar corona. As the eruptive event evolves and the associated magnetic structures reconfigure, the emission region can move, causing the observed drift in frequency.

These bursts are commonly associated with significant solar phenomena, such as flares and CMEs. They provide important insights into the release and propagation of energetic particles during these events. The characteristics of Type IV bursts, such as their duration, spectral shape, and intensity profile, can be used to study the properties of the accelerated particle populations and the magnetic structures associated with the eruptive processes.

Type IV radio bursts are of particular interest for space weather forecasting and the prediction of potential impacts on Earth's magnetosphere and technological systems. The energetic particles associated with these bursts can have adverse effects on satellites, spacecraft, and even terrestrial communication systems. Monitoring and analyzing Type IV bursts contribute to our understanding of space weather dynamics and help in developing predictive models to mitigate the potential risks associated with solar activity.

Type V radio bursts are a class of solar radio emissions that are characterized by their short-duration, broadband, and highly dynamic spectral features. They occur across a wide frequency range, from a few hundred kilohertz to a few kilohertz, and are associated with intense solar flares and eruptive events. Type V bursts are among the most powerful and intense types of solar radio bursts.

The generation mechanism of Type V radio bursts is related to the acceleration and interaction of energetic electrons with the solar corona and interplanetary medium. During solar flares, a large amount of energy is released, resulting in the acceleration of electrons to high energies. These energetic electrons interact with the ambient plasma and emit radio waves through various processes, including plasma emission and coherent emission mechanisms.

Type V bursts exhibit a highly dynamic behavior in both frequency and intensity. They can occur as a single burst or as a series of bursts with irregular temporal patterns. The spectral features of Type V bursts can show rapid frequency variations, intensity spikes, and even fine structures within the burst. These dynamic characteristics are a result of the complex and rapidly changing conditions in the solar corona during the flare and eruptive processes.

The analysis of Type V radio bursts provides valuable insights into the acceleration and propagation of high-energy electrons during solar flares. These bursts offer information about the energy release and

transport processes involved in the flare dynamics. By studying the properties of Type V bursts, such as their spectral shapes, intensity profiles, and fine structures, scientists can infer the characteristics of the accelerated electron populations and the underlying physical processes at play.

Type V radio bursts are also of great importance for space weather forecasting and the prediction of potential impacts on Earth's space environment. The high-energy particles associated with these bursts can affect the Earth's magnetosphere, ionosphere, and radiation belts, posing risks to satellites, space-craft, and even astronauts. Monitoring and studying Type V bursts contribute to our understanding of space weather phenomena and aid in the development of models to mitigate potential hazards.

Solar flares and coronal mass ejections (CMEs) are known to produce intense radiation, and the primary emitters of this radiation are the accelerated electron beams. The most widely accepted mechanism for the production of radiation in these events is gyrosynchrotron emission, which occurs when energetic electrons spiral in the strong magnetic fields present in the solar atmosphere.

The conventional mechanism of solar radio bursts, which involves the gyrosynchrotron radiation, plasma emission, and electron-cyclotron maser emission processes, has been successful in explaining a wide range of observed phenomena. However, there are certain limitations to this conventional mechanism that warrant further investigation and refinement.

Fine Structure and Substructures: Solar radio bursts often exhibit fine structures and substructures within their overall spectral and temporal profiles. These features include narrowband bursts, split-band bursts, and zebra patterns, among others. The conventional mechanism struggles to explain the origin and detailed characteristics of these fine structures, indicating the need for additional physical processes or interactions that contribute to their formation.

Polarization Properties: The polarization properties of solar radio bursts, such as the degree and position angle of polarization, provide valuable information about the magnetic field configurations and emission mechanisms involved. While the conventional mechanism can account for certain polarization characteristics, there are cases where the observed polarization properties are not fully consistent with the expected predictions, suggesting the presence of additional mechanisms or complex plasma interactions that contribute to the observed polarization signatures.

Low-Frequency Radio Bursts: The conventional mechanism primarily focuses on explaining the emission processes at higher radio frequencies. However, recent observations have revealed the presence of low-frequency radio bursts associated with solar flares. These bursts exhibit unique characteristics that challenge the conventional mechanism's ability to explain the emission mechanisms and properties at these lower frequencies.

High Brightness Temperature: One of the challenges faced by the conventional mechanism is explaining the exceptionally high brightness temperatures observed in some solar radio bursts. While coherent emission processes such as electron-cyclotron maser (ECM) emission can account for intense bursts, the reported brightness temperatures in the range of 10^9 to 10^{13} Kelvin suggest the presence of highly localized and energetic emission sources that may require additional or alternative mechanisms to be fully understood.

Among the many unsolved limitation of conventional theory, The high brightness temperature ob-

served in some solar radio bursts remains an intriguing and unsolved problem within the conventional theory. The reported brightness temperatures ranging from 10^9 to 10^{13} Kelvin raise questions about the underlying mechanisms responsible for such intense emission.

The ECM emission can be highly directional and produce focused bursts of radio waves. The emitted radiation can be concentrated within a relatively narrow beam, which gives the appearance of localization. This beam-like emission is often observed in the form of coherent radio bursts associated with intense solar flares.

Gyro-synchrotron radiation and electron-cyclotron maser are two distinct processes involved in the generation of radio emission by energetic electrons in the presence of a magnetic field. While both processes are related to the interaction between electrons and magnetic fields, there are key differences in their underlying mechanisms and characteristics.

Key features of gyro-synchrotron radiation include:

- Broadband emission: Gyro-synchrotron radiation covers a wide range of frequencies, typically spanning from radio to X-ray wavelengths.

- Continuous spectrum: The emitted radiation forms a smooth continuum with no distinct spectral features.

- Isotropic emission: The radiation is emitted in all directions perpendicular to the magnetic field lines, resulting in a generally isotropic distribution of radiation.

Key features of electron-cyclotron maser emission include:

- Narrowband emission: ECM emission is often characterized by narrowband bursts of radio waves, exhibiting a distinct spectral structure.

- Highly directional emission: The emitted radiation is highly directional and can form well-collimated beams of radiation.

- Coherent emission: The radiation is emitted coherently, meaning that the waves are in phase, resulting in high-intensity bursts of radiation.

- Resonant interaction: The emission occurs when the gyrofrequency of the electrons matches the frequency of the plasma waves, leading to resonant amplification.

The ECMI (Electron Cyclotron Masers Instability) model has been found to be applicable to spontaneous magnetic reconnection, providing insights into the electromagnetic radiation emitted by electron holes in this process. This model is now being applied to the study of reconnection in strong current-aligned magnetic guide fields. These guide fields play a passive role in reconnection, as the actual reconnection occurs in the antiparallel components on either side of the guide field-aligned current sheets, with the current carried by kinetic Alfvén waves.

During reconnection in the presence of strong guide fields, electron exhaust regions are generated at the X point of the reconnection site. These exhaust regions extend perpendicular to both the current and

the guide fields, spanning a considerable distance of hundreds of electron inertial scales. Within these exhausts, a distinct population of hot electrons with significantly reduced density is observed. These exhaust regions exhibit properties similar to electron holes, which are localized plasma structures with specific characteristics.

The momentum space distributions of electrons within these exhaust regions are highly deformed, displaying steep gradients transverse to both the reconnecting and guide fields. These properties suggest that the ECMI mechanism, with its fundamental ECMI X-mode emission, may be applicable in localized source regions beneath the nonrelativistic guide field cyclotron frequency. In these regions, the ECMI process may amplify and emit coherent radio waves.

However, it is important to note that not all ECM emission sources exhibit the same degree of localization. The extent of localization can vary depending on several factors, including the properties of the accelerated electron population, the strength and configuration of the magnetic field, and the plasma conditions in the surrounding environment.

In certain scenarios, the ECM emission can exhibit broader spatial distributions, resulting in a more diffuse or extended source of radio emission. This can occur when the conditions for beam-like emission are not met, or when the electron distribution is more spatially dispersed. In such cases, the ECM emission may not appear as highly localized as in the beam-like bursts.

The Langmuir wave collapse hypothesis is a proposed mechanism for explaining certain characteristics of solar radio bursts, particularly the short duration and high intensity of bursts associated with type III and type V bursts. This hypothesis suggests that the collapse of Langmuir waves, which are plasma waves involving electron density fluctuations, plays a crucial role in the generation of these bursts.

The Langmuir waves are excited in the solar corona by the accelerated electron beams resulting from processes such as magnetic reconnection or plasma instabilities during solar flares. These waves propagate through the plasma and can experience a phenomenon known as wave collapse. Wave collapse occurs when the Langmuir waves reach a critical amplitude and interact non-linearly with the ambient plasma.

During wave collapse, the Langmuir waves transfer their energy to other plasma waves, such as ion acoustic waves or electromagnetic waves, through various nonlinear processes. This energy transfer leads to the conversion of Langmuir waves into intense radio emission at the plasma frequency or its harmonics. The emitted radio waves are then observed as solar radio bursts.

The Langmuir wave collapse hypothesis provides an explanation for the short duration and high intensity of type III and type V solar radio bursts. The collapse of Langmuir waves results in a rapid and efficient conversion of wave energy into radio emission, leading to the observed intense bursts of radiation. The short duration of these bursts is attributed to the rapid collapse and subsequent decay of the Langmuir waves.

While the Langmuir wave collapse hypothesis offers a plausible mechanism for certain characteristics of solar radio bursts, it is important to note that it is not the only explanation and may not account for all observed phenomena. Solar radio bursts are complex events influenced by a variety of factors, including plasma conditions, magnetic field configurations, and the dynamics of accelerated particles.
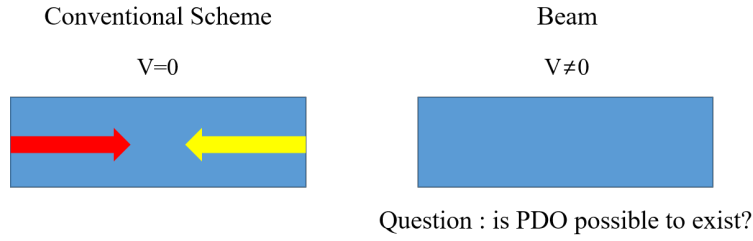
Figure 37: PDO generation schemes considering astrophysical aspect

Additional research and observations are needed to further validate and refine the Langmuir wave collapse hypothesis and to gain a comprehensive understanding of the underlying physics driving solar radio bursts.

The other possible complement to the conventional models is the PDO model. The PDO model suggests that the high brightness temperatures in solar radio bursts can be attributed to the excitation of dipole oscillations in the plasma. In this model, the intense radio emission is produced by the collective motion of charged particles in the plasma, which results in enhanced radiation at specific frequencies.

The PDO model offers an alternative perspective on the generation of high brightness temperatures by emphasizing the role of collective plasma motion. It suggests that the intense emission arises from the coordinated behavior of charged particles within the plasma, rather than solely relying on individual electron interactions. The dipole-like oscillations of the plasma enhance the radiation efficiency and contribute to the high observed brightness temperatures.

While the PDO model provides a complementary explanation for the high brightness temperatures, further research, especially **relativistic PDO and also investigate the possibility of coherent radiation emissions by the multiple PDO**. observational evidence are needed to validate its applicability in specific solar radio burst events. Exploring the interplay between the conventional mechanisms, such as gyrosynchrotron radiation and plasma emission, and the PDO model can shed light on the complex nature of solar radio bursts and help elucidate the physical processes responsible for the observed phenomena.

5.3   PDO astrophysics

How to generate PDO in the corona or plenatary plasma have not been studied until now. The most similar phenomenon is the particle bunching generated by the cyclotron maser instability, which is possible to argue that PDO is naturally generated and becomes one candidate for radio burst mechanism. Laser based PDO generation scheme is to use colliding two detuned lasers in the stationary plasma strip. To model the PDO in the beam, idealized configuration is considered. Plasma strip has constant velocity and two beams are identical except for the directions. This one is physically equivalent to the previous scheme. Difference is the frame. If the frame is stick to the plasma, each electromagnetic waves undergo Doppler shift kv, where k is ω_p/v. This one naturally produces the frequency detuning. The simulation results indicate that the PDO is stably generated.
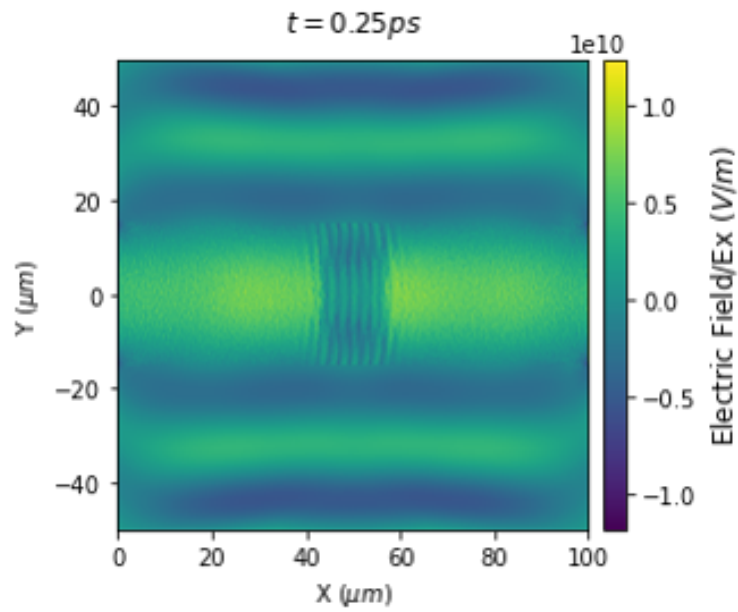
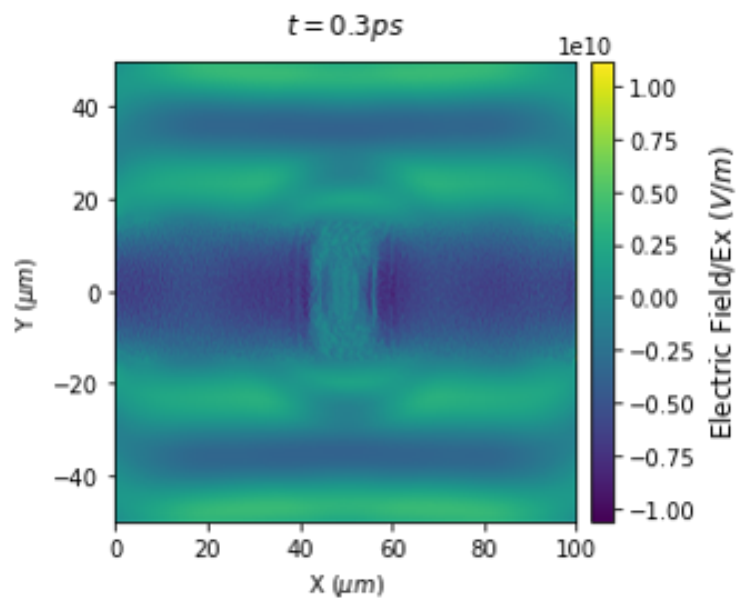Figure 38: Electric fields when the laser pulses are overlapped

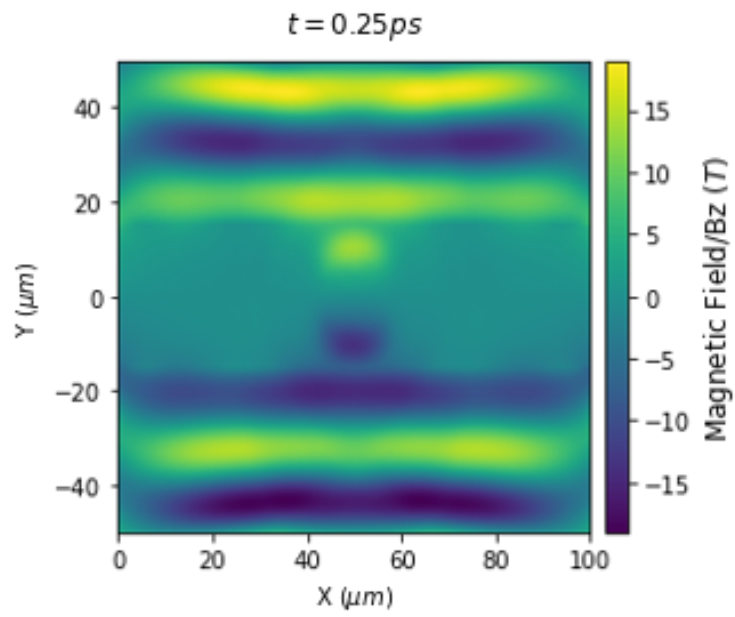Figure 39: Electric fields when the laser pulses pass

Figure 40: Magnetic fields when the laser pulses are overlapped
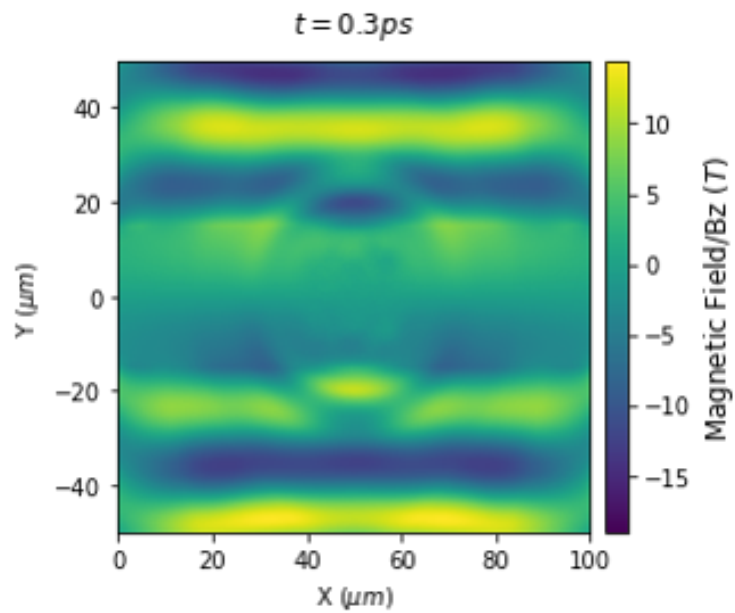

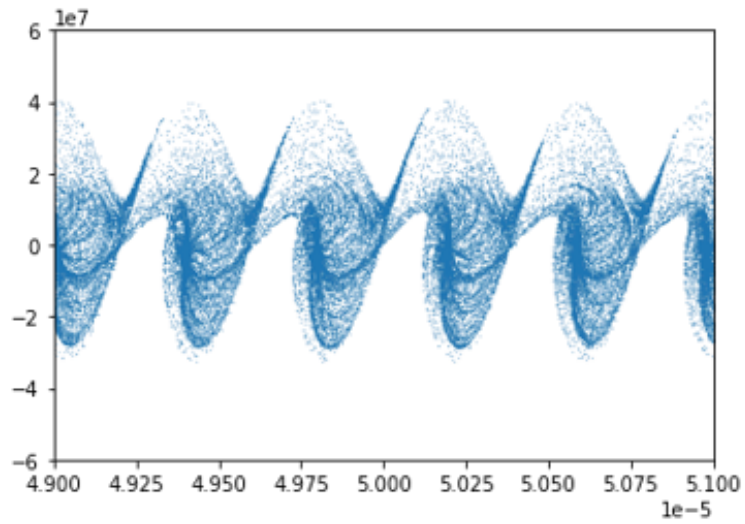Figure 41: Magnetic fields when the laser pulses pass

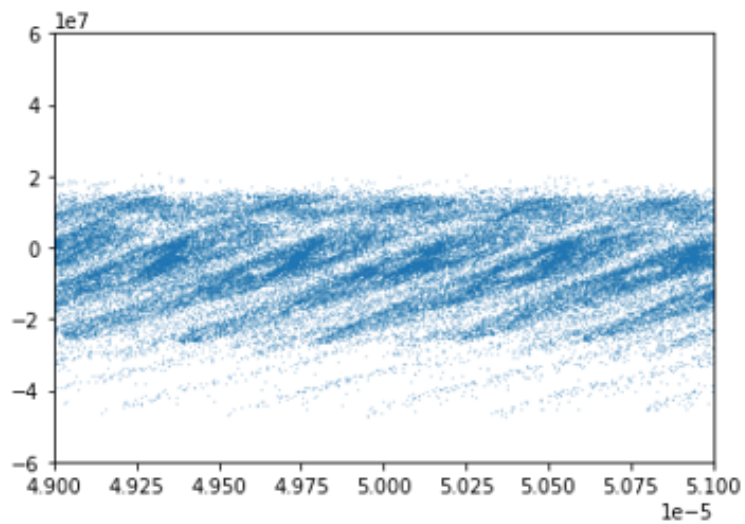Figure 42: Electron distribution in phase space when the laser pulses are overlapped

Figure 43: Electron distribution in phase space when the laser pulses pass

The electron distribution in Phase space and radiation pattern are the same as in the preceding scheme's PDO. The drift velocity is the difference between particle bunches in CME and bunches in PDO. CME bunch displacement is perpendicular to beam velocity, whereas PDO is parallel. If the PDO becomes relativistic and on the plasma beam with constant velocity, then what behavior will appear? I should firstly consider the dipole formation process in advance, but I assume the PDO is stably formed and relativistic in the plasma beam. Then the Lagrangian of it in the beam frame is like that.

$$L = -mc^2 \sqrt{1 - \beta^2} - m\frac{\omega_p^2}{2}x^2 \tag{101}$$

Obtaining equation of motion by the Lagrangian in lab frame is complex. I will obtain the equation of motion in the beam frame. Through the Lorentz transform, lab frame solution can be obtained.

$$mc^2 \gamma_\beta^3 \beta' \frac{d\beta'}{dt'} + \omega_p^2 \beta' x' = 0 \tag{102}$$

' represent beam frame. Acceleration is the

$$\frac{d\beta'}{dt'} = -\frac{\omega_p^2 x'}{\gamma_\beta^3 mc^2} \tag{103}$$

Solving this equations to get a velocity

$$\beta' = \sqrt{1 - \left(E_0 - \frac{\omega_p^2 x'^2}{2mc^3} \right)^2} \tag{104}$$

where E_0 is the initial energy of the PDO. Position and velocity in beam frame need to be also Lorentz transformed.

$$x' = \gamma_v(x + vt) \tag{105}$$

Putting X instead of $x + vt$, velocity in beam frame becomes

$$\beta' = \sqrt{1 - \left(E_0 - \frac{\omega_p^2 \gamma_v^2 X^2}{2mc^3} \right)^2} \tag{106}$$

$$\beta = \frac{\beta' - v}{\sqrt{1 - \beta' v}} \tag{107}$$

where v is the beam velocity normalized by the speed of light.

$$\beta = \frac{\sqrt{1 - \left(E_0 - \frac{\omega_p^2 \gamma_v^2 X^2}{2mc^3} \right)^2} - v}{\sqrt{1 - \left(E_0 - \frac{\omega_p^2 \gamma_v^2 X^2}{2mc^3} \right)^2} v} \tag{108}$$

When beam velocity is non-zero, unstable point appear in the trajectory of PDO in phase space. More the beam velocity is faster, displacement is shorten and unstable point is closed. That means drift PDO is unstable and hard to exist in space plasmas.
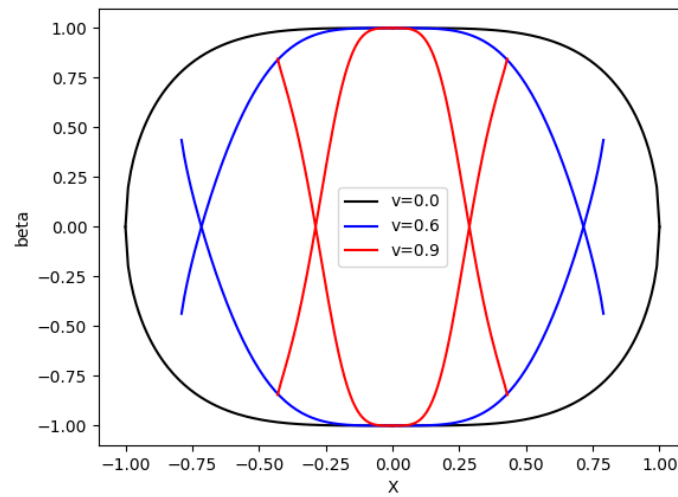
Figure 44: Trajectory of PDO in phase space

References

[1] L. Chopineau, A. Leblanc, G. Blaclard, A. Denoeud, M. Thévenet, J. Vay, G. Bonnaud, P. Martin, H. Vincenti, and F. Quéré, "Identification of coupling mechanisms between ultraintense laser light and dense plasmas," *Physical Review X*, vol. 9, no. 1, p. 011050, 2019.

[2] Y. Ping, A. Kemp, L. Divol, M. Key, P. Patel, K. Akli, F. Beg, S. Chawla, C. Chen, R. Freeman *et al.*, "Dynamics of relativistic laser-plasma interaction on solid targets," *Physical review letters*, vol. 109, no. 14, p. 145006, 2012.

[3] A. Golovanov, I. Y. Kostyukov, A. Pukhov, and V. Malka, "Energy-conserving theory of the blowout regime of plasma wakefield," *Physical review letters*, vol. 130, no. 10, p. 105001, 2023.

[4] W.-Y. Liu, X.-L. Zhu, M. Chen, S.-M. Weng, F. He, Z.-M. Sheng, and J. Zhang, "Tail-wave-assisted positron acceleration in nonlinear laser plasma wakefields," *Physical Review Applied*, vol. 19, no. 4, p. 044048, 2023.

[5] J. Rygg, P. Celliers, and G. Collins, "Specific heat of electron plasma waves," *Physical Review Letters*, vol. 130, no. 22, p. 225101, 2023.

[6] S. Cardoch, F. Trost, H. A. Scott, H. N. Chapman, C. Caleman, and N. Timneanu, "Decreasing ultrafast x-ray pulse durations with saturable absorption and resonant transitions," *Physical Review E*, vol. 107, no. 1, p. 015205, 2023.

[7] C. Tailliez, X. Davoine, A. Debayle, L. Gremillet, and L. Bergé, "Terahertz pulse generation by strongly magnetized, laser-created plasmas," *Physical Review Letters*, vol. 128, no. 17, p. 174802, 2022.

[8] B. Peng, C. Feng, Z. Wang, J. Hua, Y. Wu, H. Deng, F. Li, W. Lu, and Z. Zhao, "Generation of large-bandwidth high-power x-ray free-electron-laser pulses using a hollow-channel plasma," *Physical Review Applied*, vol. 19, no. 5, p. 054066, 2023.

[9] V. Kovalev and V. Y. Bychenkov, "Analytic theory of relativistic self-focusing for a gaussian light beam entering a plasma: Renormalization-group approach," *Physical Review E*, vol. 99, no. 4, p. 043201, 2019.

[10] M. Chen, S. Zeng, D. Lu, W. Hu, and Q. Guo, "Optical solitons, self-focusing, and wave collapse in a space-fractional schrödinger equation with a kerr-type nonlinearity," *Physical Review E*, vol. 98, no. 2, p. 022211, 2018.

[11] D. Woodbury, A. Goffin, R. Schwartz, J. Isaacs, and H. Milchberg, "Self-guiding of long-wave infrared laser pulses mediated by avalanche ionization," *Physical Review Letters*, vol. 125, no. 13, p. 133201, 2020.

[12] J. Götzfried, A. Döpp, M. Gilljohann, F. Foerster, H. Ding, S. Schindler, G. Schilling, A. Buck, L. Veisz, and S. Karsch, "Physics of high-charge electron beams in laser-plasma wakefields," *Physical Review X*, vol. 10, no. 4, p. 041015, 2020.

[13] J. Shaw, N. Lemos, L. D. Amorim, N. Vafaei-Najafabadi, K. Marsh, F. Tsung, W. Mori, and C. Joshi, "Role of direct laser acceleration of electrons in a laser wakefield accelerator with ionization injection," *Physical review letters*, vol. 118, no. 6, p. 064801, 2017.

[14] B. Dromey, M. Zepf, A. Gopal, K. Lancaster, M. Wei, K. Krushelnick, M. Tatarakis, N. Vakakis, S. Moustaizis, R. Kodama *et al.*, "High harmonic generation in the relativistic limit," *Nature physics*, vol. 2, no. 7, pp. 456–459, 2006.

[15] L. Yi, "High-harmonic generation and spin-orbit interaction of light in a relativistic oscillating window," *Physical Review Letters*, vol. 126, no. 13, p. 134801, 2021.

[16] B. Bachmann, S. MacLaren, S. Bhandarkar, T. Briggs, D. Casey, L. Divol, T. Döppner, D. Fittinghoff, M. Freeman, S. Haan *et al.*, "Measurement of dark ice-ablator mix in inertial confinement fusion," *Physical Review Letters*, vol. 129, no. 27, p. 275001, 2022.

[17] A. Goffin, I. Larkin, A. Tartaro, A. Schweinsberg, A. Valenzuela, E. Rosenthal, and H. Milchberg, "Optical guiding in 50-meter-scale air waveguides," *Physical Review X*, vol. 13, no. 1, p. 011006, 2023.

[18] C. McKinstrie, R. Betti, R. Giacone, T. Kolber, and E. Turano, "Two-dimensional stimulated raman scattering of short laser pulses," *Physical Review E*, vol. 51, no. 4, p. 3752, 1995.

[19] C. Darrow, C. Coverdale, M. Perry, W. Mori, C. Clayton, K. Marsh, and C. Joshi, "Strongly coupled stimulated raman backscatter from subpicosecond laser-plasma interactions," *Physical review letters*, vol. 69, no. 3, p. 442, 1992.

[20] S. Monchocé, S. Kahaly, A. Leblanc, L. Videau, P. Combis, F. Réau, D. Garzella, P. D'Oliveira, P. Martin, and F. Quéré, "Optically controlled solid-density transient plasma gratings," *Physical Review Letters*, vol. 112, no. 14, p. 145008, 2014.

[21] L. Shi, W. Li, Y. Wang, X. Lu, L. Ding, and H. Zeng, "Generation of high-density electrons based on plasma grating induced bragg diffraction in air," *Physical review letters*, vol. 107, no. 9, p. 095004, 2011.

[22] T. M. Jeong, S. V. Bulanov, P. Valenta, G. Korn, T. Z. Esirkepov, J. K. Koga, A. S. Pirozhkov, M. Kando, and S. S. Bulanov, "Relativistic flying laser focus by a laser-produced parabolic plasma mirror," *Physical Review A*, vol. 104, no. 5, p. 053533, 2021.

[23] B. Hafizi, A. Ting, P. Sprangle, and R. Hubbard, "Relativistic focusing and ponderomotive channeling of intense laser beams," *Physical Review E*, vol. 62, no. 3, p. 4120, 2000.

[24] H. Gould and G. F. Mazenko, "Coupling of single-particle and collective motions in a one-component plasma," *Physical Review Letters*, vol. 35, no. 21, p. 1455, 1975.

[25] P. Sprangle, E. Esarey, and A. Ting, "Nonlinear theory of intense laser-plasma interactions," *Phys. Rev. Lett.*, vol. 64, pp. 2011–2014, Apr 1990. [Online]. Available: https://link.aps.org/doi/10.1103/PhysRevLett.64.2011

[26] G. Ferrante, M. Zarcone, and S. Uryupin, "Laser even harmonics generation by a plasma embedded in a static electric field," *Laser Physics Letters*, vol. 1, no. 4, pp. 167–171, 2004.

[27] R. Balescu, "Transport equation of a plasma," *Rev. Mod. Phys.*, vol. 32, pp. 719–721, Oct 1960. [Online]. Available: https://link.aps.org/doi/10.1103/RevModPhys.32.719

[28] P. Sprangle, E. Esarey, and A. Ting, "Nonlinear interaction of intense laser pulses in plasmas," *Physical review A*, vol. 41, no. 8, p. 4463, 1990.

[29] E. Stenson, J. Horn-Stanja, M. Stoneking, and T. S. Pedersen, "Debye length and plasma skin depth: two length scales of interest in the creation and diagnosis of laboratory pair plasmas," *Journal of Plasma Physics*, vol. 83, no. 1, p. 595830106, 2017.

[30] J. M. Dawson, "Nonlinear electron oscillations in a cold plasma," *Physical Review*, vol. 113, no. 2, p. 383, 1959.

[31] A. I. Akhiezer and R. V. Polovin, "Theory of wave motion of an electron plasma," *Soviet Phys. JETP*. [Online]. Available: https://www.osti.gov/biblio/4361348

[32] D. T. Michel, S. Depierreux, C. Stenz, V. Tassin, and C. Labaune, "Exploring the saturation levels of stimulated raman scattering in the absolute regime," *Phys. Rev. Lett.*, vol. 104, p. 255001, Jun 2010. [Online]. Available: https://link.aps.org/doi/10.1103/PhysRevLett.104.255001

[33] P. Sprangle, E. Esarey, and A. Ting, "Nonlinear interaction of intense laser pulses in plasmas," *Phys. Rev. A*, vol. 41, pp. 4463–4469, Apr 1990. [Online]. Available: https://link.aps.org/doi/10.1103/PhysRevA.41.4463

[34] C.-K. Li and R. D. Petrasso, "Charged-particle stopping powers in inertial confinement fusion plasmas," *Phys. Rev. Lett.*, vol. 70, pp. 3059–3062, May 1993. [Online]. Available: https://link.aps.org/doi/10.1103/PhysRevLett.70.3059

[35] M. Thumm, G. Denisov, K. Sakamoto, and M. Q. Tran, "High-power gyrotrons for electron cyclotron heating and current drive," *Nuclear Fusion*, vol. 59, no. 7, p. 073001, 2019.

[36] A. R. Maier, N. M. Delbos, T. Eichner, L. Hübner, S. Jalas, L. Jeppe, S. W. Jolly, M. Kirchen, V. Leroux, P. Messner, M. Schnepp, M. Trunk, P. A. Walker, C. Werle, and P. Winkler, "Decoding sources of energy variability in a laser-plasma accelerator," *Phys. Rev. X*, vol. 10, p. 031039, Aug 2020. [Online]. Available: https://link.aps.org/doi/10.1103/PhysRevX.10.031039

[37] G. Gregori, U. Kortshagen, J. Heberlein, and E. Pfender, "Analysis of thomson scattered light from an arc plasma jet," *Phys. Rev. E*, vol. 65, p. 046411, Apr 2002. [Online]. Available: https://link.aps.org/doi/10.1103/PhysRevE.65.046411

[38] D. A. Burton, R. Cairns, B. Ersfeld, A. Noble, S. Yoffe, and D. Jaroszynski, "Observations on the ponderomotive force," in *Relativistic Plasma Waves and Particle Beams as Coherent and Incoherent Radiation Sources II*, vol. 10234.   SPIE, 2017, pp. 17–22.

[39] K. Nishikawa, "Parametric excitation of coupled waves i. general formulation," *Journal of the physical society of Japan*, vol. 24, no. 4, pp. 916–922, 1968.

[40] D. Pesme, G. Laval, and R. Pellat, "Parametric instabilities in bounded plasmas," *Physical Review Letters*, vol. 31, no. 4, p. 203, 1973.

[41] Y. Lee and C. Su, "Theory of parametric coupling in plasmas," *Physical Review*, vol. 152, no. 1, p. 129, 1966.

[42] R. Drake and E. Williams, "Three-wave parametric amplification in time-dependent media, with application to stimulated brillouin scattering," *Physical review letters*, vol. 67, no. 18, p. 2477, 1991.

[43] S. Coen, D. A. Wardle, and J. D. Harvey, "Observation of non-phase-matched parametric amplification in resonant nonlinear optics," *Physical review letters*, vol. 89, no. 27, p. 273901, 2002.

[44] C. Liu and M. N. Rosenbluth, "Parametric decay of electromagnetic waves into two plasmons and its consequences," *The Physics of Fluids*, vol. 19, no. 7, pp. 967–971, 1976.

[45] D. Villeneuve, H. Baldis, and J. Bernard, "Suppression of stimulated raman scattering by the seeding of stimulated brillouin scattering in a laser-produced plasma," *Physical review letters*, vol. 59, no. 14, p. 1585, 1987.

[46] A. Hruska, "Interactions between electrostatic and electromagnetic waves in a magnetized plasma," *Plasma Physics*, vol. 17, no. 12, p. 1165, 1975.

[47] S. Yatom, S. Tskhai, and Y. E. Krasik, "Electric field in a plasma channel in a high-pressure nanosecond discharge in hydrogen: A coherent anti-stokes raman scattering study," *Phys. Rev. Lett.*, vol. 111, p. 255001, Dec 2013. [Online]. Available: https://link.aps.org/doi/10.1103/PhysRevLett.111.255001

[48] M.-H. Cho, Y.-K. Kim, and M. S. Hur, "Measuring the magnetic field of a magnetized plasma using raman scattering," *Applied Physics Letters*, vol. 104, no. 14, p. 141107, 2014.

[49] C. Grebogi and C. S. Liu, "Brillouin and Raman scattering of an extraordinary mode in a magnetized plasma," *The Physics of Fluids*, vol. 23, no. 7, pp. 1330–1335, 07 1980. [Online]. Available: https://doi.org/10.1063/1.863146

[50] P. Bertrand, A. Ghizzo, S. J. Karttunen, T. J. H. Pättikangas, R. R. E. Salomaa, and M. Shoucri, "Simulations of wave–particle interactions in stimulated Raman forward scattering in a magnetized plasma," *Physics of Fluids B: Plasma Physics*, vol. 4, no. 11, pp. 3590–3607, 11 1992. [Online]. Available: https://doi.org/10.1063/1.860368

[51] J. Kim, N. Hafz, and H. Suk, "Electron trapping and acceleration across a parabolic plasma density profile," *Physical Review E*, vol. 69, no. 2, p. 026409, 2004.

[52] A. PUKHOV, "Three-dimensional electromagnetic relativistic particle-in-cell code vlpl (virtual laser plasma lab)," *Journal of Plasma Physics*, vol. 61, no. 3, p. 425–433, 1999.

[53] H. S. Song, M.-H. Cho, Y.-K. Kim, T. Kang, H. Suk, and M. S. Hur, "Measurement of local density and magnetic field of a magnetized plasma using raman scattering from a focused laser pulse," *Plasma Physics and Controlled Fusion*, vol. 58, no. 2, p. 025006, 2016.

[54] K. M. Case, "Plasma oscillations," *Annals of physics*, vol. 7, no. 3, pp. 349–364, 1959.

[55] G. Fubiani, E. Esarey, C. Schroeder, and W. Leemans, "Beat wave injection of electrons into plasma waves using two interfering laser pulses," *Physical Review E*, vol. 70, no. 1, p. 016402, 2004.

[56] A. Seaton and T. Arber, "Laser-plasma instabilities in long scale-length plasmas relevant to shock-ignition," *Physics of Plasmas*, vol. 27, no. 8, p. 082704, 2020.

[57] H. Olsen, "Thermal and electrical properties of an argon plasma," *The Physics of Fluids*, vol. 2, no. 6, pp. 614–623, 1959.

[58] R. Kulsrud, H. Furth, E. Valeo, and M. Goldhaber, "Fusion reactor plasmas with polarized nuclei," *Physical Review Letters*, vol. 49, no. 17, p. 1248, 1982.

[59] S. Bathgate, M. Bilek, and D. Mckenzie, "Electrodeless plasma thrusters for spacecraft: a review," *Plasma Science and Technology*, vol. 19, no. 8, p. 083001, 2017.

[60] M. Laroussi, "Low temperature plasma-based sterilization: overview and state-of-the-art," *Plasma processes and polymers*, vol. 2, no. 5, pp. 391–400, 2005.

[61] A. Maksimchuk, S. Gu, K. Flippo, D. Umstadter, and V. Y. Bychenkov, "Forward ion acceleration in thin films driven by a high-intensity laser," *Physical Review Letters*, vol. 84, no. 18, p. 4108, 2000.

[62] S. Banerjee, A. Valenzuela, R. Shah, A. Maksimchuk, and D. Umstadter, "High harmonic generation in relativistic laser–plasma interaction," *Physics of Plasmas*, vol. 9, no. 5, pp. 2393–2398, 2002.

[63] B. Ritchie, "Relativistic self-focusing and channel formation in laser-plasma interactions," *Physical Review E*, vol. 50, no. 2, p. R687, 1994.

[64] E. Yablonovitch, "Self-phase modulation of light in a laser-breakdown plasma," *Physical Review Letters*, vol. 32, no. 20, p. 1101, 1974.

[65] H. Hartfuss, T. Geist, and M. Hirsch, "Heterodyne methods in millimetre wave plasma diagnostics with applications to ece, interferometry and reflectometry," *Plasma Physics and Controlled Fusion*, vol. 39, no. 11, p. 1693, 1997.

[66] J. Glasser, J. Chapelle, and J. Boettner, "Abel inversion applied to plasma spectroscopy: a new interactive method," *Applied optics*, vol. 17, no. 23, pp. 3750–3754, 1978.

[67] J. Howard, "Vector tomography applications in plasma diagnostics," *Plasma physics and controlled fusion*, vol. 38, no. 4, p. 489, 1996.

[68] G. Conway, J. Schirmer, S. Klenge, W. Suttrop, E. Holzhauer, A. U. Team *et al.*, "Plasma rotation profile measurements using doppler reflectometry," *Plasma Physics and Controlled Fusion*, vol. 46, no. 6, p. 951, 2004.

[69] C. M. Laperle, P. Wintermeyer, J. R. Wands, D. Shi, M. A. Anastasio, X. Li, B. Ahr, G. J. Diebold, and C. Rose-Petruck, "Propagation based differential phase contrast imaging and tomography of murine tissue with a laser plasma x-ray source," *Applied Physics Letters*, vol. 91, no. 17, p. 173901, 2007.

[70] F. F. Chen, "Langmuir probe diagnostics," in *Mini-Course on Plasma Diagnostics, IEEEICOPS meeting, Jeju, Korea*. Citeseer, 2003, pp. 20–111.

[71] F. Snik and C. U. Keller, "Astronomical polarimetry: polarized views of stars and planets," *Planets, Stars and Stellar Systems. Volume 2: Astronomical Techniques, Software and Data*, p. 175, 2013.

[72] G. Vieux, B. Ersfeld, J. P. Farmer, M. S. Hur, R. C. Issac, and D. A. Jaroszynski, "Plasma density measurements using chirped pulse broad-band Raman amplification," *Applied Physics Letters*, vol. 103, no. 12, 09 2013, 121106. [Online]. Available: https://doi.org/10.1063/1.4821581

[73] M. A. Gigosos, "Stark broadening models for plasma diagnostics," *Journal of Physics D: Applied Physics*, vol. 47, no. 34, p. 343001, 2014.

[74] S. Zhang, X. Wang, M. He, Y. Jiang, B. Zhang, W. Hang, and B. Huang, "Laser-induced plasma temperature," *Spectrochimica Acta Part B: Atomic Spectroscopy*, vol. 97, pp. 13–33, 2014. [Online]. Available: https://www.sciencedirect.com/science/article/pii/S0584854714000615

[75] S. Kylychbekov, H. S. Song, K. B. Kwon, O. Ra, E. S. Yoon, M. Chung, K. Yu, S. R. Yoffe, B. Ersfeld, D. A. Jaroszynski, and M. S. Hur, "Reconstruction of plasma density profiles by measuring spectra of radiation emitted from oscillating plasma dipoles," *Plasma*

Sources Science and Technology, vol. 29, no. 2, p. 025018, feb 2020. [Online]. Available: https://dx.doi.org/10.1088/1361-6595/ab6756

[76] S. S. Harilal, E. J. Kautz, and M. C. Phillips, "Time-resolved absorption spectroscopic characterization of ultrafast laser-produced plasmas under varying background pressures," *Physical Review E*, vol. 103, no. 1, p. 013213, 2021.

[77] S. Bhandari and C. Flynn, "Probing the universe with fast radio bursts," *Universe*, vol. 7, no. 4, 2021. [Online]. Available: https://www.mdpi.com/2218-1997/7/4/85

[78] "A bright millisecond-duration radio burst from a galactic magnetar," *Nature*, vol. 587, no. 7832, pp. 54–58, 2020.

[79] T. Bastian, A. Benz, and D. Gary, "Radio emission from solar flares," *Annual Review of Astronomy and Astrophysics*, vol. 36, no. 1, pp. 131–188, 1998.

[80] N. Gopalswamy, S. Yashiro, M. Kaiser, R. Howard, and J.-L. Bougeret, "Characteristics of coronal mass ejections associated with long-wavelength type ii radio bursts," *Journal of Geophysical Research: Space Physics*, vol. 106, no. A12, pp. 29 219–29 229, 2001.

[81] G. Mann, F. Breitling, C. Vocks, H. Aurass, M. Steinmetz, K. Strassmeier, M. Bisi, R. Fallows, P. Gallagher, A. Kerdraon *et al.*, "Tracking of an electron beam through the solar corona with lofar," *Astronomy & Astrophysics*, vol. 611, p. A57, 2018.

[82] J. M. Cordes and S. Chatterjee, "Fast radio bursts: an extragalactic enigma," *Annual Review of Astronomy and Astrophysics*, vol. 57, pp. 417–465, 2019.

[83] C. D. Bochenek, V. Ravi, K. V. Belov, G. Hallinan, J. Kocz, S. R. Kulkarni, and D. L. McKenna, "A fast radio burst associated with a galactic magnetar," *Nature*, vol. 587, no. 7832, pp. 59–62, 2020.

[84] T. Török and B. Kliem, "Confined and ejective eruptions of kink-unstable flux ropes," *The Astrophysical Journal*, vol. 630, no. 1, p. L97, 2005.

[85] J. Feynman and A. Ruzmaikin, "A high-speed erupting-prominence cme: A bridge between types," *Solar Physics*, vol. 219, pp. 301–313, 2004.

Acknowledgements

울산과학기술원에 석사 과정으로 시작하여, 우여곡절 끝에 박사 과정을 잘 마무리 하게 되었습니다. 먼저 하나님께 감사드립니다. 중요한 순간마다 날카롭고 예리한 질문으로 저를 성장시켜주신 허민섭 교수님께도 감사드립니다. 오랜 기간 동안 지도를 받으면서 항상 "교수님 이었다면 어떤 관점으로 데이터를 보았을까" 또는 "어떤 부족한 점이 있는가" 라는 생각으로 고민 해왔던 것 같습니다. 그런 시간이 없었다면 저는 물리학자로 거듭날 수 없었을 것 같습니다. 그리고 국제광공학회를 통해 교수님과 자주 협업하는 디노 교수님과 그룹원들 그리고 노벨상 수상자 머로우 등을 볼 수 있었던 것은 제게 큰 행운이었습니다.

제가 학부 전공이 전자공학이다 보니 물리학이라는 학문에 대한 기초가 없었는데, 기초를 세우는데 도움을 주셨던 정모세 교수님과 곽규진 교수님께도 감사드립니다. 고에너지 천체물리 연구센터 워크샵을 통해, Electron Beam Ion Trap(EBIT) 장치 개발과 별의 진화에 대한 흥미로운 연구 과정을 볼 수 있어서 다채로운 물리 분야를 경험 할 수 있었습니다.

그리고 졸업 심사에 참여 해주신 광주과학기술원의 석희용 교수님, 포항가속기 연구소의 남인혁 박사님께도 감사드립니다. 한국물리학회, 울산과학기술원의 세미나, 플라즈마 컨소시움 등을 통해 레이저 플라즈마 이론을 현실로 구현화 해나가시는 수고와 노력이 매우 인상적이었습니다.

연구실에서 만난 조명훈 박사님께 Particle In Cell(PIC)을 배웠던 시간을 되돌이켜 보면, 박사님께 실무적인 배움을 얻었던 것 같습니다. 그리고 정모세 교수님 소속으로 PIC를 배우기 위해 짧은 시간 동안 건너온 문국진 박사님에게도 감사를 합니다. Fourier-Bessel PIC(FBPIC)을 함께 공부하면서 연구에 대한 꿈을 키워갔던 시간을 돌이키게 됩니다. 연구실을 늘 밝게 만들어 주었던 라욱주, 권규빈 박사님들과의 시간은 즐거운 추억으로 남습니다. 여러 일들이 있었지만 좋은 결과를 얻게 해준 살리잔에게도 감사를 표시합니다. 마노즈 쿠마르 박사님과 코로나-19 라는 어려운 시기를 함께 이겨나갔던 일들이 제가 다른 문화권 사람을 이해하는데 많은 도움이 되었습니다. 깊이 있는 토론을 할 수 있었던 태원준에게도 감사합니다.

연구실 세대 교체가 되며 들어온 김승윤, 이윤규, 이재호에게 같이 연구실 생활을 하면서 즐거운 시간을 보낸 것에 감사를 전합니다. 전산 물리 및 플라즈마 물리 수업 때, 조교로서 만났던 김현석과 박도현, 두 사람과 같은 연구실 소속이 되어 많은 도움이 되었습니다. 온전하지 않았던 컴퓨터 사이언스에 대한 지식을 채워주었던 김현석에게 감사를 전합니다. 마지막으로 학위 과정을 무사히 할 수 있도록 묵묵히 있어준 아버지 송문근, 돌아가신 어머니 서금희 그리고 동생 송누리에게 사랑한다는 말을 전합니다.